EXPERIMENTAL INVESTIGATION OF THE IMPEDANCE MEASUREMENT METHOD FOR DETECTING DUST AND GAS FLAMES IN A FLAME ACCELERATION TUBE

Development of Experimental Apparatus

Gisle André Enstad

A thesis submitted in partial fulfilment of the
requirements for the degree of *Master of Science* in
the subject of Physics; Process Safety Technology

Department of Physics and Technology
University of Bergen
Bergen, Norway
June 2009

Abstract

This master thesis describes an impedance measurement device built for investigating flame propagation in a Flame Acceleration Tube, FAT. This tube is 3.6 m long, and has been instrumented with thermocouples, pressure sensors and optical measurement probes in addition to the impedance probe. A control and data acquisition system built around a NI CAD 6259 card were developed and used during the experiments.

The impedance is measured by finding damping and resonance coil and an unknown capacitor/impedance. The methodology gave satisfactory results during initial testing in a 20 litre vessel. However, problems with implementation in the FAT limited the qualitative value of the impedance measurements to basic flame arrival information. Experiments with lean fuel-air mixtures gave weaker readings of the flame, making some of the measurements uncertain.

Kalvatn (2009) describes optical measurements of the same experiments. A tailor made probe has been developed. The probe contains both the optical and impedance based measurement techniques. This allows simultaneous measurements in the same cross sectional of the flame. The experiments were also filmed with a high speed camera. Results obtained with the methods and analyses of the video are compared. In general the video and optical measurements tend to detect the flame before the impedance measurements.

Closed vessel experiments were performed in the FAT with both gas and dust. Three concentrations of propane were tested: 3.0%, 4.5% and 6.0%; as well as two nominal dust concentrations: 250 and 500 g/m^3. The dust used were maize starch. The gas explosions produced much higher flame speeds than the dust explosions.

The main drawback of the impedance measurements found is the time resolution. This problem is not easily solved if both the resistance and capacitance of the flame is of interest. However, if one can manage without separating out resistance and capacitance information the principle could offer very high time resolution. The experiments in the 20 litre vessel show that the combined impedance is possible to measure.

Acknowledgements

I would direct my grateful thank both my supervisors Trygve Skjold and Bjørn Arntsen. A great deal of thanks goes to Werner Olsen, who has been invaluable in order to develop and understand the electronics needed to the experiments. He helped despite not being responsible for the project. Ivar B. Kalvatn has been a good cooperator throughout this project, and deserves many thanks. A special thank goes to the staff at the mechanical workshop at UiB, Kåre Slettebakken, Leif Egil Sandnes and Roald Langøen. They made much of the mechanical equipment, including the measurement probe. Also the staff at the experimental workshop at GexCon has been helpful in terms of lending equipment and help to perform experiments. Many thanks are also directed to Professor Rolf K. Eckhoff for many helpful discussions. My thanks also go to my father Gisle G. Enstad and my brother Lars I. Enstad, which has helped proof reading my thesis.

Table of contents

Symbols

τ_K	Kolmogorov time scale
τ_L	Laminar flame time scale
δ_l	Flame thickness
t	Time
n	Number of elements
S	Flame velocity
Ka	Karlovitzh number
Da	Damköler number
v'	Turbulent velocity fluctuations
υ	Kinematic viscosity
l_0	Integral length scale
Δt	Time resolution
L_t	Length between probes
i_n	Current through loop n
Cc	Capacitance of coil
Cs	Capacitance of probe wires
Cx	Capacitance of probe plates
V_m	Voltage across component m
Rc	Resistance of coil
Rs	Resistance of probe wires
Rx	Resistance between probe plates

1 Introduction

The introduction is similar in Kalvatn (2009) except chapter 1.1.4

1.1 Motivation

The dust explosion phenomenon can be explained by an example from the daily life (Eckhoff, 2003). When lighting a bonfire, it is normal to whittle parts of the wood into smaller parts to make it easier to ignite. The subdivision also increases the combustion rate due to the increased specific surface area between the wood (fuel) and air (oxidizer). By dividing the wood into increasingly smaller parts, one eventually obtains dust particles with characteristic size typically below 100 μm. If a cloud, or mechanical suspension, of such wood dust is ignited, a flame can propagate rapidly through the cloud, creating a dust explosion.

Many materials can generate explosible dust clouds, including coal, sawdust, grain, flour, maize starch, sugar, plastics, aluminium, and titanium. Explosible dust clouds are more likely to occur inside process equipment, rather than outside. They can arise from activities such as pneumatic transport, milling, spray drying, etc., and can involve equipment such as bucket elevators, silos, grinding mills, and filters. Hence, dust explosions represent a hazard in a variety of industries.

1.1.1 Accidental dust explosions

Throughout the years, many people have lost their lives and/or been injured in accidental dust explosions. Material damages from dust explosions also result in considerable economic loss. Recent statistics from the U.S. Chemical Safety and Hazard Investigation Board (CSB, 2006) show that dust the explosion hazards is still a major problem in the powder handling industry. Figure 1-1 suggests that the problem has worsened in the recent years, but this trend may be influenced by lack of reporting of minor incidents in the early years.

The following examples from Eckhoff (2003) and CSB (2006) illustrates that dust explosions can occur in many different types of industries:

- Wheat grain dust explosion in silo, Stavanger port silo, 1970
- Dust explosion in a silicon powder grinding plant at Bremanger, Norway 1972, five workers killed
- Fish meal factory, Norway 1975, one person killed
- Atomized aluminium powder production plant at Anglesey, UK 1983
- Methane/coal dust explosion in a coal storage silo at a cement works in San Bernardino County, California 1984
- Smoldering gas explosion in a silo plant in Stavanger, November 1985
- Polyethylene dust explosion, Kinston, North Carolina 2003, six workers killed
- Resin dust explosion, Corbin, Kentucky 2003, seven workers killed
- Sugar dust explosion at Imperial Sugar, Savannah, Georgia, February 7, 2008, 14 deaths and 38 injuries

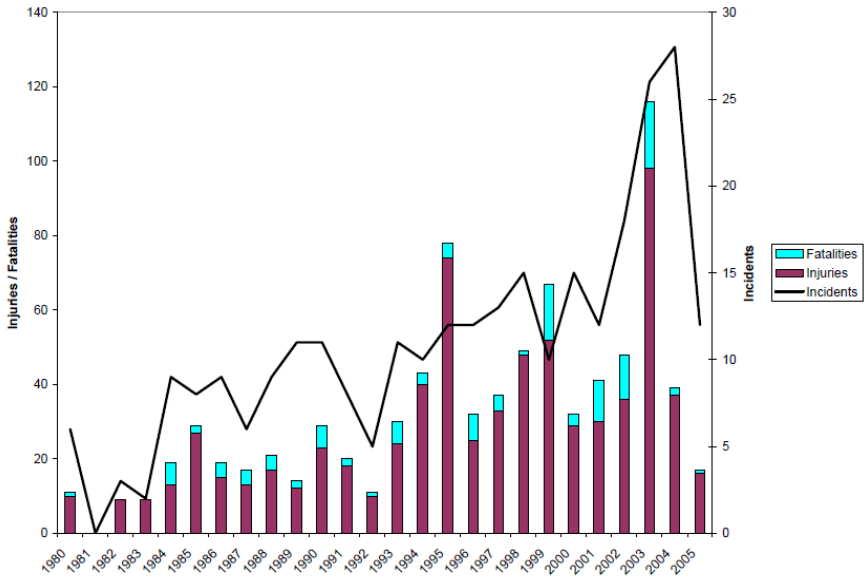

Figure 1-1 *Dust incidents, injuries, and fatalities in the US from 1980 to 2005 (CSB, 2006)*

1.1.2 Prevention and mitigation

The risk associated with an activity is determined by the probability and the consequence of events that inflict various types of loss: fatalities, injuries, material damage, downtime, loss of reputation, etc. There are two main categories of measures to reduce the risk posed by dust explosions (Eckhoff, 2003): prevention and mitigation. Prevention reduces the probability, and mitigation reduces the consequence. Table 1-1 provides an overview of the means for preventing and mitigating dust explosions in the process industries.

Table 1-1 *Overview of means for preventing and mitigating dust explosions in the process industries (Eckhoff, 2003)*

Prevention		**Mitigation**
Preventing explosible dust clouds	**Preventing ignition sources**	
Inerting by N_2, CO_2 and rare gases	Smouldering combustion in dust, dust flames	Reduce explosible cloud size
		Partial inerting
Intrinsic inerting	Other types of open flames (*e.g.* hot work)	Isolation (sectioning)
Inerting by adding inert dust	Hot surfaces	Venting
Dust concentration outside explosible range	Electric spark and arcs, electrostatic discharges	Pressure resistant construction
	Heat from mechanical impact (metal sparks and hot spots)	Automatic suppression
		Good housekeeping (dust removal/cleaning)

Preventive measures may in some situations be sufficient to reduce the dust explosions risk to acceptable levels. However, it is often necessary to apply mitigating measures, either passive such as explosion venting or pressure resistant constructions or active such as automatic suppression and isolation systems. Sensors that detect the explosion in its incipient stages, either from the increase in pressure or the flame itself, trigger active mitigation systems. Reliable and robust methods for flame detection are therefore important to realise fast and effective suppression and isolation systems.

1.1.3 Flame detection – an overview

A flame can be detected by instruments that measures properties of the flame directly, or through phenomena that could result from flame propagation (*e.g.* increased pressure or smoke). Flame detection by measuring IR and/or UV radiation is the most used principle in instruments that are commercial available today, but other principles are also in use. Ray (1978) provides a useful review of the physical techniques that can be used to detect and give warning of fire. Figure 1-1 shows some of the different instruments available today.

Figure 1-2 *Instruments for detecting flames or flame related properties: 1) combined IR and UV flame detector from Net-Safety Monitoring Inc., 2) IR smoke detector from Det-Tronics, 3) piezoelectric pressure sensor from Kistler, 4) and thermocouples from Jackson O*

Flame detection is important both for industry and in research. In industry, it can be used to monitor combustion processes, or for activating suppression and isolation systems. In the context of research, quantitative information about flame propagation and flame-related properties is needed to investigate and understand combustion phenomena (*e.g.* through the validation of numerical models). Thus, the purpose of flame detectors differs in the two cases.

It is very important that instruments designed for industrial applications are reliable and can run for a long time with minimum maintenance. Instruments intended for dust explosion protection will usually operate under relatively harsh conditions inside process equipment such as bucket elevators, mills, filters, etc. Most flame sensors will never be activated by an explosion, but should a flame occur, the sensor should detect the flame fast enough for the active mitigation system to isolate or extinguish the flame.

Robustness and lifetime is usually less important in research, but it is desiarable that the sensor provides additional information about the flame, such as temperature and flame thickness. The flame sensor will not run for long periods, but rather in short intervals during the experiments, and some maintenance between tests can usually be afforded.

The following principles for flame detection/measurements have been identified in the context of active mitigating systems:

- pressure measurements in partially or fully closed systems (*e.g.* pressure transducers)
- measuring flame temperature (*e.g.* thermocouples and photosensors)

- measuring the dielectricity and/or resistivity in the flame (*e.g.* ionization gauges and impedance probes)
- measuring the speed of sound (*e.g.* acoustic transducers and receivers)

In the context of dust explosion research it is of interest to combine two or more of these principles to get additional information about the flame propagation, and to compare the results from the different principles. The use of pressure transducers and thermocouples are quite common in dust explosion experiments. Different versions of optical probes (usually photodiodes) are used to some extent. However the remaining principles are rarely used and combination of different principles within the same probe is even rarer.

1.1.4 The impedance measurement principle in dust explosions

In the last decades methods to measure very small capacitors and impedances have made it possible to measure the dielectricity and resistivity of different mediums for use in various applications. Some of the applications involve flame measuring. It is possible to make impedance tomograhpic pictures of a combustion process, something which is useful in many applications. The method described in this thesis has a main purpose of flame detection, and secondly measure the capacitance change and resistivity of the flame.

1.2 Present Work

1.2.1 Experimental approach

The present work involves an experimental study of flame detection by various means in the 3.6-meter flame acceleration tube (FAT) illustrated in Figure 1-3. The experiments involve constant volume explosions with ether propane-air mixtures or clouds of maize starch in air. In the basic experimental setup, an ignition source initiates the combustion process in one end of the tube, thermocouples measure flame propagation along the length of the tube, and piezoelectric pressure transducers measure pressure development inside the tube. The experimental approach is similar to that of Pu *et al.* (1988), but with a somewhat larger apparatus, and with an up to date data acquisition systems.

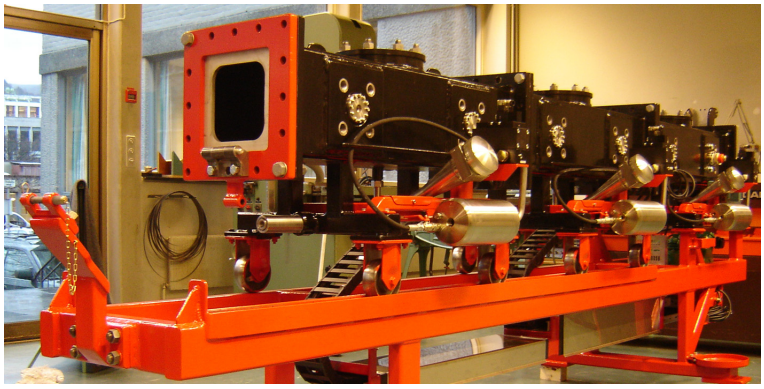

Figure 1-3 *The 3.6 meter flame acceleration tube used in the experiment; the internal cross-section of the tube is 0.27m × 0.27 m.*

The experiments were performed in co-operation with fellow master student Ivar Kalvatn and PhD student Trygve Skjold. This thesis focuses on impedance flame detection/measurement principle, whereas Kalvatn describes the optical principle. Instrumentation and small-scale laboratory work took place at the Dust Explosion Laboratory at the Department of Physics and Technology, University of Bergen. Prototyping of the flame sensors were done in a 20-litre explosion vessel of the USBM type (Skjold 2003). Prior to testing of the measurement

systems, the FAT was equipped with power supplies for instrumentation and automation, as well as a dust dispersion system, a gas-filling system, and an ignition system.

1.2.2 Aim

The aim of the present work is to identify reliable and robust means of detecting turbulent flames in dust-air suspensions and gaseous mixtures. Such measurements are important both for practical applications (*e.g.* suppression and isolation systems), and for fundamental experimental and computational studies of turbulent flame propagation (*e.g.* the determination of burning velocity and the flame thickness of the turbulent flame brush). This thesis will focus on the impedance flame detection/measurement principle, and in particular on the development of a probe that fits both industrial and research related demands.

2 Basic concepts, previous work and theory

This chapter is similar to chapter 2 in Kalvatn (2009) except from 2.2.2 and 2.2.3.

2.1 Concepts and definitions

The following section introduce some fundamental concepts relevant to the thesis. These concepts and definitions is fundamental to understand measurements and conclusions.

2.1.1 Turbulence

Turbulence is a property of the flow, not the fluid. In the present context turbulence influences the dispersion process, the residence time of the dust cloud, ignitability, and not the least the burning velocity. Eckhoff (2003) describes turbulence in the context of a dust cloud as "*a state of rapid internal, more or less random movement of small elements of the dust cloud relative to each other in three dimensions*". One may distinguish between two sources of turbulence in the case of a dust explosion. First, the initial turbulence, is the turbulence which is at place where the dust cloud is formed, typically within process equipment. Second, the Turbulence generated ahead of the flame front by expansion-induced turbulence, is depending on the flow and geometry of the system.

In the case of dust dispersion, turbulence is the most important property of the flow. In fact, turbulence is needed for the dust to be dispersed at all. A common way to disperse dust in experiments is to use pressurised air and disperse the dust through some kind of a nozzle or perforated tube/pipe, thus generating turbulence.

Turbulence determines the residence time of the dust cloud. The more turbulence, the longer it will take before the dust in the dust cloud settles out. Therefore, a simple way to study the influence of turbulence on the explosibilty of a dust cloud is to vary the delay between dispersion and ignition. The longer delay, the lower is the level of turbulence.

The ignitability of a dust cloud is highly influenced by the turbulence, because the turbulence cools the ignition zone by convective heat transfer. Hence, the ignition energy required to ignite a dust cloud increases with increasing level of turbulence. The ignition source itself creates turbulence and affect the combustion process. A chemical igniter for instance, will create more turbulence than an electric spark.

In a burning dust cloud, turbulence will promote mixing of hot burned/burning dust with the unburned cloud. Hence, the flame front is not a well-defined planar surface, but rather a mixture of burned, burning, and unburned parts. As a result, the burning velocity of a turbulent dust cloud is much larger than that of a laminar dust cloud. In experiments, expansion-induced turbulence that affects the flame speed can be generated by inserting objects in the explosion vessel, thus changing the geometry, and the flame speed can be measured for different levels of turbulence (Pu *et al*., 1988).

2.1.2 Combustion

Combustion involves exothermic chemical reactions between a fuel (usually a hydrocarbon) and an oxidant usually. In the context of chemical explosions, combustion is not always straight forward to define precisely, because of various borderline cases, which complicate a precise definition. According to Arrhenius the reaction rate will never equal zero, thus there will always be some rate of combustion whenever a fuel is mixed with an oxidiser. The question is then how to define combustion in a useful way. In this thesis, combustion is

defined as a the rapid oxidation of a fuel accompanied by heat release, light emission and ion generation in the reaction zone. This definition fits the different measurement methods, light emission and heat release suits optical and thermocouples while ion generation fits impedance method.

2.1.3 Flames

A flame can be defined as the zone where the combustion processes takes place. Thus combustion characteristic, such as heat release, ion in the form of free radicals and emission of light, will define the flame.

Exothermic combustion often results in emission of visible light, although this is not always the case. For instance, hydrogen flames are not readily visible. Several processes are taking place in a flame, such as heat release, heat transport and mass transport. Decomposition of the reacting molecules at high temperature produces free radicals, such as OH and CH among others. It is possible to measure these radicals, as they alter the physical behaviour of the medium. For example both the electrical conductivity and the dielectric constant in the flame are different from the unreacted mixture. These effects are utilised for making flame sensors.

Radiation from a flame is due to heat production and emission of light. The light is a result of both black body radiation and spectral band emission, which gives the flame a specific colour. Spectral band emission is used to identify different species of molecules within the flame with laser spectroscopy. Black body emission however, requires a surface to emit light. In dust explosions the dust particles provides the surface. Fuel-rich hydrocarbon flames form small particles of carbon, or soot. These particles radiate bright light. In premixed flames close to stoichiometric concentrations, the combustion is more complete, resulting in less carbon particles, thus less red/yellow colour of the flame. Such flames often have a blue colour, associated with the spectrum band of CH and C_2.

Pyrolysis of organic dust particles releases gas from the surface. The gasses mix with the oxidiser, by diffusion and turbulence, and burn. At moderate turbulence level, the mixing of fuel and oxidizer is the slowest process, and defines how fast the dust cloud burns. If the turbulence level is high, the slowest process is the surface reaction. The surface reaction depends on the temperature and the specific surface area of the particles. For metal particles melting and evaporation replace pyrolysis.

Table 2-1 summarizes the main categories of flames according to the initial conditions and mode of fluid motion. In explosions, the fuel and oxidizer is always premixed. However, expansion induced turbulence can determine the mixing state of fuel/oxidizer. In coal mine explosions, for instance, a methane air explosion can whirl up layers of coal dust which again is ignited by the primary explosion.

Table 2-1 *Characterization of flames based on flow conditions and mixing*

Fuel/Oxidizer mixing	Fluid Motion	Examples
Premixed	Turbulent	Gasoline engines
	Laminar	Bunsen burner
Nonpremixed	Turbulent	Torch
	Laminar	Candle

In some cases the dispersion is due to dust falling through air, thus turbulence is not needed. The turbulence level of the flame is one of the key parameters to predict the violence of an explosion. Turbulence can in extreme cases lead to detonation, making the explosion much more devastating. This mechanism is almost as important as the reactivity of the fuel, making it a crucial point in venting area dimensioning.

Figure 2-1 illustrates the Borghi diagram (Borghi, 1984) developed a diagram, shown in. This diagram shows the relation between turbulence parameters and the reaction rate of the mixture. If the turbulent velocity fluctuations are smaller than the laminar flame speed (v` < S_L), the flame will be wrinkled or laminar, depending on the length scale of the turbulence (the x-axis of the diagram). Length scale is associated with the size of the turbulent eddies. At the smallest length scale, Kolmogorov length scale l_K, the time for ½ revolutions equals the diffusion time across the diameter. The geometrical dimensions of the system define the largest length scale, the integral length scale l_0

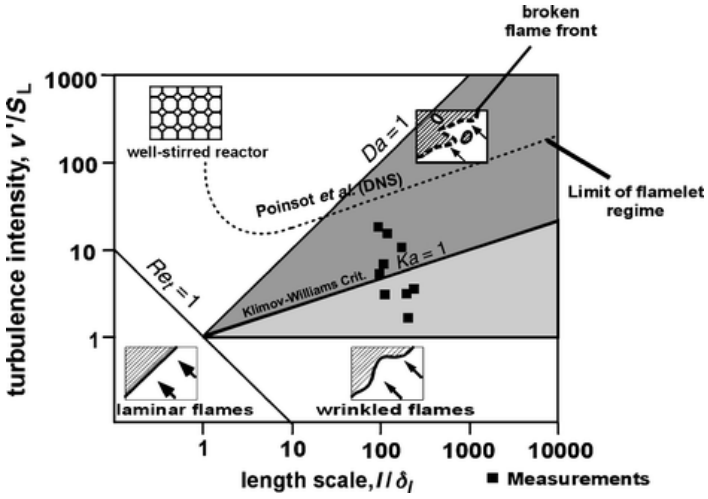

Figure 2-1 *Borghi diagram. (from Borghi 1984)*

If the flame thickness is smaller than the smallest length scale the flame is characterized as a laminar premixed flame, embedded in turbulence. This occurs under the line where *Ka = 1*, where the Karlovitz number *Ka* is given by:

$$Ka = \frac{\tau_L}{\tau_K} \tag{2.1}$$

where τ_L is the time scale of the laminar flame, $\tau_L = \delta_L/S_L$, and τ_K the Kolmogorov time scale, $\tau_K = (\upsilon/\tilde{e})$ ^ 0.5. δ_L laminar flame thickness, S_L is the laminar burning velocity, υ is the kinematic viscosity and $\tilde{e}$ is the dissipation rate. The Damkölher number *Da* relates the chemical time scale to the turbulent time scale (2.2). If the fluid motion is faster than the reaction (*Da > 1*) it results in well stirred reaction. The flame can be very thick under these circumstances. If the number is smaller than 1 the flame will be torn apart, resulting in a large area of reaction. The Damkölher number is given by:

$$Da = \frac{l_0 \cdot s_L}{v` \cdot \delta_L} \tag{2.2}$$

Where l_0 is the integral length scale, δ_L the laminar flame thickness, S_L laminar burning velocity and *v'* the turbulent velocity fluctuations.

2.1.4 Explosions

The word ‘explosion’ is often used for rapid release of energy resulting in the propagation of a pressure wave through the surrounding medium. Explosions can have devastating consequences, and great efforts are made to both prevent them from happen and mitigate the consequences. In the present context, an explosion defined as rapid combustion resulting in pressure build up. Five fundamental criteria must be satisfied for a chemical explosion to occur.

I) Fuel – flammable material

II) Oxidizer – usually oxygen from the air

III) Explosible mixture of fuel and oxidiser

IV) Confinement – some degree of confinement is usually required for pressure build-up to occur.

V) Ignition source – electrical sparks are besides chemical igniters usually applied for experimental work. The ignition source can influence the progress of the explosion.

2.1.5 Some differences between gas and dust

Explosive gas mixtures and dust clouds exhibit similar ignition and combustion properties Eckhoff (2005):

- reasonable well-defined flammability and explosibility limits
- laminar burning velocities and quenching distances
- strong influence of turbulence on the burning velocity
- detonation made of flame propagation
- adiabatic constant-volume explosion pressure of similar magnitudes
- reasonable well-defined minimum ignition energies
- minimum ignition temperatures for given experimental conditions

However, there is a vast difference in the way explosive clouds/mixtures arise and behaves. Whereas explosive gas mixtures are most likely to arise from a leak, an explosible dust clouds often exist within various types of process equipment such as filters and bucket elevators under normal operating conditions. Furthermore dust layers accumulated outside process equipment can generate secondary dust clouds and secondary dust explosions. Finally, a cloud of dust particle suspended in air will settle after a while, unlike a gas mixture.

Another important difference is that dust is flammable both as a dust cloud, with concentrations between the lower and upper flammability limits, and as a settled layer of dust. In combustible gas however, flame propagation is only possible with gas concentrations within the lower and upper flammability limits. It is therefore important to remove dust between tests when dealing with experiments. If not, dust from previous tests will take part in the combustion. This makes testing with dust time-consuming compared to testing with gas because of the time needed for cleaning.

2.2 Previous work

2.2.1 Flame propagation in dust explosions

Limited attention has this far been given to the investigation of the effect of obstacles on flame propagation in dust clouds. This is nevertheless a relevant topic for both explosion safety and the modelling of dust flames, since turbulence induced by the air/dust mixture passing such obstacles will result in flame acceleration.

The first large-scale experiments to investigate flame propagation in large length to diameter galleries were the ones described by Hall (1890). Similar work has been done later in response to the many disastrous explosions in coalmines. Many of these experiments were performed in large scale, with tubes 100 – 250 m long, and turbulence induced by wall friction. The flame velocities measured in these experiments vary from 50 to 800 m/s. Detonation can also be achieved, if the tube is long enough or the wall roughness increased.

Bartknecht (1971) investigated flame propagation in tubes with one end open. He used an external dispersion system, which generated a dust cloud along the whole tube length. This was achieved by injecting dust from externally pressurised reservoirs. By using this technique, he was able to avoid the use of a primary explosion to initiate the dust explosion. This resulted in well-defined conditions for the experiment, and more reproducible results. However, one may discuss whether these conditions are comparable to the ones in more realistic situations. Bartknecht also conducted experiments by placing the dust as a layer inside the tube, and let the air velocity in front of the explosion generate the dust cloud. The deflagration was initiated with a turbulent methane/air explosion at the closed end of the tube. This resulted in lower flame speeds and maximum pressures, and shows the importance of performing experiments as close to the realistic condition as possible. His work showed a close agreement between the K_{St} value and violence of the explosion in the tubes. The K_{St} values were measured in a 1 m^3 closed explosion vessel. The 1 m^3 vessel used by Bartknecht was the prototype of the International Standards Organization method to determine K_{St} values (ISO, 1985).

A lot of work has been done in explosion vessels without expansion-induced turbulence during combustion. By varying the delay between dispersion and spark ignition, and vary the strength of the dispersion, one can correlate the measured rate of pressure rise (dP/dt) and turbulence. Kauffman *et al.* (1984) investigated the effect of turbulence on dust explosions in a 0.95 m^3 vessel. It was assumed isotropic turbulence, and a hot wire anemometer measured the level of turbulence in the absence of dust. The presence of dust complicates the turbulence measurements, but Kauffman *et al.* was unable to account for this. Tezok *et al.* (1985) extended the work of Kauffman *et al.* His results corresponded with what Kauffman found. Tezok also used an optical probe for measuring the flame thickness, which was found to be in the range of 0.15 to 0.7 m.

Pu *et al.* (1988) investigated the influence of obstacles on a propagating dust flame. Pu used two tubes, one 0.91 and one 1.86 m long. Both tubes were equipped with rings to induce turbulence. The small tube was equipped with two high-quality schlieren glasses for visualizing the process. The dispersion system consisted of a dust feeder on the top of the vertical tube. The dust fell down, forming an explosible dust cloud. Pictures from the schlieren system were used for analysing the flame. In the larger tube it was used one piezoelectric transducer, for pressure measurement, and eight ionization probes, to investigate the flame velocity. The dust was dispersed through two dispersion pipes located at one of the tube walls. Experiments were performed for both methane-air mixtures and clouds of maize starch in air. It was found that flame propagation in lean methane-air mixtures had similarities

with flame propagation in the dust clouds. This result may suggest that there are similar processes in the gaseous phase, which is not further discussed in her article.

Klein (2005a, 2005b) experimented with dust explosions in a closed vessel system at TNO. The apparatus consisted of two 1 m^3 vessels connected with pipes of various lengths, with or without obstacles and a 90° bend. The dust was ignited in one of the 1 m^3 vessels. It was also conducted tests with different types of dusts, such as coal, silicon and potato starch, and with various configurations of ignition position and venting. The introduction of either obstacles or a 90° bend in the connecting pipe resulted in enhanced pressure piling for all the dusts, because of delayed jet ignition in the secondary vessel.

Holbrow (2004, 2005a, 2005b) performed tests on a larger system, consisting of two cylindrically vented vessels (20 m^3 and 2 m^3) connected by a pipe with a sharp bend of 90°. The pipe was of diameter 0.5 or 0.25 m. The dust was dispersed from four 2.3 l pressurized reservoirs, one at the 2 m^3 vessel, and three at the 20 m^3 vessel. The ignition source was located in the larger vessel and consisted of electric fuse heads and 25 g of black powder (50 kJ). Six pressure transducers located in both vessels and pipe, and 8 thermocouples located in the centreline of the pipe measured the flame speed, as it propagated through the system. Holbrow found that the explosion more readily transmitted through the larger pipe (0.50 m) than the smaller one (0.25 m). The experiment produced results of poor repeatability. One of 25 tests produced significantly high pressure in the smaller secondary vessel (3 bar).

2.2.2 Impedance measurements

Impedance consists of two components: a reactance and resistance. The reactance is a function of the frequency and a capacitor and/or an inductor. An inductor is defined as ability to store energy as a magnetic field. Capacitance is shortly told the ability to store an electrical charge. A capacitor is often used in the electronics, and consists of two plates electrically isolated from each other. The ability to store an electrical charge is determined by the distance between the plates as well as the isolating material, also called dielectricum. This can be used to measure changes in a medium, for example an exploding mixture of fuel and air, in order to investigate the phenomenon more closely. Resistance is defined as the electrical potential needed to transport a given charge/time between two points. Both these parameters, resistance and dielectric constant, changes during combustion of gas, due to ion production in the reacting zone.

Huang *et al*. (1988) describes various methods for measuring/determine unknown capacitances for use in industrial applications. They points out the problem of stray capacitance in the measurement circuit, which must be minimized to achieve good and precise measurements. Huang *et al.* describes four different principles for measuring an unknown capacitance:

- One can determine an unknown capacitance by introducing an inductor of known size in parallel with the capacitance. The resulting resonance response will be a function of resistance and capacitance. This requires a sine generator with tuneable frequency. The disadvantage of this method, according to Huang *et al.*, is that the circuit must be tuned manually. However this is the method used in this thesis. One can, if the capacitor of question only varies within relative small boundaries, omit the manually tuning by use of a frequency sweep generator. The achieved resonance response curve of the circuit will give both the resistance and the dielectric constant of the medium to measure. Huang *et al*. also states that this is an accurate way of small capacitor.

- The second circuit Huang *et al.* discusses is an oscillation circuit. The principle is to make an oscillator with a LC circuit as the frequency reference. This method is not very sensitive to the loss component in the capacitor, since the resonant frequency is little affected by loss. In this circuit the stray capacitance will influence the measurement.
- Huang *et al.* thirdly describes a charge - discharge circuit. This principle builds on measuring the current which is required to charge the capacitor to a certain voltage. This includes some switches, and some integrator coupled amplifiers, which integrates the current. This method has the advantage of low drifting, good measurement accuracy even at high measuring frequency and that the resistance parallel to the capacitor can also be measured.
- Last Huang *et al.* describes various methods for AC – bridging. This is in general methods which is comparing the unknown impedance to an impedance of known value. Some of these methods can be very accurate. However, in pneumatic transport applications, static electricity can result in nonlinear effects that disturbing the measurements.

Waterfall *et al.* (1997) describes dielectric measurements in a piston engine. To measure the capacitors Waterfall *et al.* (1997) used a charge-discharge circuit. The aim was to prevent knocking, by studying where the gas ignited. They used 6 capacitors, placed on the cylinder, from which they makes a tomographic picture of the process. The spark is a major noise generator. The electronics and the materials used in the sensor will also be affected by temperature drift, and the materials used as insulators often are piezoelectric, creating dc-offset if exposed to pressure. These problems must be overcome to make a successful monitoring system in this type of systems they conclude.

Eckhoff (2003b) used a charge-discharge circuit in order to investigate the burning velocity in dusts.

2.2.3 Ionization gap measurement

Ionization gaps have often been used to investigate flame propagation in tubes, silos and other configurations. I. G. William *et al.* (1958) first described the Flame Ionization Detector (FID). The method is very simple, and is highly linear. The electrodes is almost unaffected by temperature variation and other sources of noise. One electrode was coupled in series with a battery and a resistor. The voltage across the resistor will depend on the current flowing through the flame gap, from the electrode to the ground potential, and hence the conductivity of the medium.

Ionization gap was also used in the experiments of Pu *et al.* (1988). The Ionization gaps were placed along the centreline of the experimental tube, and a oscilloscope recorded the voltage across the resistor in series.

3 Measurements

This thesis focused on impedance flame measurements. The idea is that the plasma in a flame alters both the dielectric constant and the resistance of the medium between two plates. Work has been done on this before but, mainly for gas. GexCon, CMR, has also developed a capacitive measurement probe for dust flames (Eckhoff, 2003b). Previous work on the issue is mainly based on an integrator circuit to measure the current charging the opposing plates (charge-discharge circuits). However it is also possible to measure the resonant frequency between a coil and the capacitor/impedance which are to be measured.

3.1.1 Impedance measurements

The basic idea of impedance measurements is to place two metal plates in such a way that they form a capacitor, where an electrical potential between the plates creates electrical field lines that pass through the medium to measure. Since both the resistivity and dielectricity changes the most correct name of the measurement is not capacitive measurement, but impedance measurement.

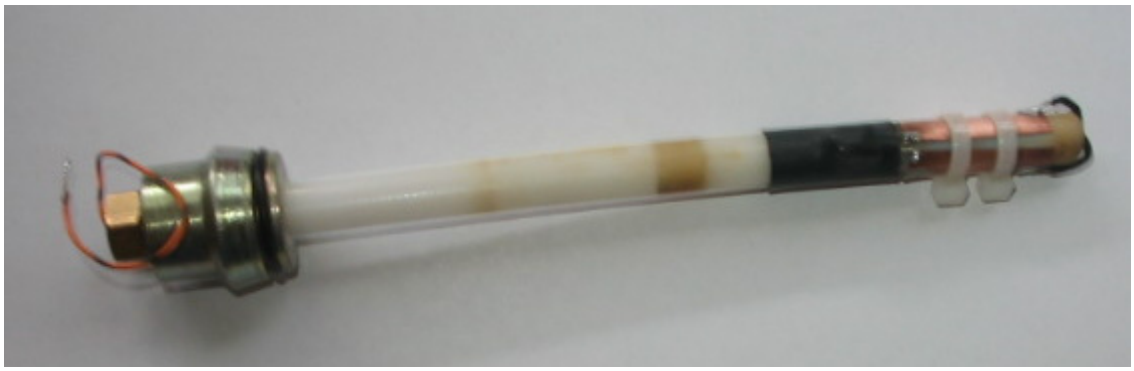

Figure 3-1 *The probe used in 20 litre vessel. The copper plates are attached with strips*

The first attempt to measure the impedance involved the use of an AC-bridge. However this method was not suitable for measuring dust explosions, because it was observed in experiments that the dust dispersion process interfered with the actual measurement by introducing a DC-voltage across the capacitor to be measured. The plates were attempted discharged by a relay, but no significant change in the noise was observed. The plates were attached to a plastic rod using plastic strips (Figure 3-1). The strips may be the reason why the plates were not properly discharged.

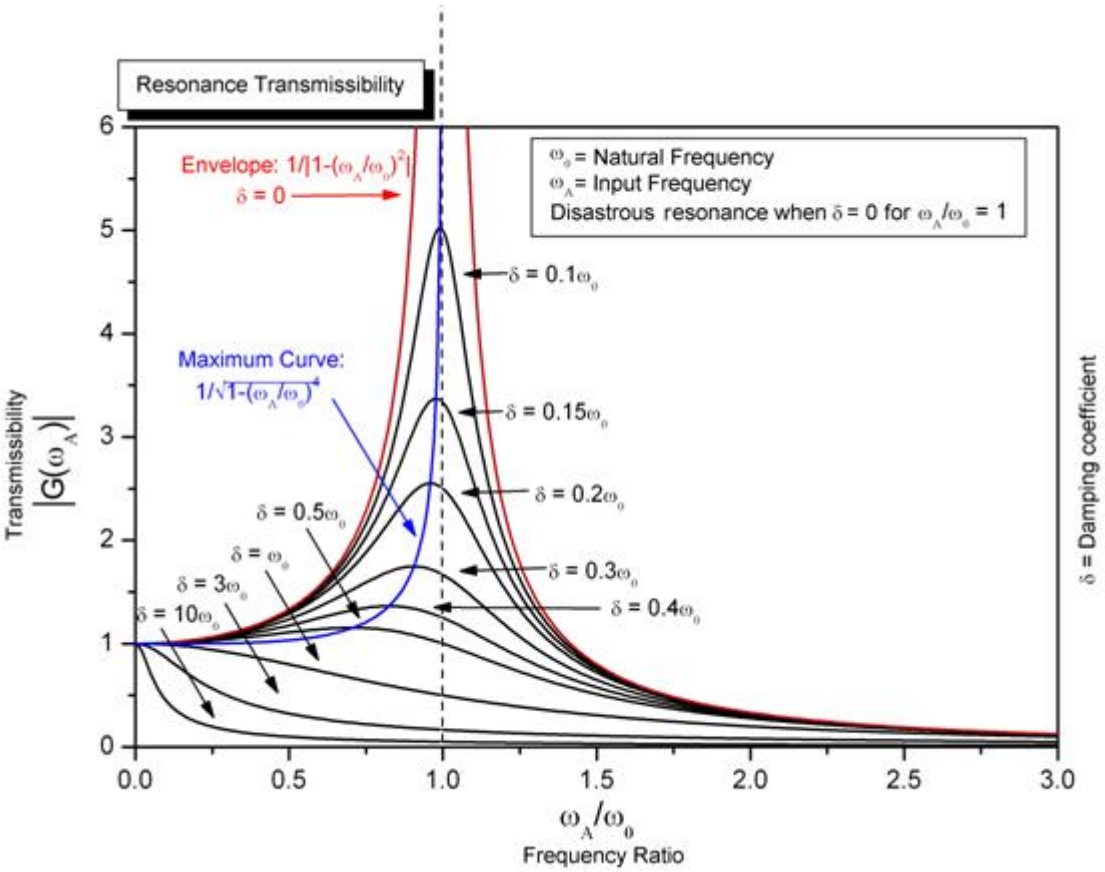

Figure 3-2 *Resonant curve for a damped system (Wikipedia, 2009)*

The second attempt was to measure the resonance frequency between the unknown capacitor and a known inductor. This was achieved by using a sweep frequency generator, which varies the frequency within a predefined range. The sweep is performed once every milli-second. The frequency and amplitude of the response from the circuit is measured and recorded. The frequency response curve, similar to the one shown in Figure 3-2 is then obtained. The actual circuit used is shown in Figure 3-3 Note that the components in the blue field are an equivalent scheme of stray capacitance and resistance. This scheme is not exact. Stray capacitance is defined as the electric field lines not passing through the region to measure. The capacitance between the wires (Cw) connecting the coil to the capacitor are therefore stray capacitance. Also some of the probe capacitance is stray capacitance (Cx). The capacitor Cc represents internal capacitance in the coil. There is also resistance in the wires and the coil, Rc, and through wires, Rw. In order to analyze results produced by the equipment it is very important to measure the different stray capacitances and resistances. These parasitic capacitances and resistances can be found by measuring the resonant frequency for different capacitors in parallel with the plates to be measured.

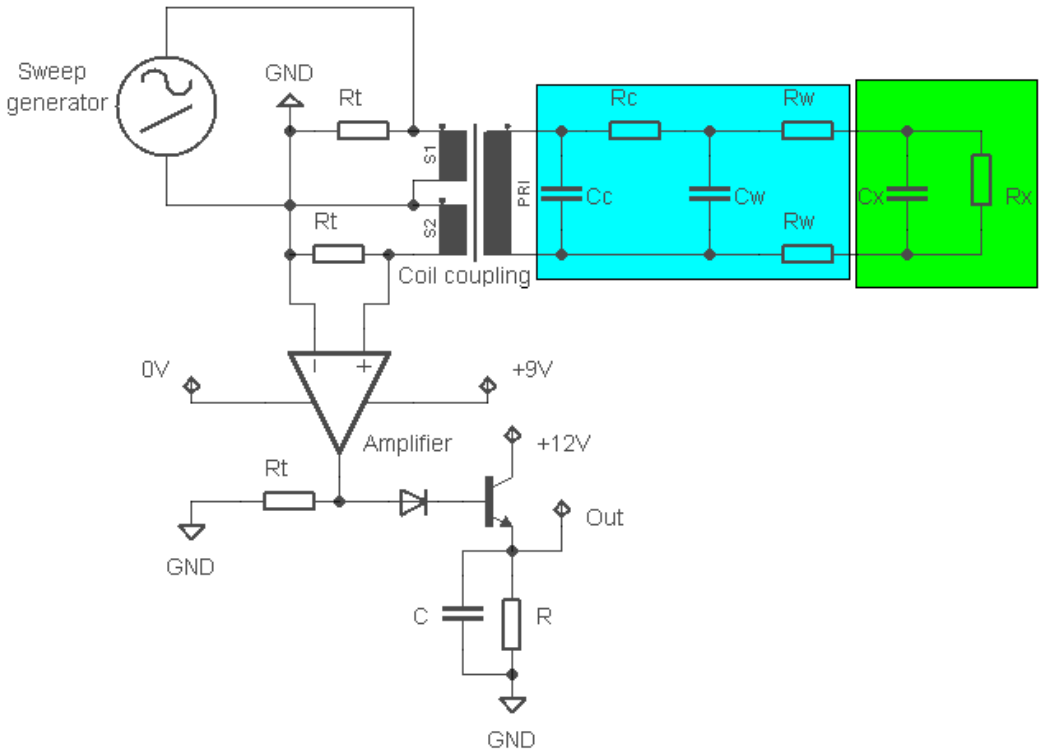

Figure 3-3 *Schematic of the measurement circuit.*

For industrial applications it is of primary interest to achieve positive flame detection, and this can be accomplished without the sweep generator. If the circuit is tuned to resonate at a known frequency, and subjected to an oscillator that produces this frequency, the amplitude of the response determine weather there is a flame or not in the electrical field of the capacitor plates. The probe developed in this thesis is primarily for use in fundamental experimental work, and it would be of interest to obtain both the capacitance and the resistance in the flame. However, the attempts to calculate capacitance and resistance were unsuccessful, due to various distorting effects. The measurements obtained from the curves are therefore a resonant frequency, mostly dependent upon the capacitance, and damping, mostly dependent upon resistance.

In general, to measure a frequency, one will have to use frequency counters, to get an accurate measurement. This can be done in two ways: one can measure the time of one period, or count the number of edges within a known time. If the frequency is low, compared to the clock frequency of the counter device, it is preferable to measure the period. If the frequency is high, one usually measures the number of edges within a known time. The accuracy of this method depends on how many edges one counts before the frequency is determined.

The frequency range is in the order of 40-50 MHz, depending on the actual probe, and the coil. The sweep frequency is set to be 1 kHz. This makes rather difficult to measure the frequency by counters. As many measured points on the resonance curve as possible are wanted at the same time as accurate frequency measurements are required (Figure 3-4 show a measured resonance curve with and without a flame present). As pointed out previously these requirements are conflicting, and a compromise is necessary. The frequency counters used in this thesis had a clock frequency of 20 MHz, but this was not sufficient to yield good measurements. A counter device with higher clock frequency, maybe in the order of GHz, would give much more accurate results. The counters also had difficulties acquiring data at

the same rate as the analogue/digital-converter, used to determine the amplitude, and made it troublesome to analyse the results.

The sweep generator used in these experiments has two outputs: the sweep frequency, and the other is a voltage corresponding to the frequency (frequency-voltage). This frequency-voltage is used as the x-axis, when an oscilloscope displays the measurements. (The measurements were recorded by a a NI-CAD 6259 card connected to a pc). Because the counters could not measure frequency accurately, the voltage-frequency was used as a reference for the frequency in a similar way as if an oscilloscope were used. The generator is suspected to drift somewhat in terms of frequency versus voltage. Satisfying methods to determine the precision of this frequency-voltage directly has not been found, since this would include a counter device. If one assumes the amplitude of the resonant curve to be unaffected by the sweep frequency, and to have an exact amplitude corresponding to a specific frequency, one can estimate the accuracy of the frequency-voltage from the generator. The Matlab software ('Voltagefrequency') developed to analyse the results uses a linear correlation with the frequency (appendix B). This is a simplification of the actual situation. Maybe a higher degree polynom would be more preferable.

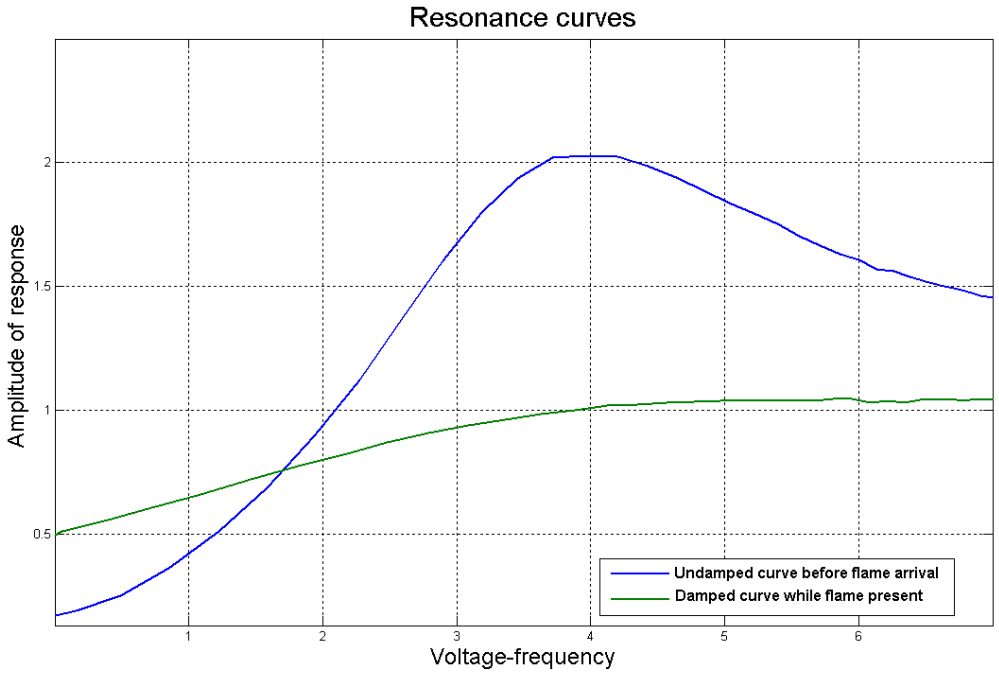

Figure 3-4 *The effect of the flame has on the resonance response curve*

The amplifiers and diodes will distort the signal. This noise is more dominant if the signal is weak, since rectifying requires some voltage. In the actual experiments, some of the probes are further away from the electronics, causing more attenuating of the signal and more distortion from the diodes. The amplifiers require some power from the signal they are amplifying, which will influence on the resonant circuit as additional damping. The amplifier will also tend to amplify certain frequencies more than others.

The coupling between the generator and the probe is a loose transformer coupling (shown as S1 and PRI in Figure 3-3). This is done to allow the circuit to oscillate freely. The probe is connected to the amplifier in a similar way (S2 and PRI), for the same reasons. The first and third (S1 and S2) coils has five windings, the second (PRI) has 21 windings. To reduce internal capacitance, the coil is wound on helical coil, allowing some space between the wires.

Some mathematics is required to analyse the results. Some rather complex equations are required to describe circuit shown in Figure 3-3. The block diagram in Figure 3-5 represents the differential equation for the circuit shown in Figure 3-3. The lines symbolises numbers going from one mathematical operation to the next, the circles add the numbers, the rectangles multiply the number by the factor inside, and the triangles integrate the numbers. It is straight forward to simulate the circuit with software as Matlab (the simulink application) or LabView. It is also very easy to transform the model into the frequency domain by using Laplace transformation. This is simply done by replacing the integrator box with rectangles holding the factor 1/S, where S is the complex angular velocity of the frequency of Vin. When the Laplace transform is applied, the equation is not time dependent, which means that the sweep frequency is not taken into account. Since the sweep frequency (1kHz) is much smaller than the resonance frequency (40MHz), this error is considered small.

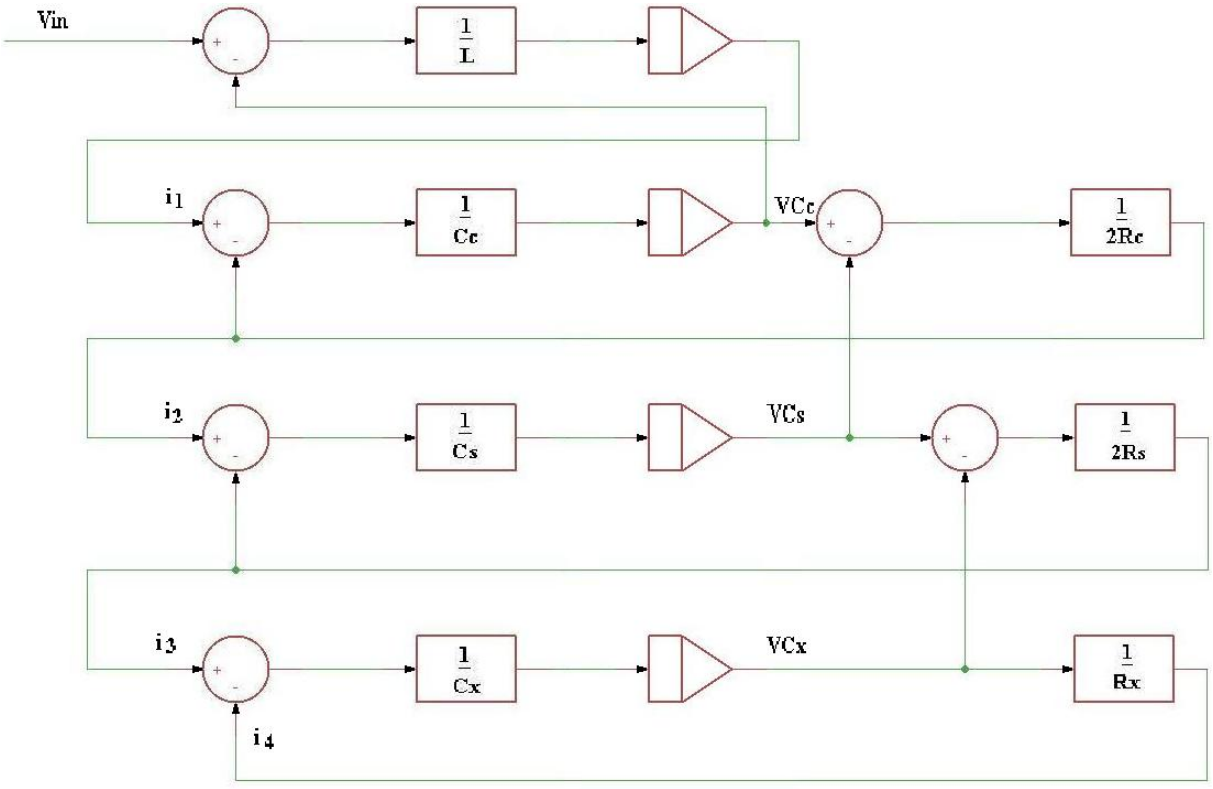

Figure 3-5 *The circuit in the time – domain*

From Figure 3-5 one can retrieve the equation which controls the resonant circuit. From the schematic the system of equations is:

$$VCc = \frac{i_1 - i_2}{Cc \cdot S} \qquad 3.1$$

$$VCs = \frac{i_2 - i_3}{Cs \cdot S} \qquad 3.2$$

$$VCx = \frac{i_3 - i_4}{Cx \cdot S} \qquad 3.3$$

$$i_1 = \frac{Vin \ - VCc}{L \cdot S} \tag{3.4}$$

$$i_2 = \frac{VCc - VCs}{Rc} \tag{3.5}$$

$$i_3 = \frac{VCs - VCx}{2Rs} \tag{3.6}$$

$$i_4 = \frac{VCx}{Rx} \tag{3.7}$$

Matlab is used to solve this equation system symbolically. The equation produces results quite close to what is measured in reality, where the components are known. This equation can be used to analyse the results from the experiments. However, the results from the measurements were not good enough to perform this analysis. A Matlab program ('titled', appendix B) calculates the resonant curve with different Cx and Rx.

3.1.2 Electrical field lines, and probe design

Consider a flame between two plates with different electrical potentials, represented as 1 and 4 in Figure 3-6. There is no direct resistive path between the plates, but small islands of plasma which has a higher conductivity than the surrounding gas. Ca_1 is the capacitance between plate 1 and the plasma. C_b and R_b are the capacitance and resistance in the flame plasma respectively, and Ca_4 is the capacitance between plate 4 and the plasma. C_s represents the stray capacitance, as well as the field lines going elsewhere. Ca_1 and Ca_4 depend upon the distance between the plasma and the flame. C_b and R_b depend on the properties of the flame. It is uncertain if it is an acceptable simplification to assume a constant value for the properties of the flame, such as conductivity and dielectric constant. The assumption could make it possible to measure fluctuations of the flame area in the measured zone. The main value influencing these properties is the density of ions in the flame, which is a function of the chemical reaction and the temperature. There might be inhomogenities introduced by the combined flow and combustion processes in the ion density of the flame.

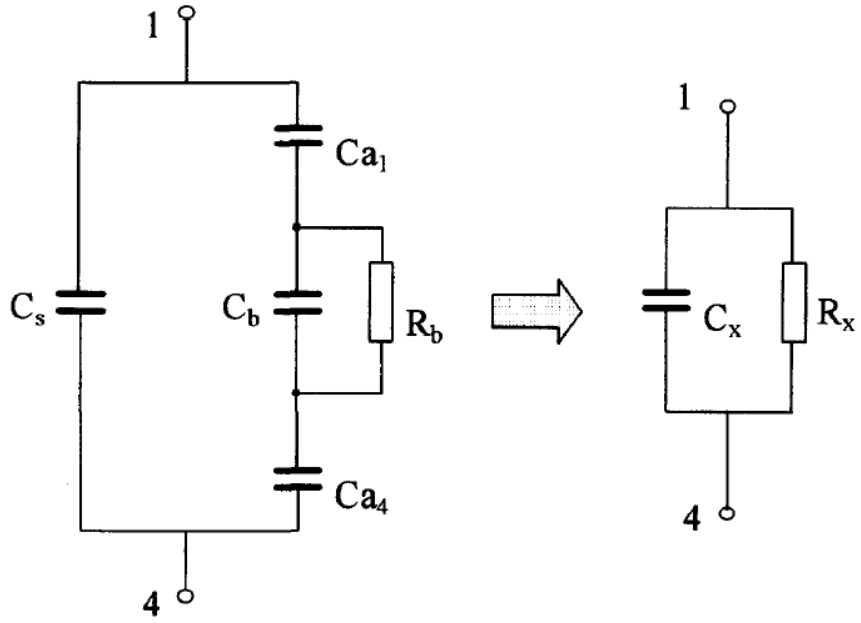

Figure 3-6 *Equivalent scheme of a flame in between two plates (From Waterfall 1997 et al.)*

The sensor will not be equally sensitive to the position of the flame, since the plates are placed along a circle (Figure 3-7). The probe is a little bit more sensitive if the flame is close to one of the plates, as the field strength is highest there. A test with a bottle of water proves this effect. The resonant frequency without the bottle was 41 MHz, with the bottle placed in the centre of the circular probe gave 40.6 MHz and the bottle placed close to one of ether plates 39.5 MHz. Also the probe used in the FAT experiment has aluminium extension rings that will influence the electric field (this is done to make the probe more aerodynamic). Figure 3-7 illustrates the electrical field lines. The denser the field lines are in an area, the more sensitive the probe is to a change in the area. The figure is only schematic and the field lines are most dense close to the capacitive plates. Some of the lines will pass to ground potential, without going through the area to measure (stray capacitance). It is possible to omit this stray capacitance by active guarding *i.e.* holding the shield at the same potential as the plates. This would make the measurements more precise, but it requires some more electronics, and perhaps a little more complex probe design.

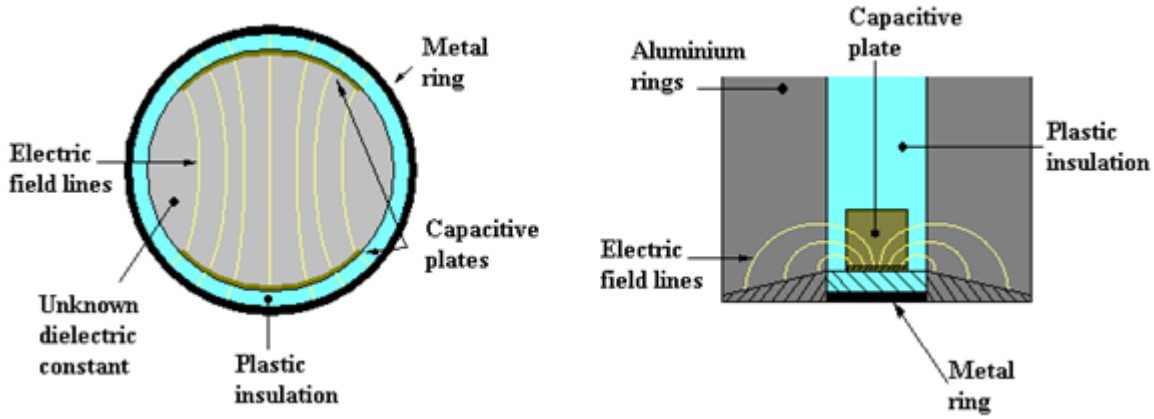

Figure 3-7 *Illustration of electric field lines in the flame probe: top view (left) and side view (right)*

The probe design (Figure 3-7) could make it possible to measure the change in cross sectional area of the flame. It would be necessary to add two more plates, in order to calculate the cross

sectional area of the flame. Also more studying of the changes of the propeties due to a flame present and high temperature must be done. A time resolution of 1 ms is also a very course time step, since the flame can travel with up to 40 – 60 m/s.

Measured sizes, probe used in 20 litre vessel

The probe must be analysed In order to calculate the capacitance and resistance. By using different capacitors in parallel with the coil, the inductance of the coil was found. Table 3-1 shows the results of these measurements under "measurement of coil" header. The capacitors Cw and Cx were found by introducing them one at the time to the circuit. The resulting resonant frequency gives the desired measures of the capacitances. Table 3-1 shows the results.

Table 3-1 *Measured coil for use in experiments*

Measurement of coil			
Parallel capacitor [F]	**Farad [F]**	**Frequency [Hz]**	**Inductance [H]**
C1	7.00E-12	8.44E+07	5.07E-07
C2	1.50E-11	5.85E+07	4.92E-07
Measured inductor [H]			5.00E-07

Table 3-2 *Measured capacitances of 20 litre probe*

Measurement of probe		
Capacitor connected	**Frequency [Hz]**	**Farad [F]**
Cw	6.35E+07	1.26E-11
Cw + Cx	5.67E+07	1.58E-11
Cw + Cx + 10 pF	4.23E+07	2.84E-11

As seen from Table 3-2 $Cx = (Cw + Cx) – Cw = 3.2$ pF and $Cx = (Cw + Cx+10) – Cw = 5.8$ pF. These results vary around 4.5 pF +/- 1.3 pF, which is quite a large range. The reason for this error might be that the more current that passes through the wires, the larger capacitance in the end of the wires, thus damping will increase. Therefore the most correct answer will be $Cx = 3.2$ pF, since this result includes least damping.

The probe used in the FAT experiment:

The metal plates in the probes used in the FAT experiment were connected to the measurement circuit with a 0.3 m coaxial cable (96 pF/m). This results in two capacitors in series: $Cw = 96*0.6/2 = 28.8$ pF. By introducing the capacitance plates into the circuit a resonance frequency of 41 MHz corresponds to a capacitance of 3 pF. However, this capacitance is mainly through the plastic on the inside of the plates and is in fact stray capacitance (Figure 3-7). The coil is the same used in the 20 litre vessel experiment. The results of these measurements, and of response of the

3.1.3 Accuracy and precision of measurements

Analysing the results from the FAT experiments showed clearly that furthermore improvement of the equipment is needed to make good capacitive and resistance measurements. The various amplifiers, cables and probes differed slightly, making it necessary to tune the sweep generator to a wide frequency range. The amplitude of the signal was also different, probably because of variations in cable lengths. This resulted in significant noise for some of the probes, while others gave better measurements. Since the measurements were distorted, the capacitance and resistance could not be separated out. The damping were most prominent feature of the measurements, and therefore the area under the resonance curve is the most pronounced parameter. Also, the maximal point of the curve and the resonance frequency voltage can be used, but as seen on Figure 3-4 the damped curve is very flat. A false resonance peak at somewhat higher frequency than the sweep frequency also distorts the signal, and in some cases the resonance to be measured is shadowed by this. Therefore the measured response does not form a top in some cases.

The accuracy of the flame detection measurements relates to the response-time of the probe and the time resolution. Table 3-3 shows the standard deviation of different values calculated from the measurements. The table illustrates which parameters that is suitable as flame arrival indicators, due to less natural drifting. As seen from the table, the calculated area is the least noisy parameter. This is reasonable, since the indicator uses all of the measured values. The area under the curve is divided by the mean area under the 100 first measured curves, to get a relative measure of the area change. When the flame arrives the area parameter drops quite pronounced, as is easily seen in Figure 3-8. The green line is defined as $1-4\cdot\sigma$. σ is the standard deviation. The calculated parameters are normalized, so the value is 1 before experiment starts.

Table 3-3 *Showing standard deviation of different parameters calculated. All the numbers are relative so the values are dimensionless.*

Standard deviation of different measured values					
Probe	**1**	**2**	**3**	**4**	**5**
Maximum point	7,06E-04	1,46E-03	2,23E-02	7,83E-03	8,76E-01
Resonant frequency	1,73E-03	4,16E-03	2,55E-02	2,25E-02	7,10E-02
Area under resonance curve	1,46E-03	3,25E-03	1,19E-02	4,21E-03	7,05E-03

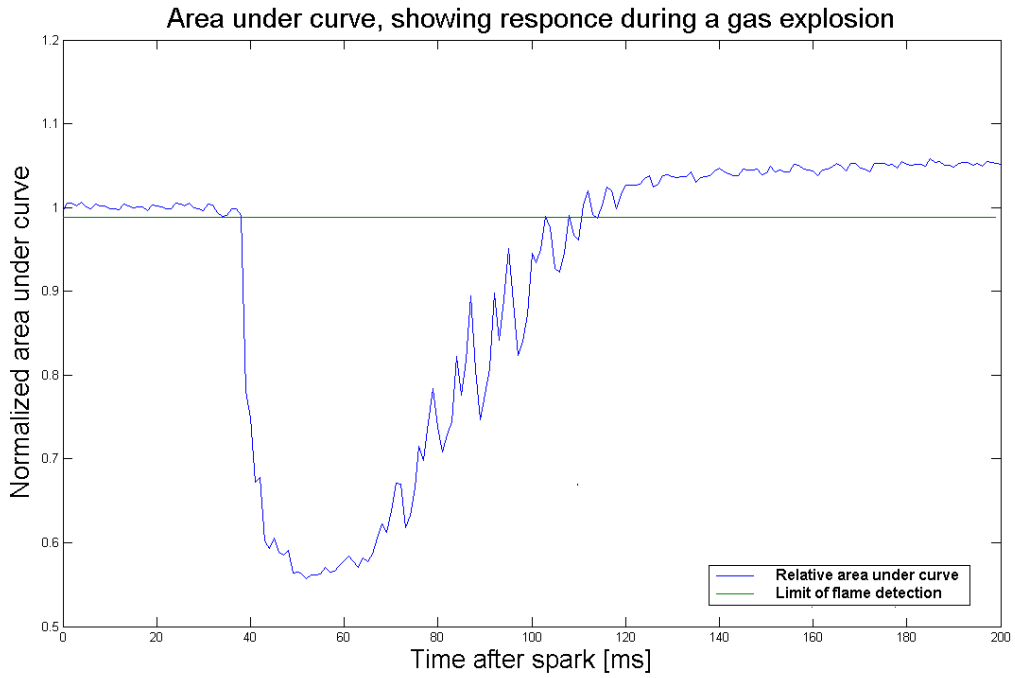

Figure 3-8 *The area under resonance curve*

The variations in the damping during the experiments are due to generator sending signal at different strength at different frequencies, drifting in the amplifiers due to temperature changes, high frequency going through rectifying diodes as noise and accuracy of sampling. A capacitor is used to smooth the signal from the rectifying diode. This will result in some time delay between flame arrival and voltage change. The capacitor used in the experimental setup is 33 pF, connected in parallel with a resistor of 10 kΩ, giving the circuit a time constant of 330 ns. The accuracy of flame arrival detection will therefore be limited by the time resolution of 1 ms.

Since the measurement only holds approximately 50 points per resonant curve, some numerically inaccuracies may occur. Linear interpolation has been used to find values between points. To find the maximum point of curve a third degree polynomial is fitted to the curve, using least square method (the 'polyfit' function in Matlab). Derivation of this function gives the top point. Resistance and capacitance could in principle be calculated from the two parameters: resonant frequency, and the second derivative of the maximal point of resonant curve.

4 Experiments

This chapter describes the experimental equipment and experimental procedure. Apart from chapter 4.1.2, and chapter 3.3.6 in Kalvatn(2009), this chapter is similar to chapter 3 in Kalvatn (2009).

4.1 Preliminary tests in the 20-litre vessel at the UiB

The different measurement systems have been tested in the 20-litre USBM vessel at the Dust Explosion Laboratory, UiB (Skjold, 2003). Figure 4-1 shows a simplified schematic of the test facility, and Figure 4-2 shows a picture of the 20-litre vessel. A more detailed description of the test facility is given by Skjold(2003). The powder used in these tests is maize starch, usually at a nominal concentration of 500 g/m^3, which correspond to 10 g in the 20-litre vessel. The main purpose was to verify the functionality of the different measurement probes and the associated electronics.

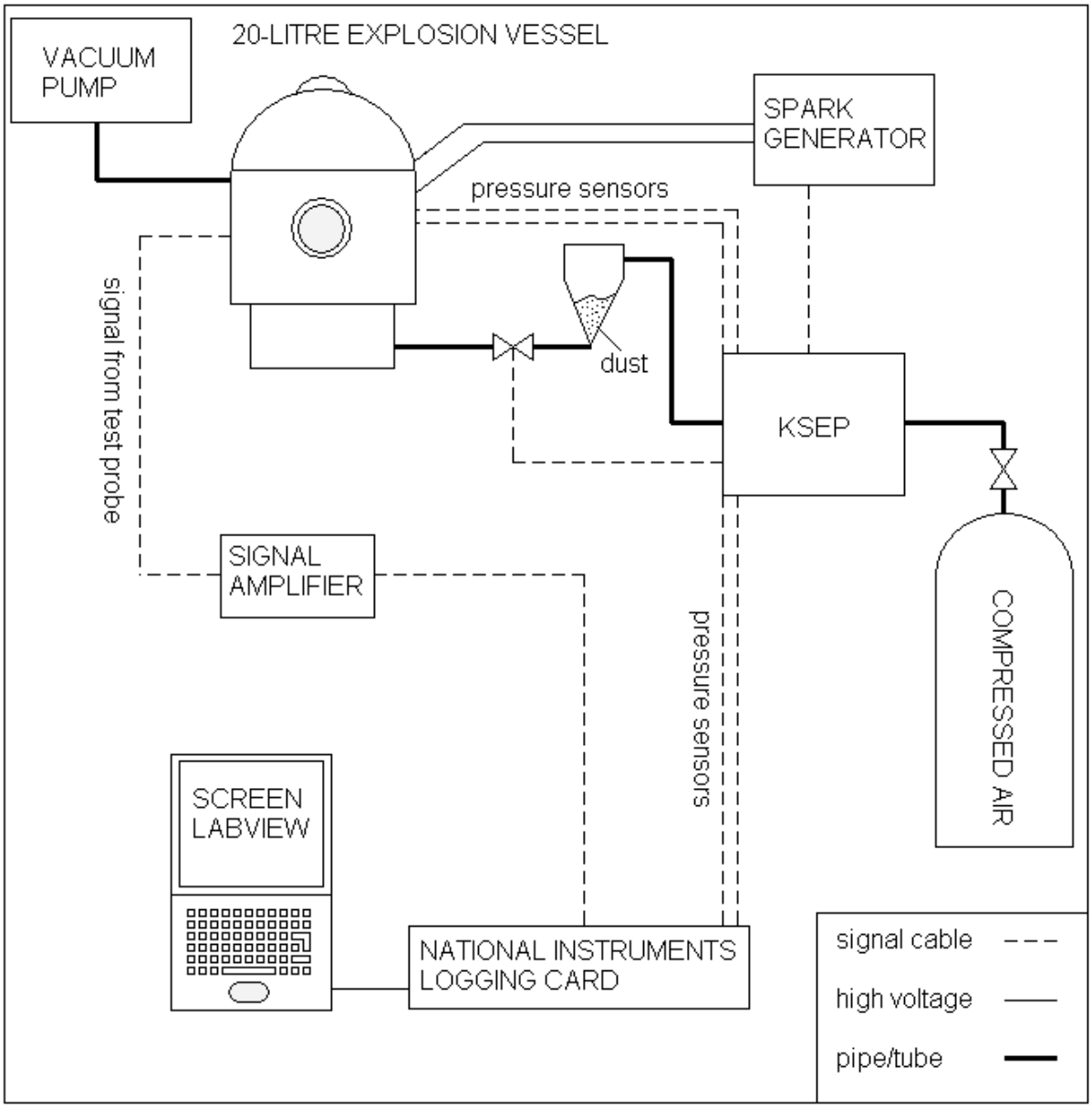

Figure 4-1 *Simplified schematic for the 20-litre test facility at UiB*

4.1.1 Experimental procedure

The spark gap is checked before the lid is closed. The vacuum pump lowers the pressure inside the vessel to 0.4 bar(a). A digital pressure indicator monitors the pressure inside the vessel. A desired amount of dust is then placed in the dust reservoir before a lid seals the reservoir. The reservoir is pressurised to 20 bar(g) with air from a 50 litre compressed air bottle. A digital pressure indicator monitors the pressure inside the reservoir. The spark generator is turned on and a flashing blue light indicates that the spark ignition is ready to be triggered. The Measurement and Control Unit, KSEP, runs the dust dispersion, triggering of the ignition source, and pressure measurements. A computer in the dust laboratory runs the KSEP software, that initiates and controls the sequence of events. The dust is dispersed through a dispersion nozzle and is ignited by an electrical arc discharge, or alternatively a chemical igniter. Two piezoelectric pressure sensors from Kistler measure the pressure development inside the vessel. Two separate charge amplifiers in the KSEP amplify the signal from the pressure sensors, and the resulting signals is registered by the logging card from National Instruments (NI USB-6259), transferred to a laptop, and processed by LabView. The signal from the test probe is processed in the same way i.e. with a signal amplifier, the NI-card, and a laptop. After the test, the spark generator is manually turned off and the remaining dust inside the vessel is removed with a brush and vacuum cleaner.

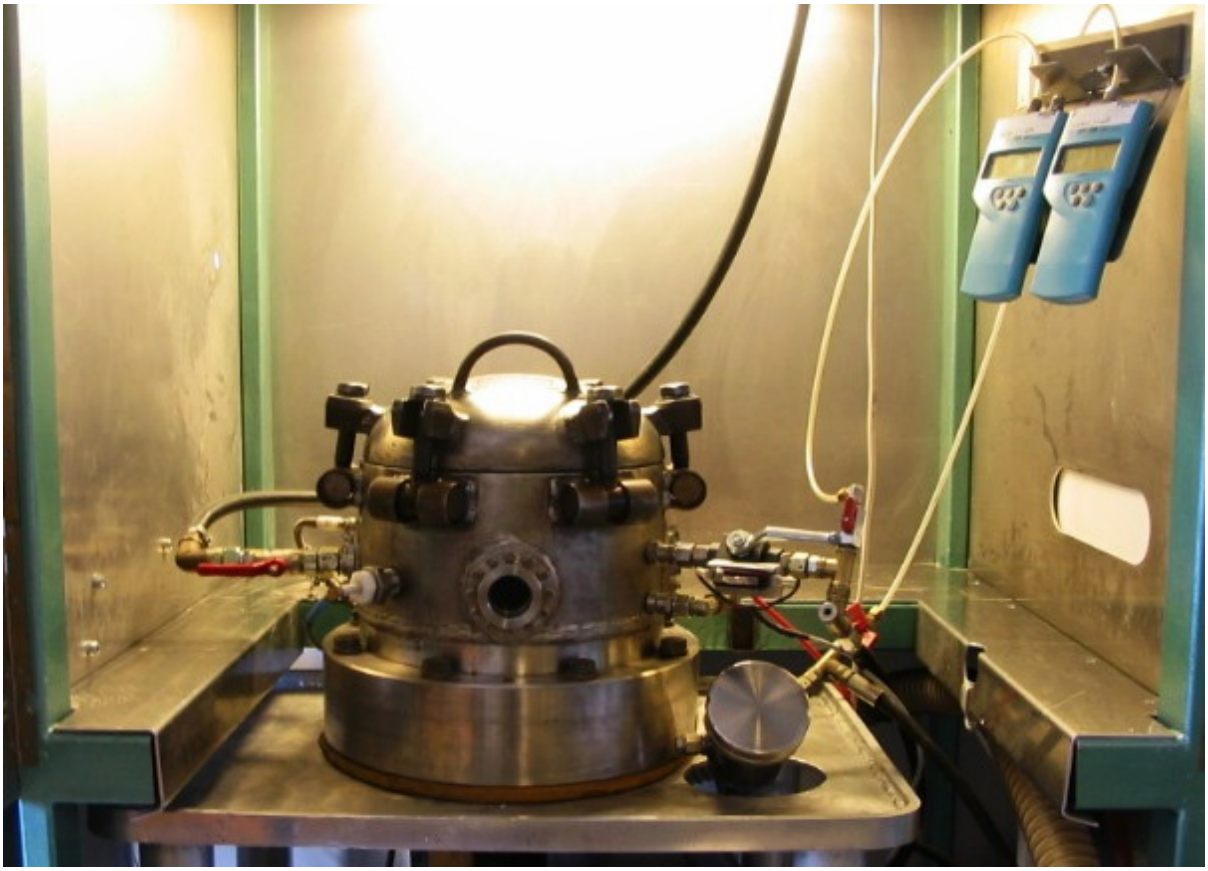

Figure 4-2 *20-litre explosion vessel situated at the dust-explosion laboratory at the UiB. The two blue displays in the upper right corner are the digital pressure indicators for controlling the pressure in the vessel and dust reservoir.*

4.1.2 Probe used in the 20 litre vessel

Preliminary tests in a 20 litre vessel proved the functionality of the measurement equipment, and the measurements in the FAT and the 20 litre vessel involved much of the same

equipment. However, the actual flame probe differs. Figure 3-1 shows the probe used in the 20 litre vessel, and section 3.1.2 discusses the probe used in the FAT. The different designs of the probes result in different properties. The probe used in the 20 litre vessel provides more local and focused measurements than the circular probe in the FAT, since the electrical field lines are more concentrated in the area closer to the probe. The reason for designing different probes for the two experiments was to be able to compare different measurement techniques in the FAT experiments.

The 20 litre vessel, and this reduced the load for the frequency generator. Therefore it was not necessary to buffer the signal through an amplifier, which was the case for the FAT experiments. Figure 4-3 shows the schematic of the experimental setup. The distance between the probe and spark gap is 4 cm.

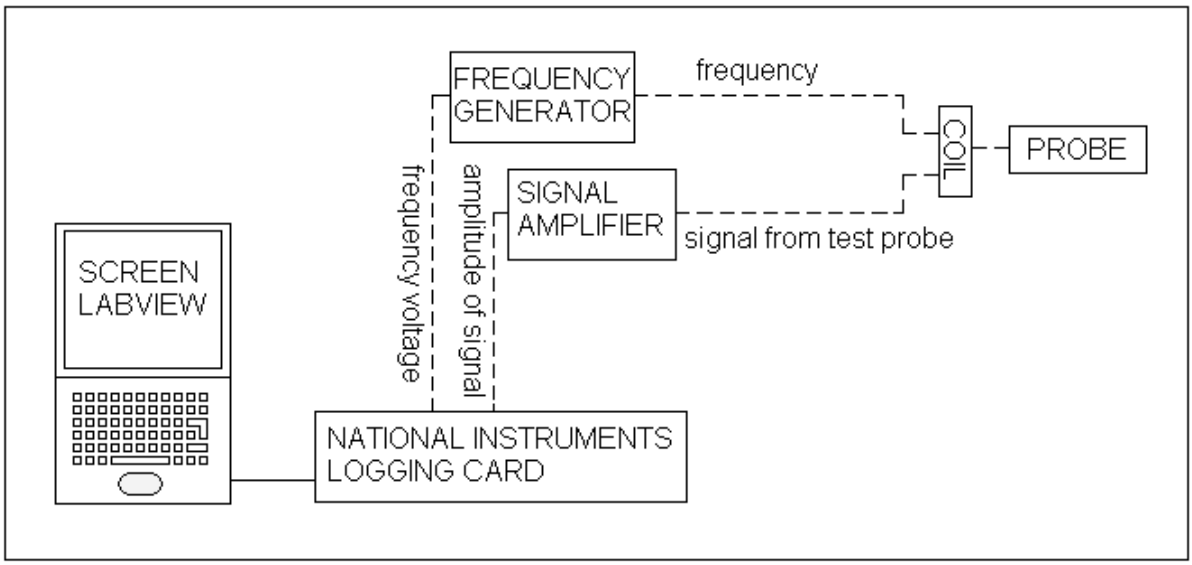

Figure 4-3 *Experimental measurement configuration for tests in the 20-litre vessel*

Some experiments were performed with the ionization probe shown in Figure 4-4. The probe consists of a metal housing with an electrode in the middle. 10 V source were connected to ground and the electrode. Flame arrival will change the resistance through the medium near the tip of the probe, altering the current through the probe. The current is determined by measuring the voltage over a resistor in series with the electrode. However, these tests were not successful, because of to weak amplifying, hence mainly noise were measured. It was not prioritized to go further with this since the capacitive is able to obtain the same information over an entire cross sectional area. The ionization probe was not used in the FAT experiment.

Figure 4-4 *The ionisation probe used in some preliminary experiments in the 20-litre vessel.*

4.1.3 Preliminary dispersion experiments

The dispersion system is a crucial part of the experimental setup, and has been tested separately to document its ability to create well-dispersed dust clouds. The tests were performed in a section replica which was mounted with a plexiglas in front (Figure 4-6). A high speed camera was used to investigate the effectiveness of the nozzle to evenly distribute the dust and the shape of the dust cloud, with and without confinement. The time delay between the dispersion signal, to the first dust seen coming out of the nozzle gives a time delay of the pneumatic operated valve. The pressure in the reservoir is not recorded in this investigation. It was later recorded in FAT experiments, and it is of interest to compare the pressure-time curves with and without dust in the cyclone. The experimental setup is shown in Figure 4-5, and the view from the camera in Figure 4-6 For timing purposes, a LED-light box was used (referred to as signal lamp on the schematics), indicating when the dispersion signal is sent. This signal is sent from a NI-CAD card. To measure the pressure in the reservoir, before the test is performed, a manometer is used. The camera can record at a rate of 1200 fps, but this will compromise the quality of the frames. The rate used in this experiment is therefore 300 fps, giving it a time resolution of 0.0033 seconds per frame. Analysis of the videos is manually done, and is therefore subjective.

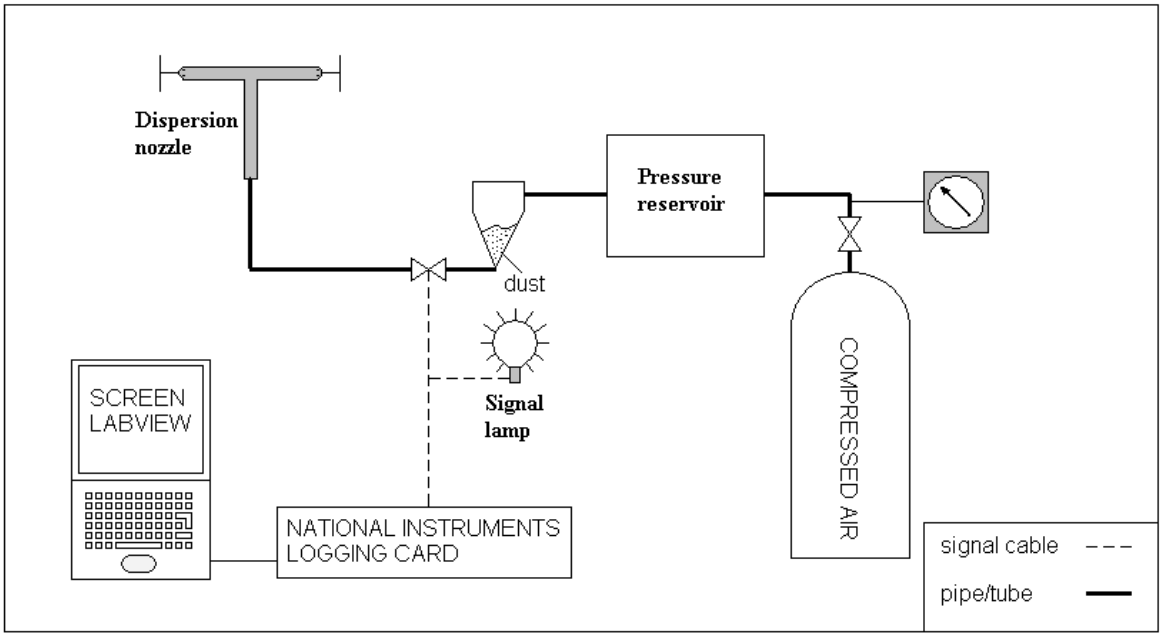

Figure 4-5 *Experimental setup schematics.*

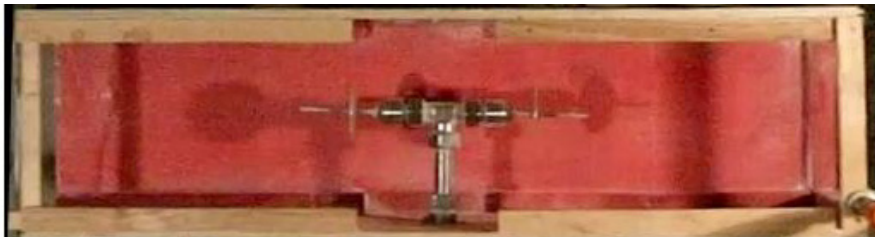

Figure 4-6 *Dispersion nozzle in its test rig*

4.2 Experiments in the Flame Acceleration Tube (FAT)

The Experiments conducted with the complete FAT setup are closed vessel experiments. Both gas (propane) and dust (maize starch) are tested, and the results are compared. Experiments of

gas mixtures were performed for 3% (often referred to as lean mixture), 4.5% (often referred to as stoichimetric mixture) and 6% (often referred to as rich mixture). The dust used in the experiments was maize starch, of nominal concentration 500 g/m^3 or 250 g/m^3. The concentrations of different tests are given in appendix A.

4.2.1 The FAT

Figure 4-7 shows the FAT. The tube consists of three 1.2 m sections with internal cross section 0.27 x 0.27 m. one section is fixed and two of them are running on rails. This allows easy access to the interior of the pipe, for cleaning and modifications. It is possible to place different types and numbers of obstructions inside the tube, to generate different levels of turbulence. One sidewall and the top of the tube are fitted with circular plexiglasses, in order to make the explosion visible from the outside. A high speed camera films the experiment.

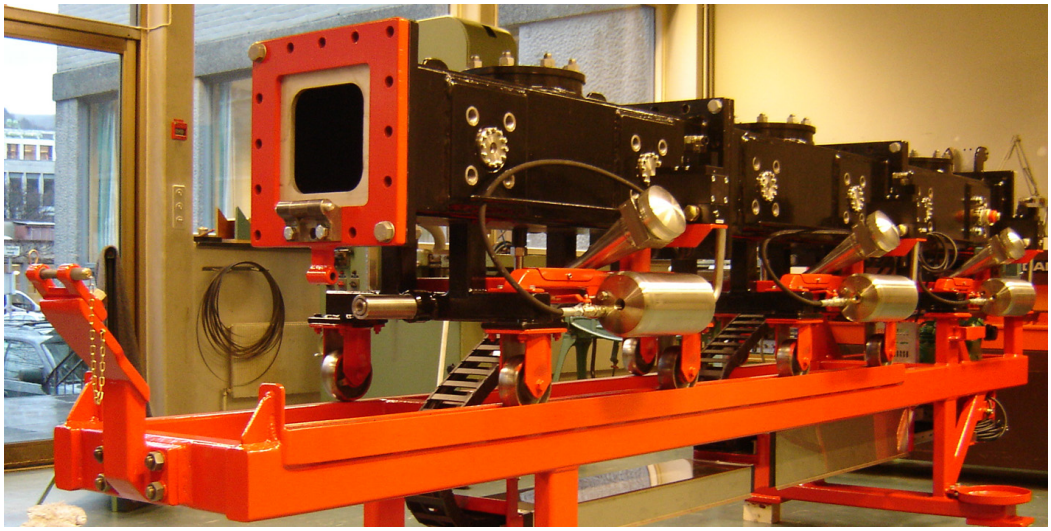

Figure 4-7 *Flame Acceleration Tube*

4.2.2 Systems for dust dispersion and gas filling

When testing with gas a separate gas filling system is applied to the FAT. It consists of a flask with gas *e.g.* propane, six tube entries alongside the FAT with belonging valves, and valves to shut off gas from the flask and to bleed the tube system to get rid of air and gas in prior to filling. The vacuum pump evacuates down the pressure inside the vessel prior to gas filling. The concentration of gas is estimated based on pressure rise inside the FAT when filling gas. If a concentration of 4-volpercentage of gas in air is desired at atmospheric pressure, a pressure rise of 0.04 atm is needed. In order to optimize the concentration distribution in the FAT, the gas is in equal amounts let in at the six entries in turn. Pressurised air from the dust dispersion system mixes the gas prior to ignition. Figure 4-9 show the system schematically.

If dust is to be tested, the dust is filled into the dust reservoirs (1A, 2A and 3A on schematics Figure 4-9). The dust is dispersed by activating a pneumatic valve, actuated by the control system. This releases the pressurised air from the air reservoirs and disperses the dust. For more detailed information, see chapter 4.1.3. Note that the dispersion air is injected for both gas and dust experiments, in order to maintain the same initial conditions.

4.2.3 Control and data acquisition system

A NI-CAD 6259 card, connected to a computer, performs both controlling and logging of the experiment. The card controls the timing of dispersion and ignition. This NI-CAD card is programmed by LabView software, which is documented in appendix A. The software enables the user to change all setup parameters, within the limitations of the card.

Control system

A tailor made power supply with opto-couplers and semiconductor relays was made to control the experiments. See switching circuits in appendix A. A NI CAD (6259) sends signals to this power supply switching on and off the opto-couplers and semi conductor relays, controlling the valves and triggers the ignition. In order to be able to pre-program the output and maximize the accuracy of timing, the analogue output of the NI-CAD card is used. Digital ports are used for: remote triggering of the experiment, to reset and activate the pressure measurement system and for turning on the LED indicator. A high speed camera records the explosion, and the LED indicates when the dispersion occurs.

A simple spark generator was built for ignitiong the gas explosion tests (appendix A). The NI-CAD card is used to trigger the spark directly through an opto-coupler. However, reliable ignition of turbulent dust clouds requires a stronger ignition source, and for this purpose a 1 kJ chemical igniter was used. This chemical igniter need 24 volt to ignite. This is achived by one of the semiconductor-relay in the switching circuit, shown in appendix A.

Sources of error, timing

The NI-CAD card is able to time trigging within 50 ns. Three separate semiconductor-relays operate the dispersion valves. The relays switch from off to on within 0.1 ms and use 0.75 ms from on to off. The valves use at most 20 ms to open, see section 5.2 Time delay for the spark-generator has not been measured, but the optocoupler trigging this system uses 5 us to switch on. The spark generator utilise a coil to generate high voltage. This coil will delay the spark, but it is probably negligible compared to the other sources of timing error. Time delay of activating the chemical igniters, was not determined.

Data acquisition system*

The experience from the work performed in this thesis shows that amplification of measured signal is important. One A/D converter reads all the channels. Switches inside the card choose which channel to read. If one channel is not satisfactory amplified, the signal from one channel would influence the signal read next. The reason may be stray capacitance, see documentation of the NI-CAD 6259, of 100 pF inside the NI-CAD card.

Sources of error, timing, A/D converters and measurements

The NI CAD card can record 1MS/s when multiple channels are in use, or 62.5 kS/s per channel. The resolution of the readings is 16 bits, which makes it possible to differentiate between 65536 levels. The maximum input voltage is +/- 10 V. The accuracy of the voltage reading in the NI-CAD card is relative to the maximum and minimum voltage set for the specific task, and varies from 0.019% (+/- 10 V) to 0.023% (+/- 2 V) (obtained from www.ni.com). Background noise and natural drifting of the electrical equipment represent additional source of error.

The light sensitivity of the high speed camera drops with increasing frame rates. This becomes a problem for lean gaseous flames, since less bright. At 600 fps the lean propane air flames were barely visible on the video. Richer mixtures give a flame easily seen, as the flame shines bright yellow. Since these results are manually processed, the results are subjective to

some extend. Especially in cases of dust flames, because of illumination of the dust ahead of the flame. The frame rate also introduces inherent limits to the time resolution of the video measurements.

The pressure measurement consists of a pressure transducer and a charge amplifier. The amplifiers precision, according to documentation, is 1 % of charge amplified. This means that constant test conditions will give results varying with 1 %. The accuracy depends upon the setup of the amplifier, and the sensors. The sensors are also temperature dependent. To protect and insulate the sensors, red silicone covers the exposed end of the sensor. However some thermal drift is expected for prolonged measurements

4.2.4 Flame probes

In order to measure flame arrival times in the same position, probes with both capacitive plates and optical diodes has been designed. The probes are distributed through out the length of the pipe 0.6 m apart (Figure 4-9). The probes are designed to carry two optical pair of one sender and one receiver. In addition it is possible to fit in two acoustic sensor pairs. The probe is shown in Figure 4-8, and more comprehensive drawings are included in appendix A.

Figure 4-8 *Probe used in FAT experiment*

Special probes with exposed junction thermocouples were designed to monitor flame arrival and to some extent flame temperature. The electronics, as well as a welding apparatus built for this application, are shown in appendix A. Thermocouples is a bit slower than the other measurements, since the temperature of the burning gas will have to heat the laminar boundary layer around the string, and the string it self. This physical restriction not only slow the response time regarding flame arrival, but also limits the information possible to retrieve from the combustion process.

4.2.5 Experimental procedure

Experimental procedure for the FAT – Gas

With reference to the schematic in Figure 4-7, the experimental procedure for the gas explosion tests in the FAT was as follows

1) start vacuum pump and open valves (16, 17 and 18) between the pump, FAT and pressure gauge P_1
2) evacuate the FAT to the desired pressure typically –0.33 bar(g) + desired partial pressure of gas monitored by the digital pressure indicator(P_1)
3) close valve 17 to pump and turn off vacuum pump
4) open valves 24, 25, 20 and 19 and fill pressurised air of 16 bar(g) from the flask into the reservoirs via the reservoir valves(11, 12 and 13) by the help of the digital pressure indicator(P2)
5) open valves 10, 9 and 1 to flush gas through the line to displace air in the system. Add 1/6 of total amount of gas, measured by partial pressure into the FAT via the valves 2, 3, 4, 5, 6 and 7. Use reduction valve (8) to control the flow accurately. The pressure inside the FAT should reach -0.33 bar(g)
6) close valve (8) to the fuel gas
7) adjust vacuum and reservoir pressure to -0.32 bar(g) and 16 bar(g), respectively, via valves (vacuum: 14 and 15, reservoirs: 21 and 22)
8) close needle valve (24) on flask of pressurised air and valve (20) between flask and FAT
9) check that the safety valve(16) is closed
10) activate the LabView program and specify filename in LabView
11) reset charge amplifiers for pressure measurements in reservoirs
12) close the reservoir valves (11, 12 and 13)
13) turn on the spark generator
14) secure the area
15) check that the test number is correct
16) turn on camera
17) push the trigger button
18) open exhaust valve
19) open FAT and connect ventilation system

Experimental procedure for the FAT – Dust

With reference to the schematic in Figure 4-7, the experimental procedure for the dust explosion tests in the FAT was as follows

1) open the door in the end of ignition and install a chemical igniter to the holder for spark gap / chemical igniter located inside tube at the point marked ignition
2) start vacuum pump and open valves (16, 17 and 18) between the pump, FAT and pressure gauge P_1
3) evacuate the FAT to the desired pressure typically –0.33 bar(g)
4) close valve 17 to pump and turn off vacuum pump
5) open valves 24, 25, 20 and 19 and fill pressurised air of 16 bar(g) from the flask into the reservoirs via the reservoir valves(11, 12 and 13) by the help of the digital pressure indicator(P_2)
6) fill desired amount of dust into dust reservoirs, 1A, 2A and 3A
7) adjust vacuum and reservoir pressure to -0.32 bar(g) and 16 bar(g), respectively, via valves (vacuum: 14 and 15, reservoirs: 21 and 22)
8) close needle valve (24) on flask of pressurised air and valve (20) between flask and FAT
9) check that the safety valve(16) is closed
10) activate the LabView program and specify filename in LabView
11) reset charge amplifiers for pressure measurements in reservoirs
12) close the reservoir valves (11, 12 and 13)
13) secure the area
14) check that the test number is correct
15) turn on camera
16) push the trigger button
17) open exhaust valve
18) open FAT and clean out remains from the experiment

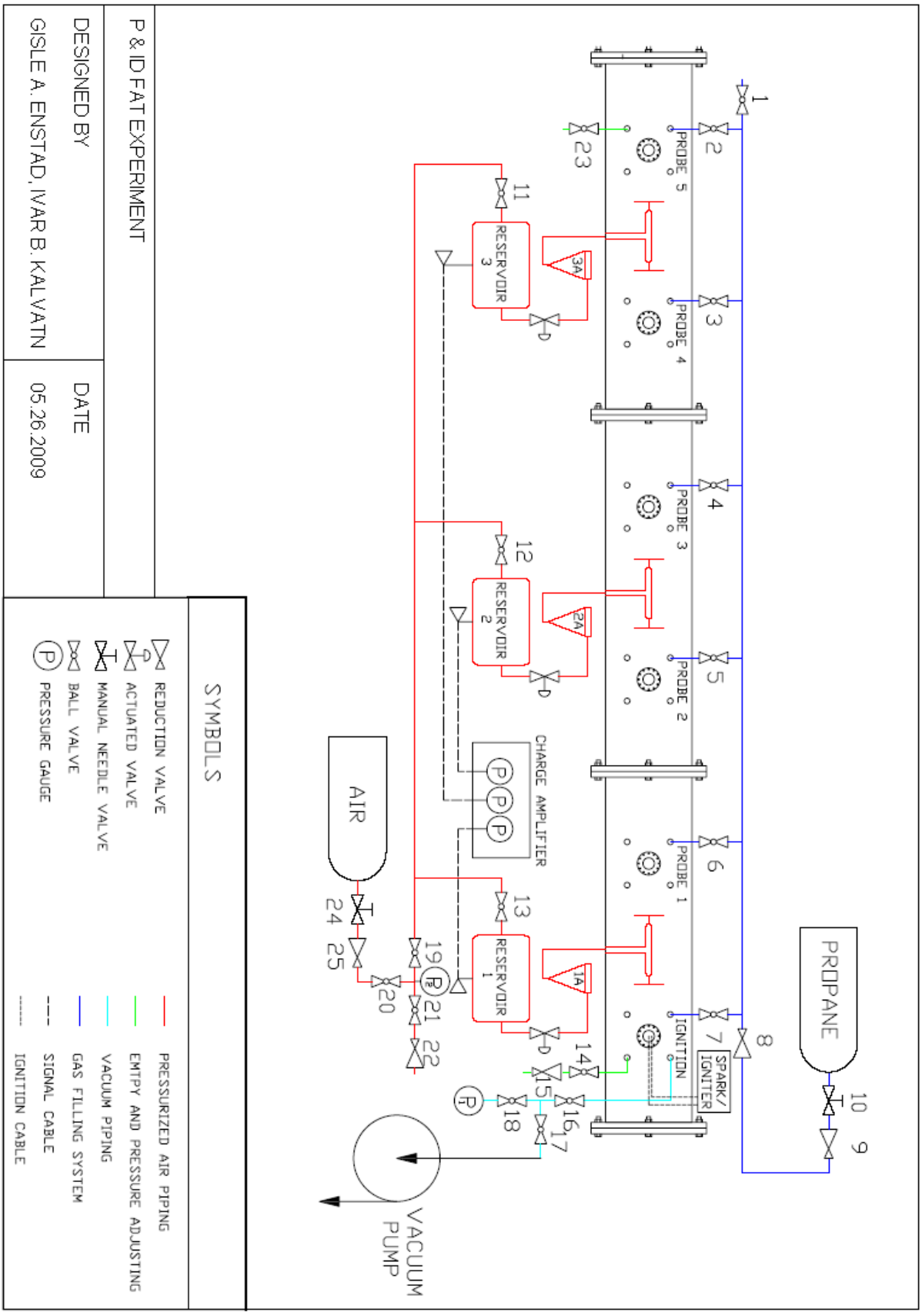

Figure 4-9 *Schematics of the FAT experimental setup*

5 Results and discussion

Chapter 5.2 is similar to 4.2 in Kalvatn (2009)

5.1 Results from the preliminary experiments in the 20 litre vessel

The flame arrival at the probe was very characteristic and easy to identify. The two inputs, frequency-voltage and amplitude of response provide both the resistive part and the capacitive part of the unknown impedance.

The experiment in the 20 litre vessel showed a clear indication of flame arrival. The damping of the resonance is the best way to indicate this, but since the resonance frequency also changed it is possible to measure both capacitance and resistance in the flame. However, the actual dielectric constant of the flame is quite problematic to derive, since the flame presumably is quite fragmented. Figure 5-1 shows a typical measurement a dust explosion. Interestingly the capacitance and resistance develops differently. The resonance frequency is mainly influenced by the capacitance and the resistivity mainly influences the damping.

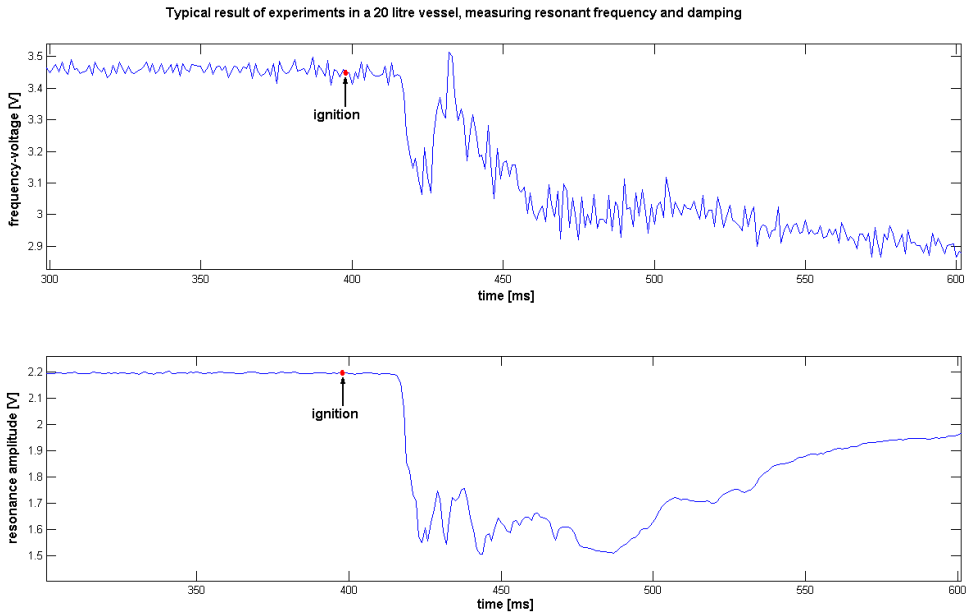

Figure 5-1 *The responce of the probe used in 20 litre vessel. Upper: resonance frequency (represented as frequency-voltage). Lower: the amplitude of the resonant peak during same time span.*

5.2 Results from preliminary dispersion experiments in the FAT

This section presents the results from preliminary dispersion experiments in the FAT. Table 5-1 shows test configurations and test results and Figure 5-2shows the pressure development in the reservoirs during dispersion. Figure 5-3 and Figure 5-4 shows images from the dispersion tests and illustrates the strong effect of confinement.

Table 5-1 *Test configuration and test results*

Test number	**Configuration**	
1	Confined within box	
2	No confinment	
Time delay of dust		
Test Number	**Frames**	**Sec**
1	13	0,043
2	14	0,047
Time to fill box		
1	75	0,250

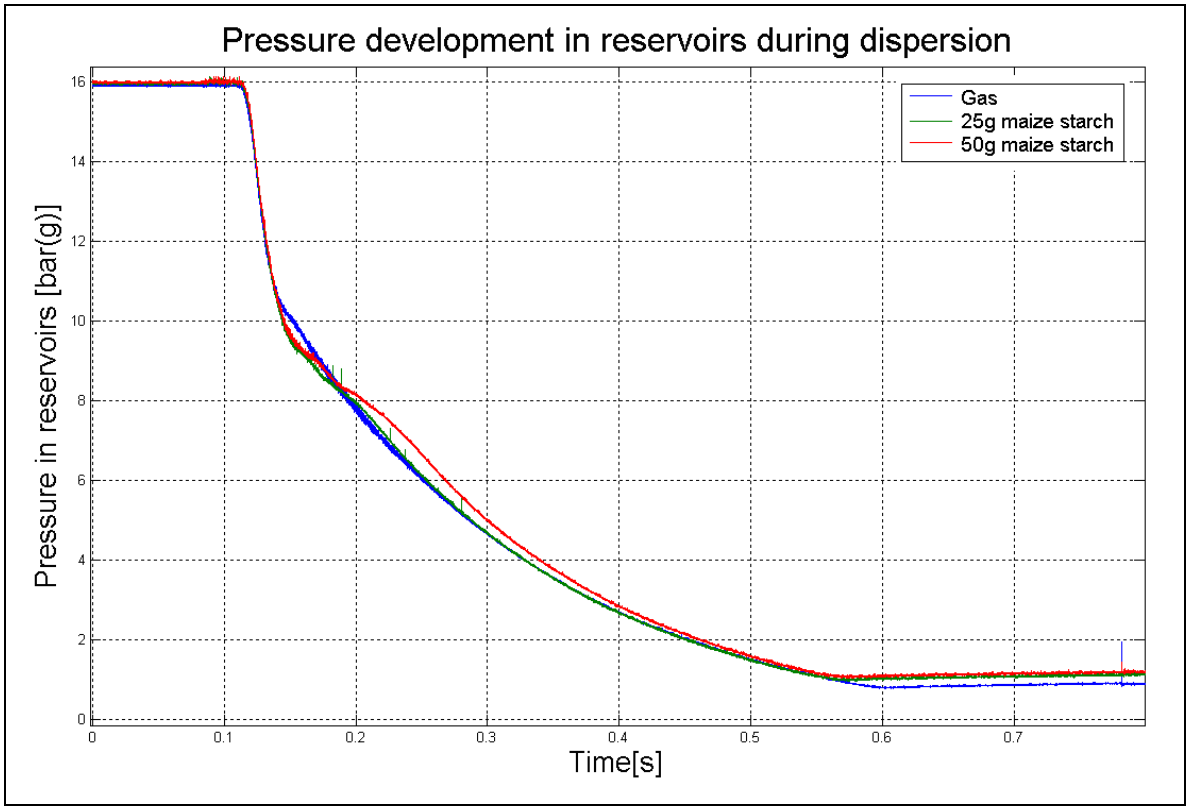

Figure 5-2 *Pressure development in reservoirs during the dispersion process*

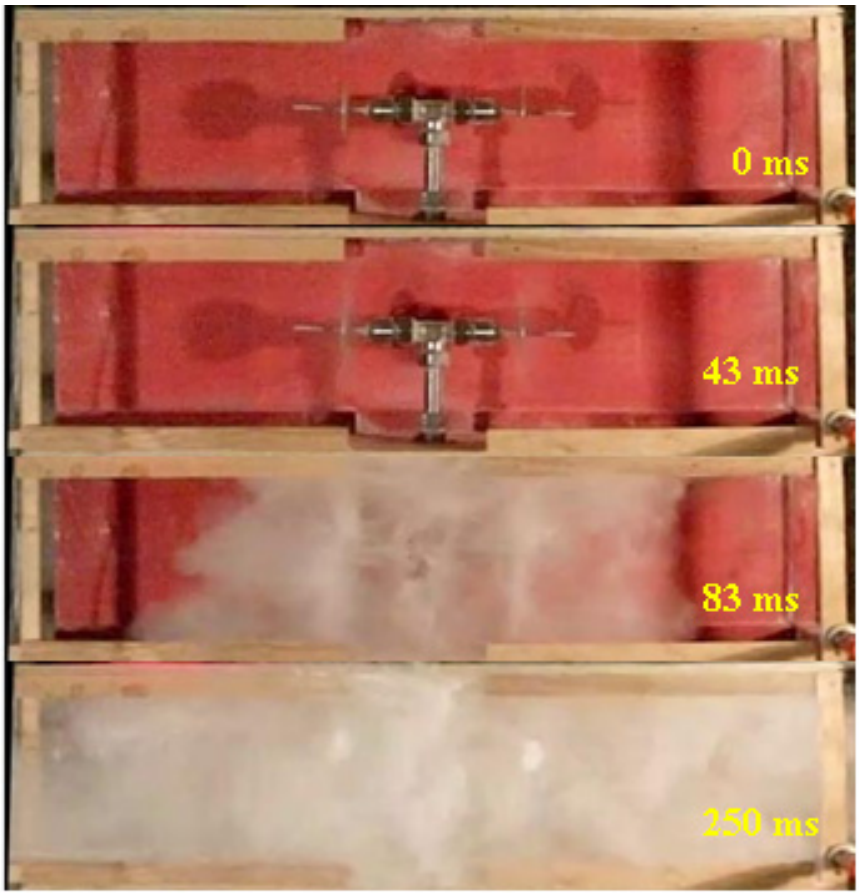

Figure 5-3 *Images from dispersion confined within box*

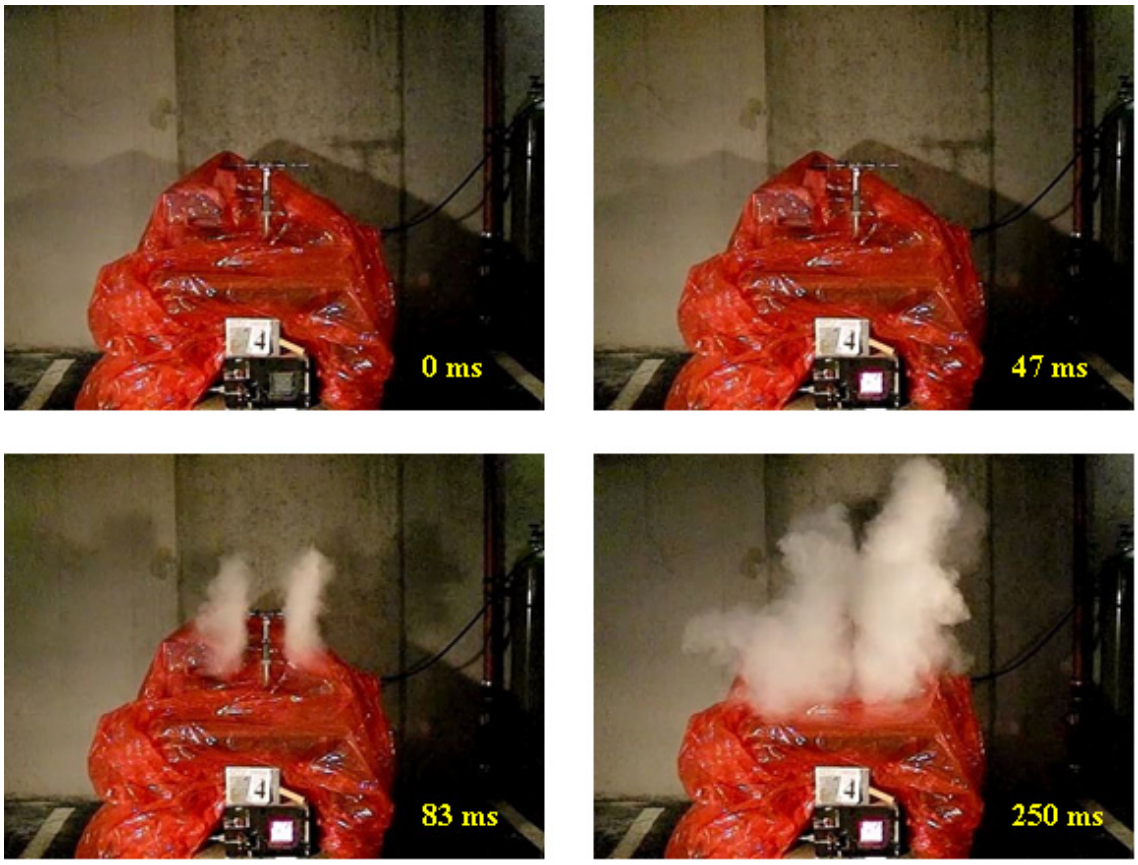

Figure 5-4 *Images from dispersion test 2.*

5.2.1 Analysis of pressure in reservoirs

Figure 4-2 shows the pressure time curves during dispersion tests. The introduction of dust in the dust reservoirs slows down the discharge rate, and hence pressure drop in the reservoir. It seems 25 and 50 gram of maize starch give approximately the same end pressure. The initial pressure drop that seems to be linear is probably sonic flow, and the reason for the linear pressure development is chocking. This sonic flow lasts a little longer in the experiments with dust.

The dispersion process is over after about 500 ms. The trigger signal is sent just before 0.1 s after the LabView program is activated, and the pressure drops up to 0.57 - 0.60 s. A shorter dispersion time would be advantageous. If the dispersion times were shorter, the dispersion could be differentiated in such a way that the last section of the FAT would disperse last. This would give more control with the mixture ratio in the pipe. To achieve this, the dispersion system would have to inflict less pressure drop, meaning that the number of bends and length of pipes must be reduced and the cross-section area of the connections increased. In some tests the valves did not close. The length of the signal sent was adjusted to 90 ms, since the valves seem to close after a certain time after the signal is stopped. Improvements to the system would be advantageous in order to get better control with the dispersion process.

5.3 Results of FAT experiment, gas and dust explosions

As pointed out earlier, the video analysis was highly subjective. For dust flames a flame times determined from video recordings were difficult since the dust cloud was illuminated in front of the flame. The optical measurements indicated the same trend, as the flame arrival detected was earlier than when the capacitive method was used.

5.4 Results, measured damped resonance curves

The curves in the Figures 5-5, 5-6, 5-7, 5-8 and 5-9 are shows the measured response when the flame arrives at probe 2 in the FAT

5.4.1 Gas experiments

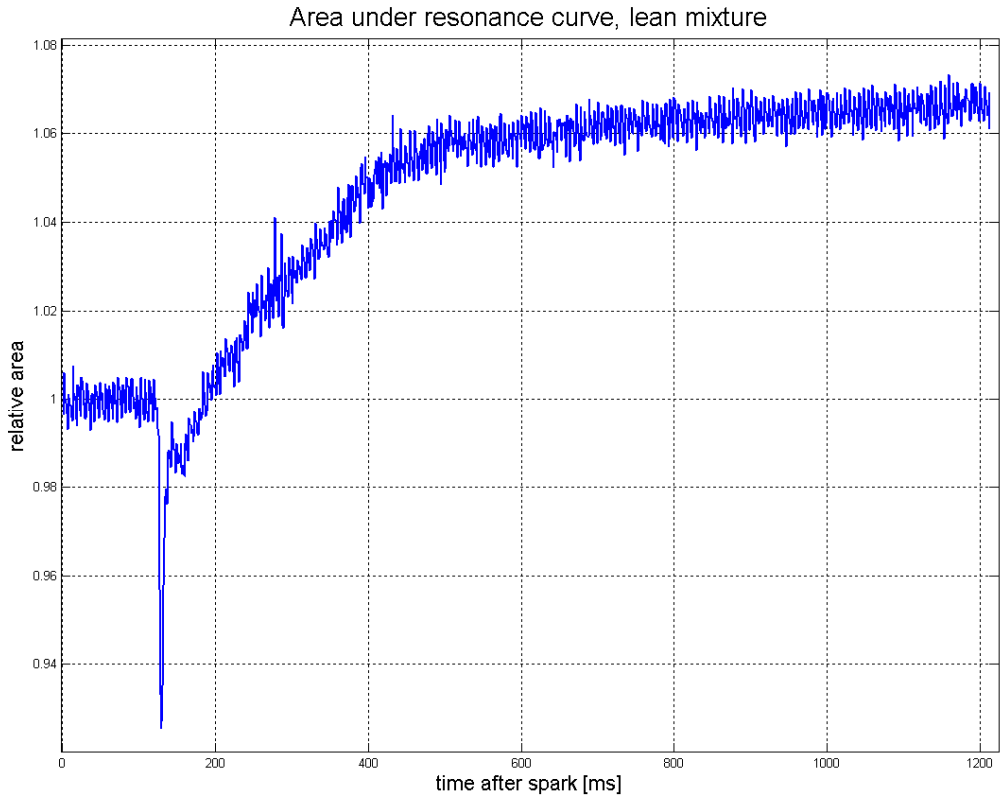

Figure 5-5 *The damping of the resonance during a gas explosion in a lean (3%) mixture*

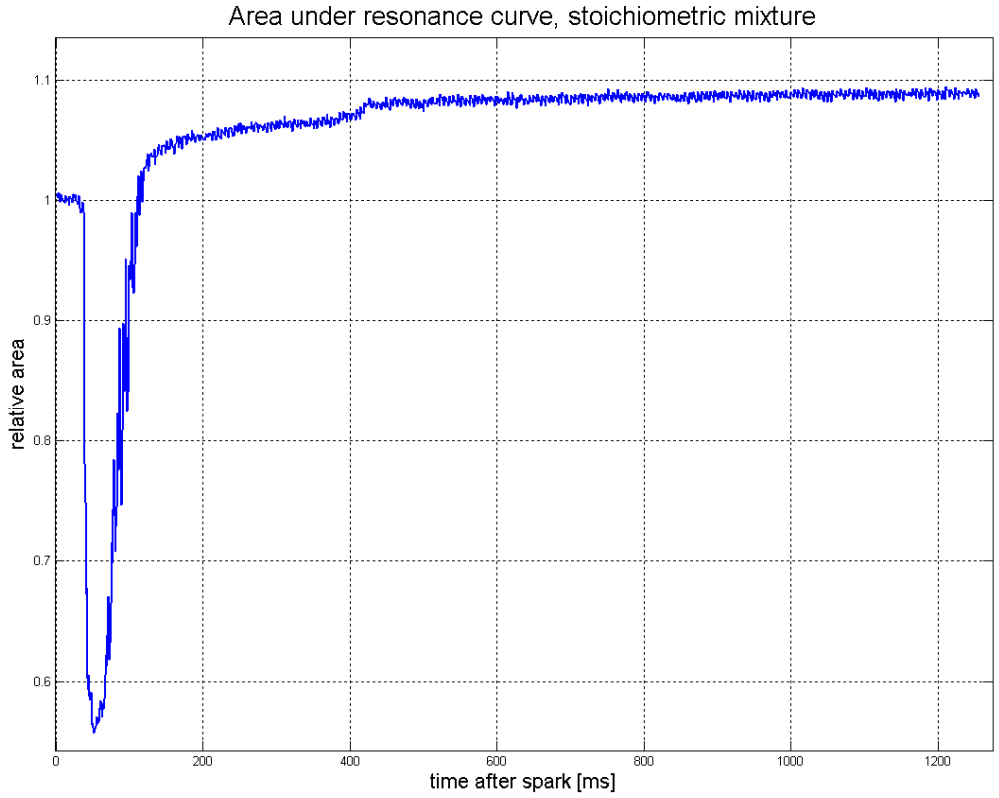

Figure 5-6 *The damping of the resonance during gas explosion in a stoichiometric (4.5%) mixture*

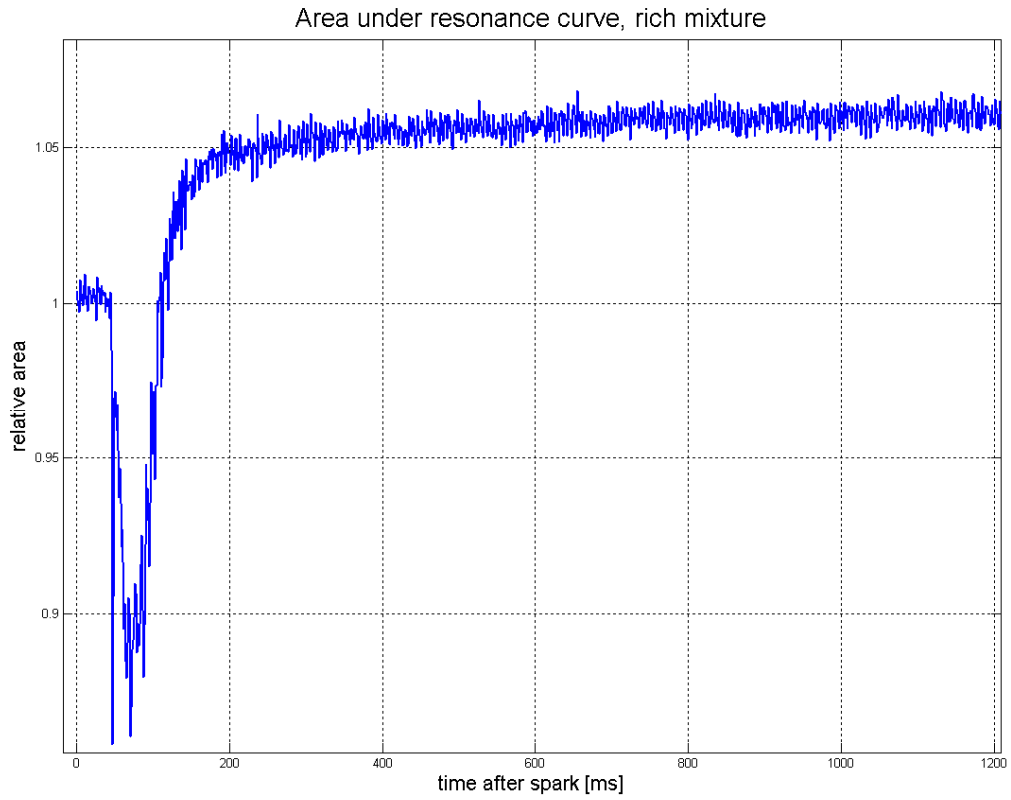

Figure 5-7 *The damping of the resonance during a rich (6%) gas explosion in a rich (6%) mixture*

5.4.2 Dust experiments

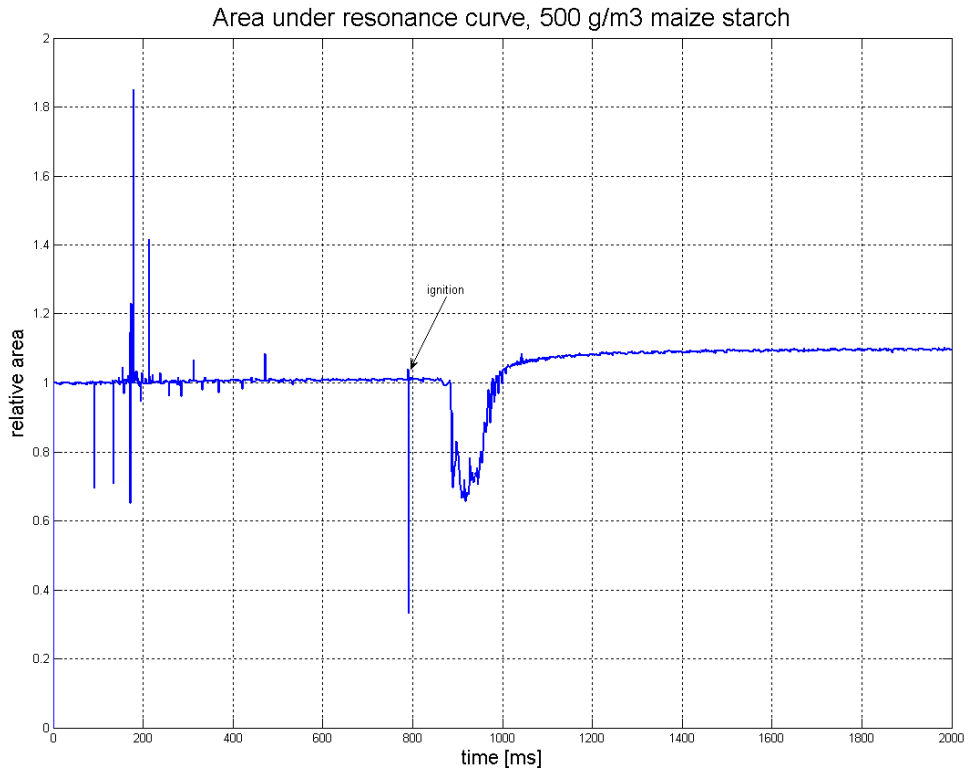

Figure 5-8 *The damping of the resonance during explosion for 500 g/m3 nominal maize starch mixture*

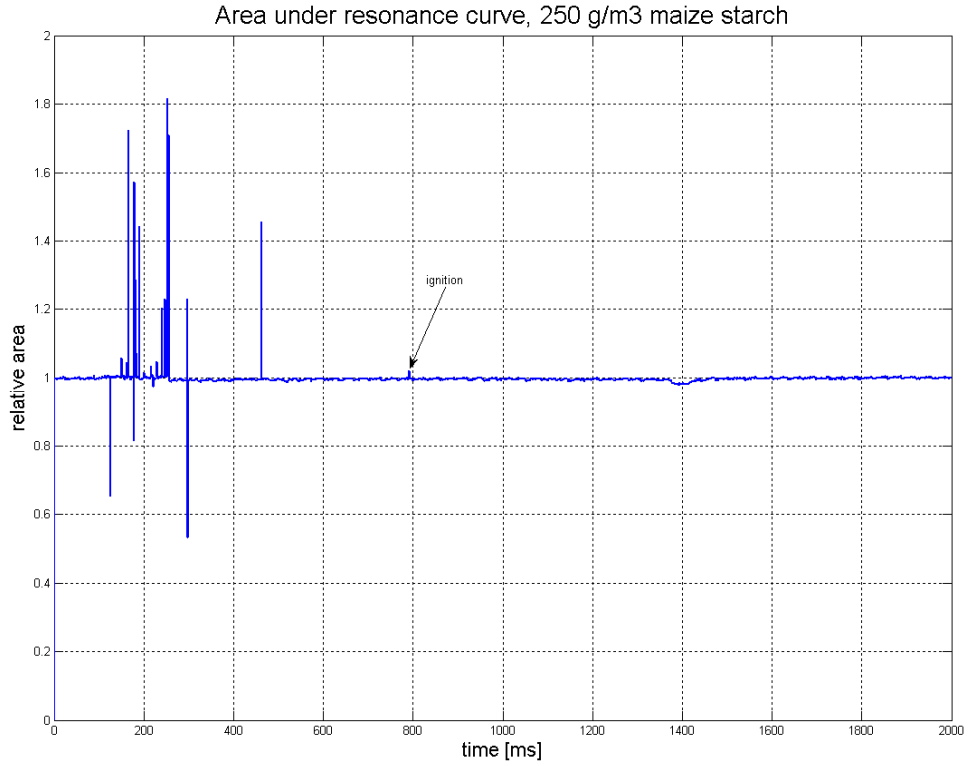

Figure 5-9 *the damping of the resonance during explosion for 250 g/m3 nominal maize starch mixture*

5.4.3 General discussion of measurements

Several methods to interpret the results of the capacitive measurements. The most efficient way to identify the flame arrival time is to simply integrate the resonance curve. In theory more damping should give less area under the curve.

In this context, some of the results obtained with different probes may seem confusing. Some of the graphs increase while others decrease (only measurements from probe 2 are represented in the previous plots). This is probably due to the rectifying diodes, which distort the signal, combined with fake resonant peaks (fake resonance peaks are peaks due to other effects as amplifiers and other noise). If the true resonant peak moves towards a fake, this would boost the amplitude in this area more than it decreases in the area the true resonant peak moved from. This is seen in the results from probes 3, 4 and 5.

Since some of the signals, especially from probes 3 and 4 are very weak, the time of flame arrival is challenging to detect automatically, and manual interpretation of the results is usually required. Probes 1 and 2 gave quite clear indications of flame arrival. The reason of these differences of the probes is discussed extensively in section 3.1.3. While probes 1 and 2 prove the functionality of the measurement principle, the other probes need fine tuning to give good measurements.

Probes 1 and 2 are capable of detecting flames in lean gas mixtures, while probes 3, 4 and 5 gave very diffuse flame indication. The times of flame arrival in these probes are therefore uncertain. Also probe 4 seems to be somewhat influenced by probe 2, as the graph jumps a little when probe 2 detects the flame. The reason is perhaps a combination of weak signal and a connection of the signals in the amplifiers. This is not a significant problem, but should be noted.

It would be interesting to see if the measurements are capable of indicating a flame thickness. The flame is defined as the zone where combustion takes place, and the presence of free radicals, see chapter 2.1.3, influences both the capacitance and resistance. As pointed out in chapter 3, the resistive part of the flame impedance is the dominant one. The ion-density in a gas is also temperature dependent, and damping of the resonance curve will also occur after the combustion zone has passed.

Figure 5-10 show the measured damping of the resonance curve during a rich mixture explosion. The spike indicated is only 1 measured point, since it is very narrow may slip through the measurements in some experiments. The spike in Figure 5-10 is only present in the experiments with rich mixture. Whereas the lean mixtures had a more narrow spike, not followed by a u-shape (Figure 5-5). The effect of the flame on the measurement was also weaker. Experiments with stoichiometric mixtures only produced one u-shape, and no spike (Figure 5-6). It is possible that the high velocity for stoichiometric mixtures hides a narrow spike in-between the measured curves, or it simply is not present. Maybe this spike is the correct indication of a flame present. In that case the time resolution is too crude to determine the flame thickness. More research is needed in order to determine these details, and the flame thickness remains an unanswered question.

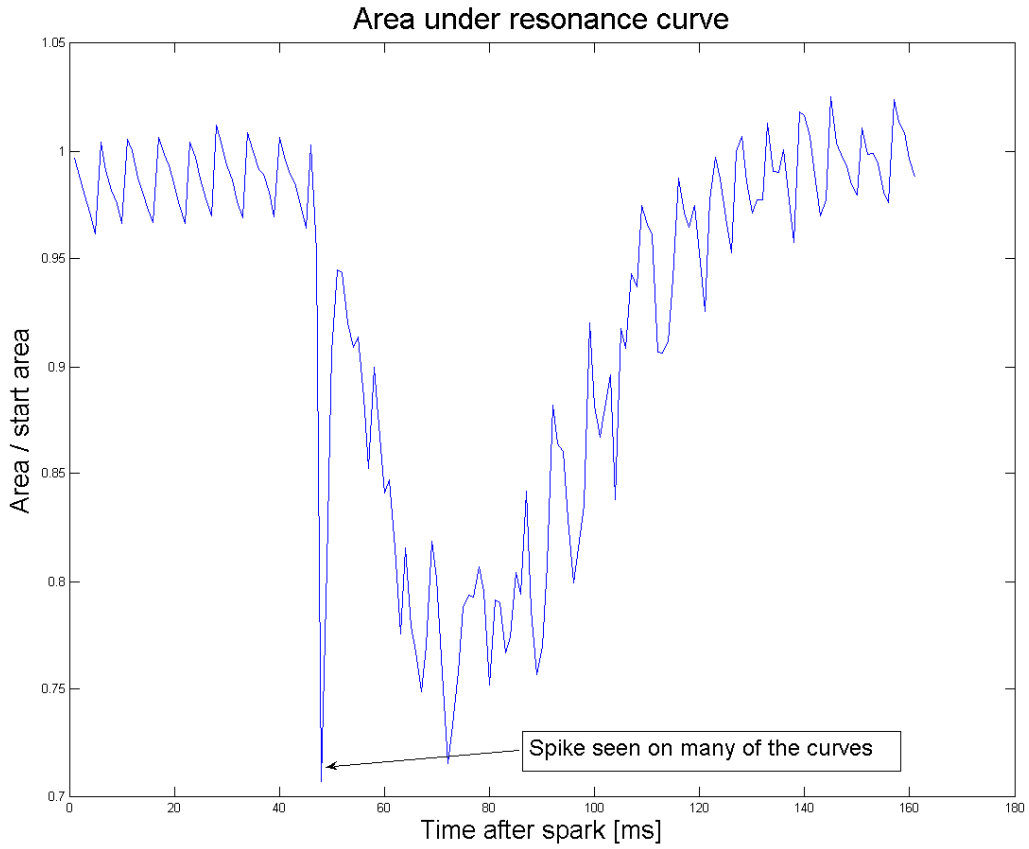

Figure 5-10 *Response of probe 2 during experiment with rich gas mixture*

In order to investigate the temperature dependence of the damped resonance, one can compare temperature development with damping. Recording thermocouples at the probe location could not measure temperatures higher than 500 ^{o}C. However, if extrapolated, the temperature measurements suggest a very high temperature even after the measurement stabilizes (after the relative area under resonance curve is back to 1). Also the pressure measurements indicate high temperatures after the resonance is back to normal. Both these measurements seem to contradict that the temperature dependency of the ion-density in the gas phase controls the "tail" of the u shape. One should keep in mind that the temperature measured by thermocouples will lag, and could indicate a rising temperature even if the temperature in reality is decreasing around the thermocouple-wire. Also, the pressure, if used as a temperature indicator, is only a mean temperature of the tube as a whole. Therefore these measurements are not necessarily contradicting that there is a correlation between the measured damping and the temperature in the gas. One may assume that the temperature will stay high long after the flame has passed.

Water forms during combustion. Water has a relative dielectric constant of 80 at 20 ^{o}C and 34 at 200 ^{o}C. This is perhaps the reason why the resonance frequency and the area under the resonance curve changes so gradually. Figure 5-6 shows the area under the resonance curve makes a little jump after approximately 420 ms. The temperature is recorded to 110 ^{o}C at the same time, indicating that this jump might correspond to condensation of the water. The gradual change of the area under the resonance curve could indicate an increase of the capacitance. The change can be explained by interaction with a fake resonant top, and the fact that increased capacitance will give a stronger resonance response. Because of the many factors distorting the capacitive measurement the interpretation of such phenomena is not obvious.

The lean mixture propane air did not cool down as fast as for the stoichiometric ones. Despite the fact that the temperature did not reach the same maximum value as for the stiochiometric mixtures, the temperature did not reach 200 ^{o}C after 4 seconds of recording. This may explain the relatively slow stabilization of the area under the resonance curve (Figure 5-5). The little jump, discussed previously, is not present.

Figure 5-8 and Figure 5-9 are taken from experiments of dust explosions. With dust there is significant noise during the dispersion process presumably due to static electricity. There is less damping of the resonance in the 250 g/m^3 experiment, compared to 500 g/m^3, at the time of flame arrival. This is the same conclusion as for the gas experiments, which gave less damping with leaner mixtures. Figure 5-8 of the 500 g/m^3 may indicate that the capacitive probe is capable of measuring the dust cloud density. The area under the resonance curve is higher after dispersion than before, something which is not seen in the experiment with 250 g/m^3.

Appendix B lists the Matlab programs that were developed to analyse the measurements. In the experiments with rich and stoichiometric mixtures the resonance top were not found during the damped period. This is because of a fake resonance top shadowing the top which is to be measured. Lean gas experiments gave a measurable resonance top. Strangely enough the resonance frequency seems to suggest a lower capacitance when the flame arrives. This result is quite the opposite of what you would expect and what was found by Waterfall (1997). Careful examination of the curve reveals a dent which suggests a fake resonance top, which distorts the signal resulting in this effect. This makes it pointless to analyse the resonance frequency. It should also be noted that the experiments performed in the 20 litre vessel agreed more with the results of Waterfall (1997). The fake resonance top is not present in these experiments, as only one probe is used. This allowed the use of a better amplifier, and the frequency generator was not pushed to its limit as was the case in the FAT experiment.

To summarize the above analysis of the results, one can conclude that perfection of the equipment is needed to analyse resistance and capacitance in different types of flames. It was, nevertheless possible to achieve reliable detection of the flame, and the results provided measurement of flame acceleration.

5.5 Results, comparing flame arrival

Figures on the next pages comparing flame arrival detection of different measurement techniques. The line indicates the mean value. The points are found from:

$$t_d = \frac{t_p \cdot n}{\sum_{m=1}^{n} t_m} - 1 \tag{5.1}$$

Where the relative deviation, t_d, equals the measured time of flame arrival, t_p, divided by the mean measured arrival time, sum(t)/ n. This would make the absolute time difference at probe 5 look like a smaller deviation, as the mean value of the flame arrival times is a greater number than the mean flame arrival at the earlier probes. Flame velocity is calculated by the time delay of flame detection between two probes divided by the distance between the probes. This gives the mean velocity between these two points. The plotted points between numbers 1, 2, 3, 4 and 5 are the calculated velocity of the flame (see x-axis). Equation 5.2 shows the similar way of calculating the velocity deviation. S_d is the relative deviation of velocity, v_p the absolute velocity and sum(S)/n is the mean velocity:

$$S_d = \frac{S_p \cdot n}{\sum_{m=1}^{n} S_m} - 1 \tag{5.2}$$

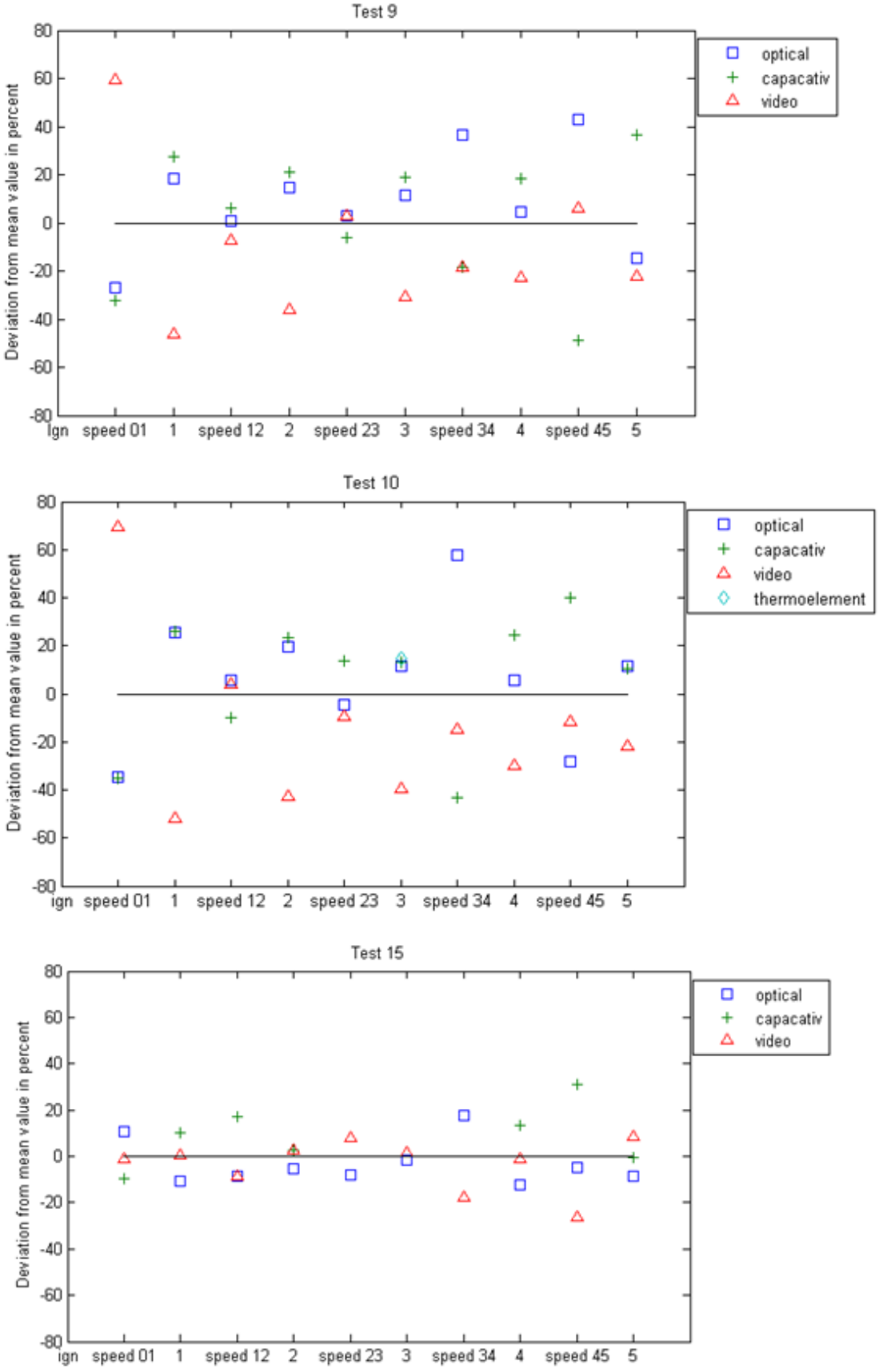

Figure 5-11 *Deviation from mean values for flame arrival/speed measurements for the different measurement principles in tests with 3.0 vol% propane in air.*

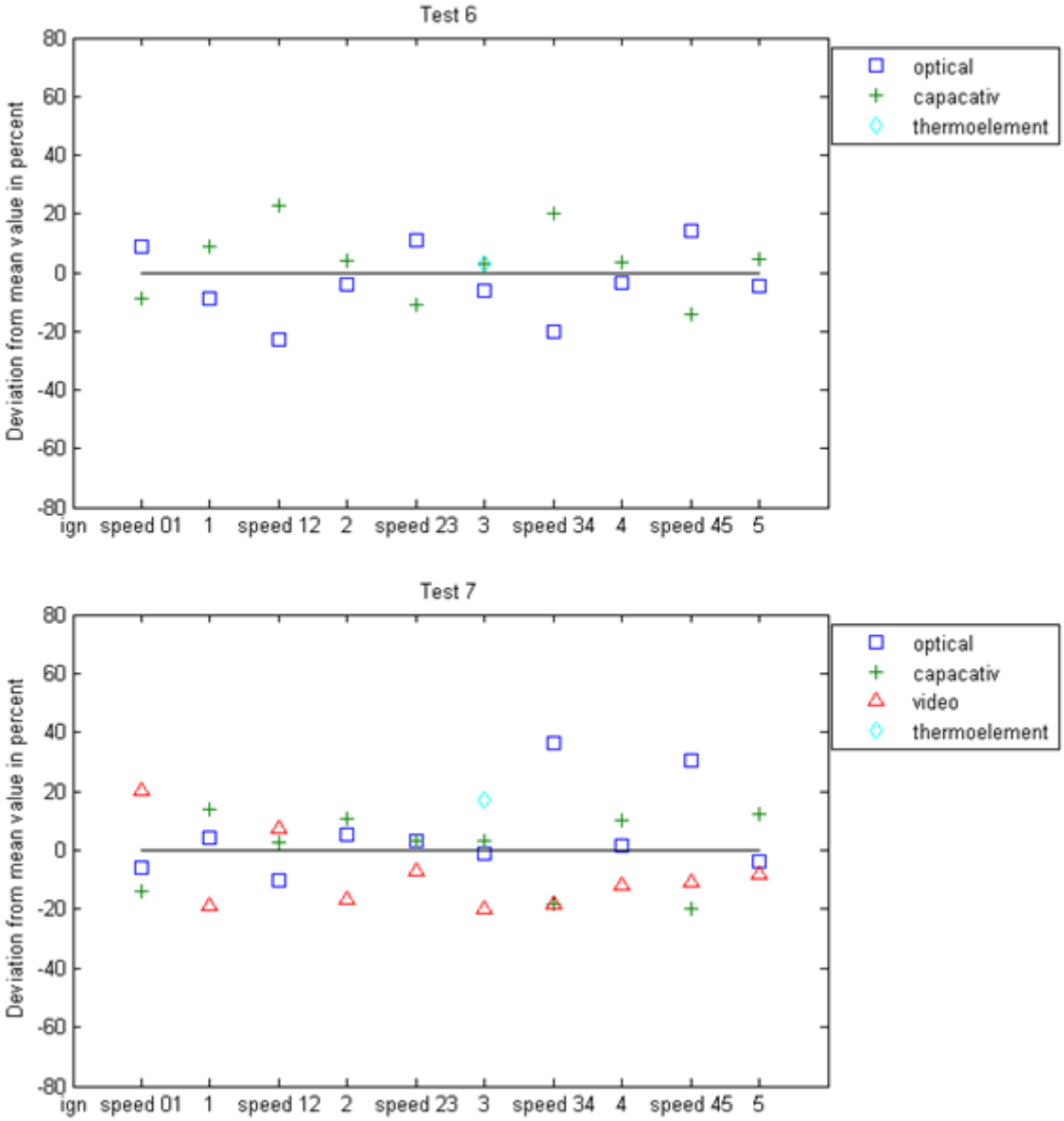

Figure 5-12 *Deviation from mean values for flame arrival/speed measurements for the different measurement*

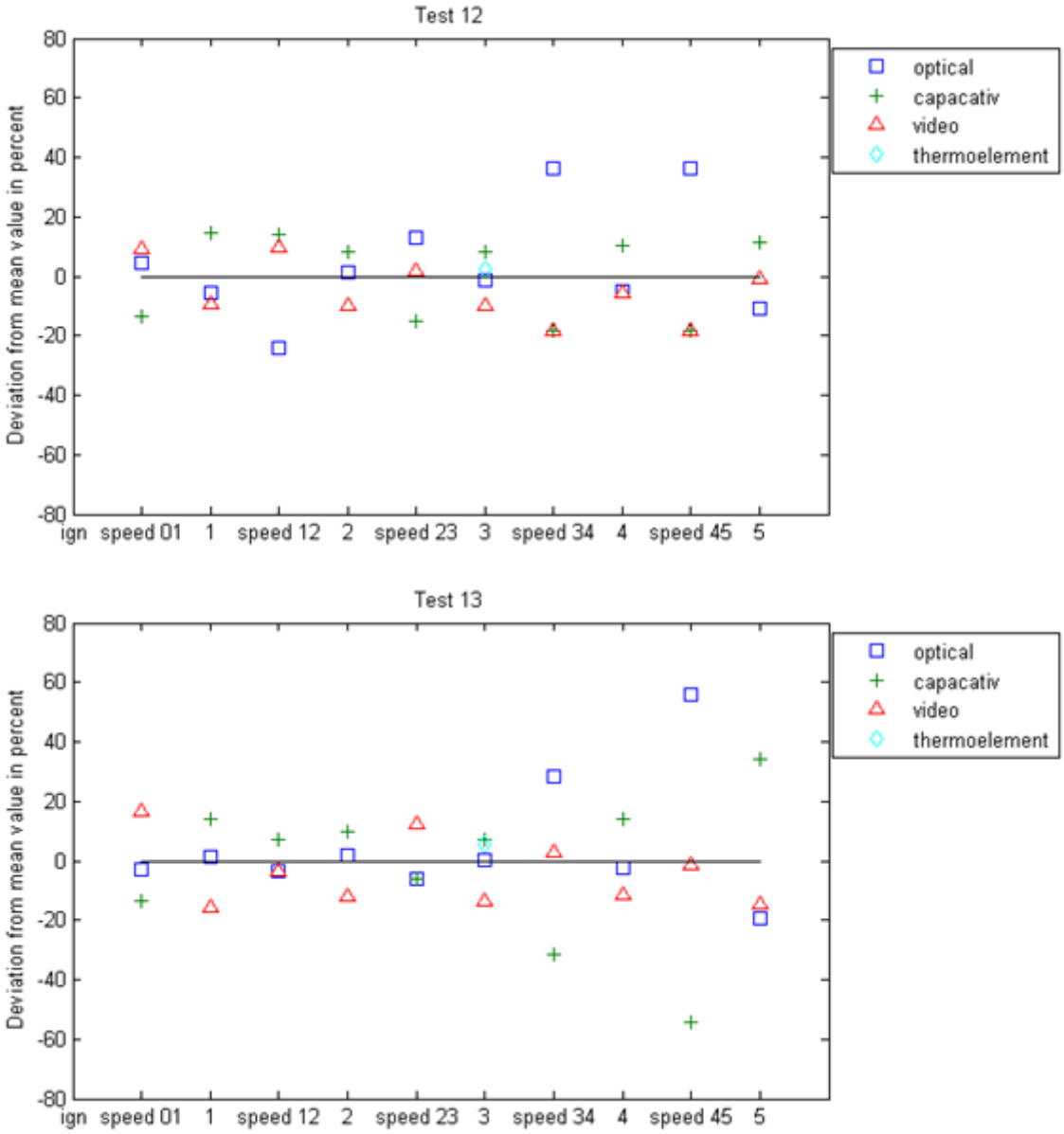

Figure 5-13 *Deviation from mean values for flame arrival/speed measurements for the different measurement principles in tests with 6.0 vol% propane in air.*

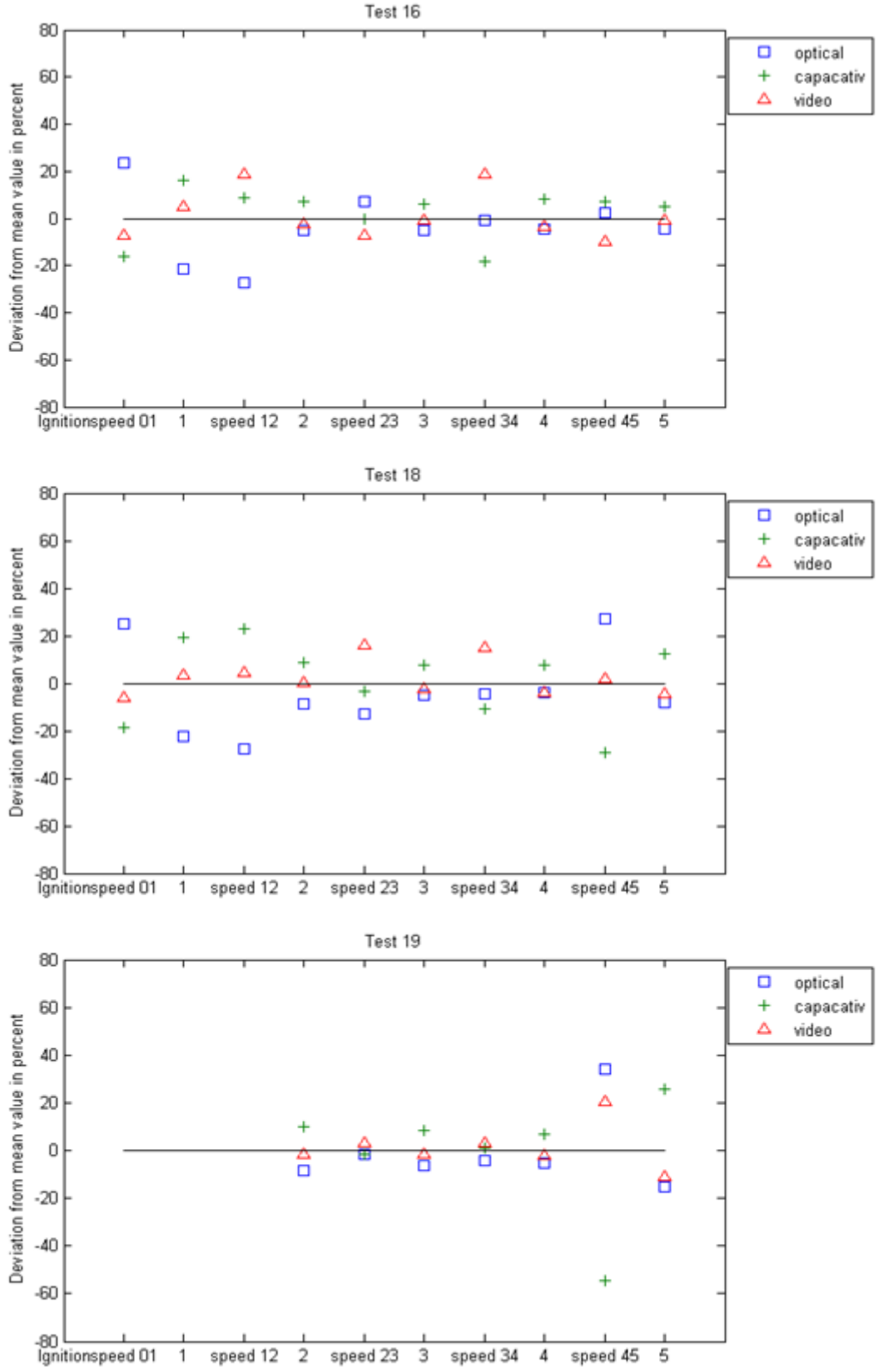

Figure 5-14 *Deviation from mean values for flame arrival/speed measurements for the different measurement principles in tests with 500 g/m3 of maize starch.*

5.5.1 Discussion of compared flame arrival times

The video analysis gave flame arrival earlier compared with the other measurements for all experiments and at all the probe stations. The measured speed between ignition and probe 1 was measured higher with the camera compared to the two comparing measurements. Furthermore, the optical measurements were generally a little earlier than the capacitive measurements, the optical and capacitive method showed better agreement than the video. A probable explanation of this phenomenon is that the measuring probe reflects the light before the actual flame arrives, looking like a flame arrival in the video. The dust explosion experiments also support this. The transparency of the dust cloud is of course lower than for the gas mixtures, and the measured flame arrival of video analysis agrees more with the other methods (Figure 5-14). The thermocouple is placed in front of the probe, and is situated closer to the wall. The measured flame arrival times is agrees quite well with optical and capacitive measurements, although the point of flame arrival does not correspond exactly to the other methods. If the thermocouples had been placed in the probe the measured flame arrival would have occur somewhat later.

The experiments showed less relative deviations. This is mainly due to the mentioned video analysis, agreeing better with the other measurements. The capacitive probe measured a much later flame arrival between probe station 4 and 5. This may indicate that both the optical measurements and the video analysis are sensing light before the actual flame arrival. This would result in a greater error at probe 5, because the flame is moving more slowly at this location. The tendency is also seen in the gas experiments. The capacitive measurements of probes 3, 4 and 5 are as mentioned in section 3.1.3 more marginal, and it is not easily detected on the curves when the flame arrives.

5.6 Results, comparing calculated speed

Figures on the next pages shows calculated speed from different measurement techniques. The lines indicate a possible velocity development. Some of the lines go through the points and are calculated using the spline method in Matlab, some are fitted to the data using a least square 3 degree polynom (polyfit in Matlab). The choice of method depends on which curve looks most natural.

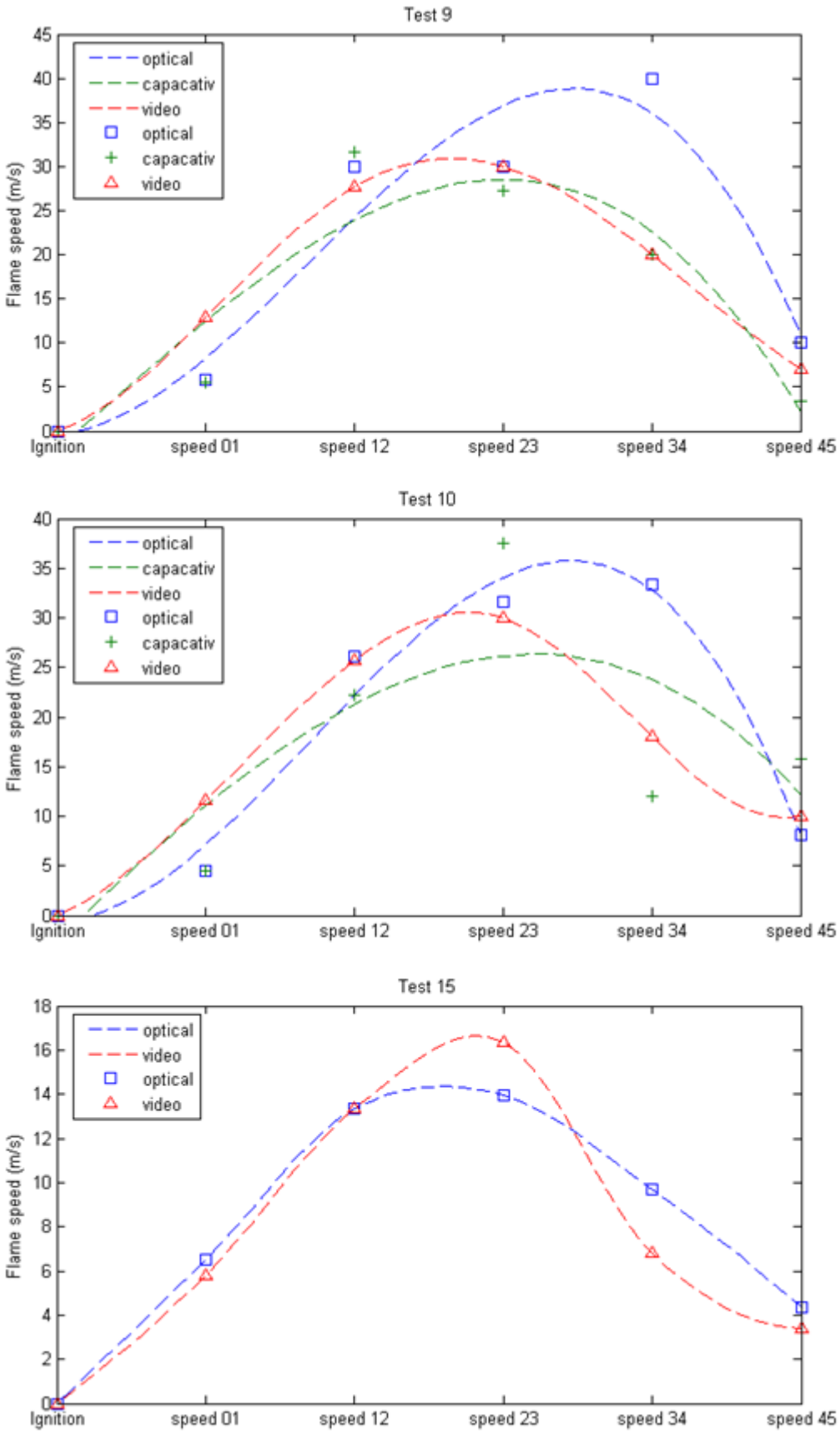

Figure 5-15 *Flame speed measurements for tests with 3 vol%*

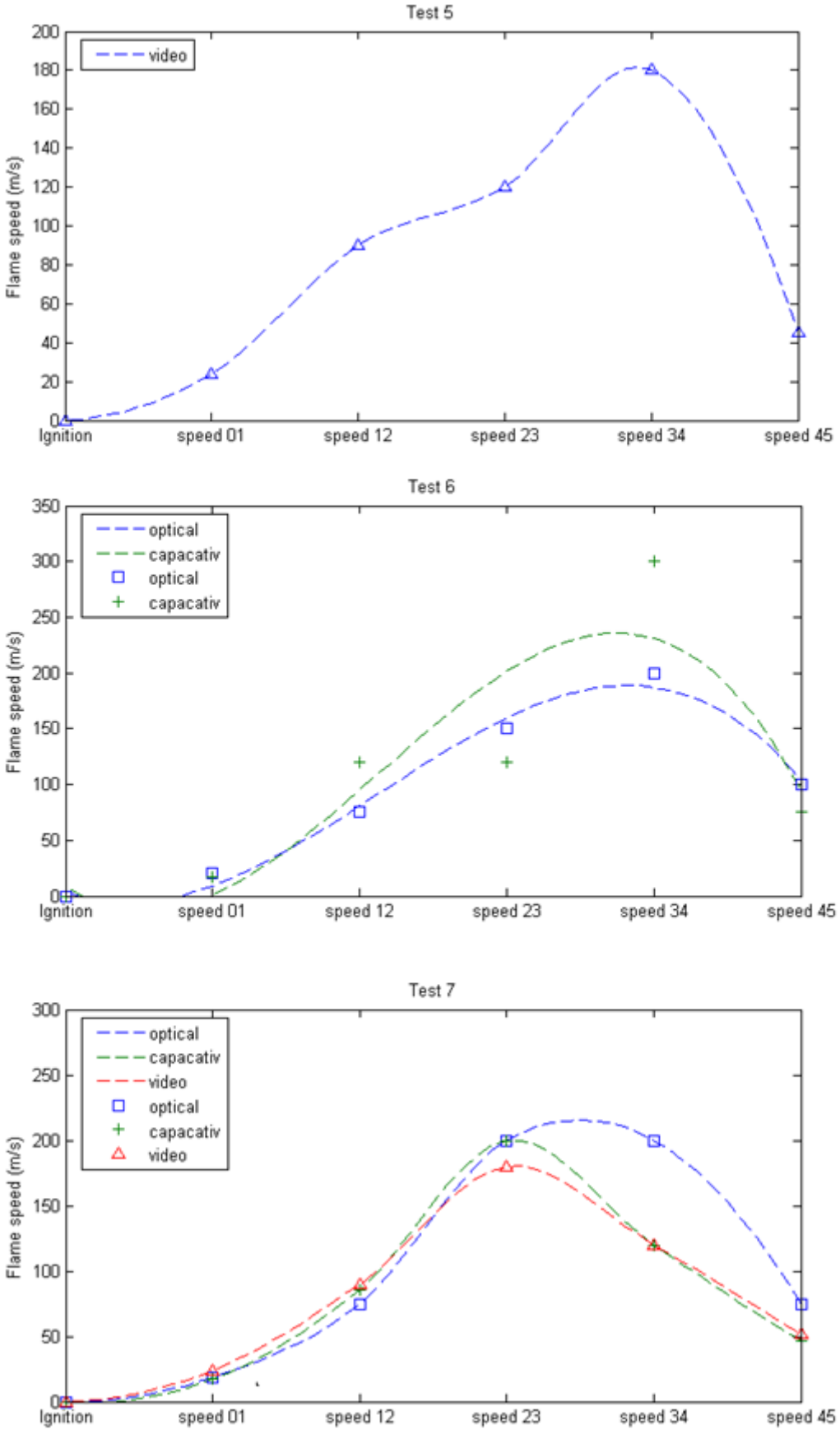

Figure 5-16 *Flame speed measurements for tests with 4.5 vol% propane in air.*

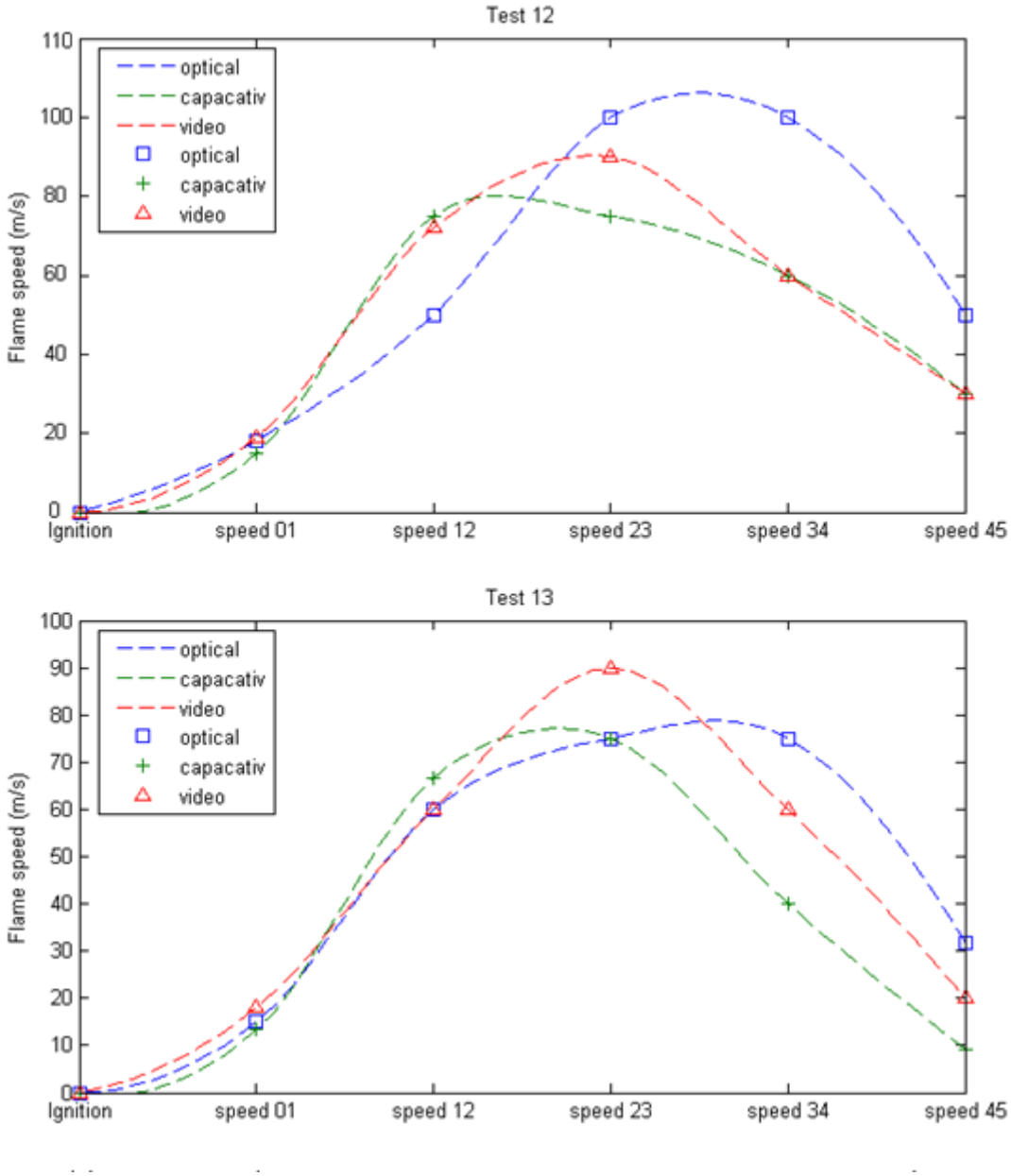

Figure 5-17 *Flame speed measurements for tests with 6.0 vol% propane in air.*

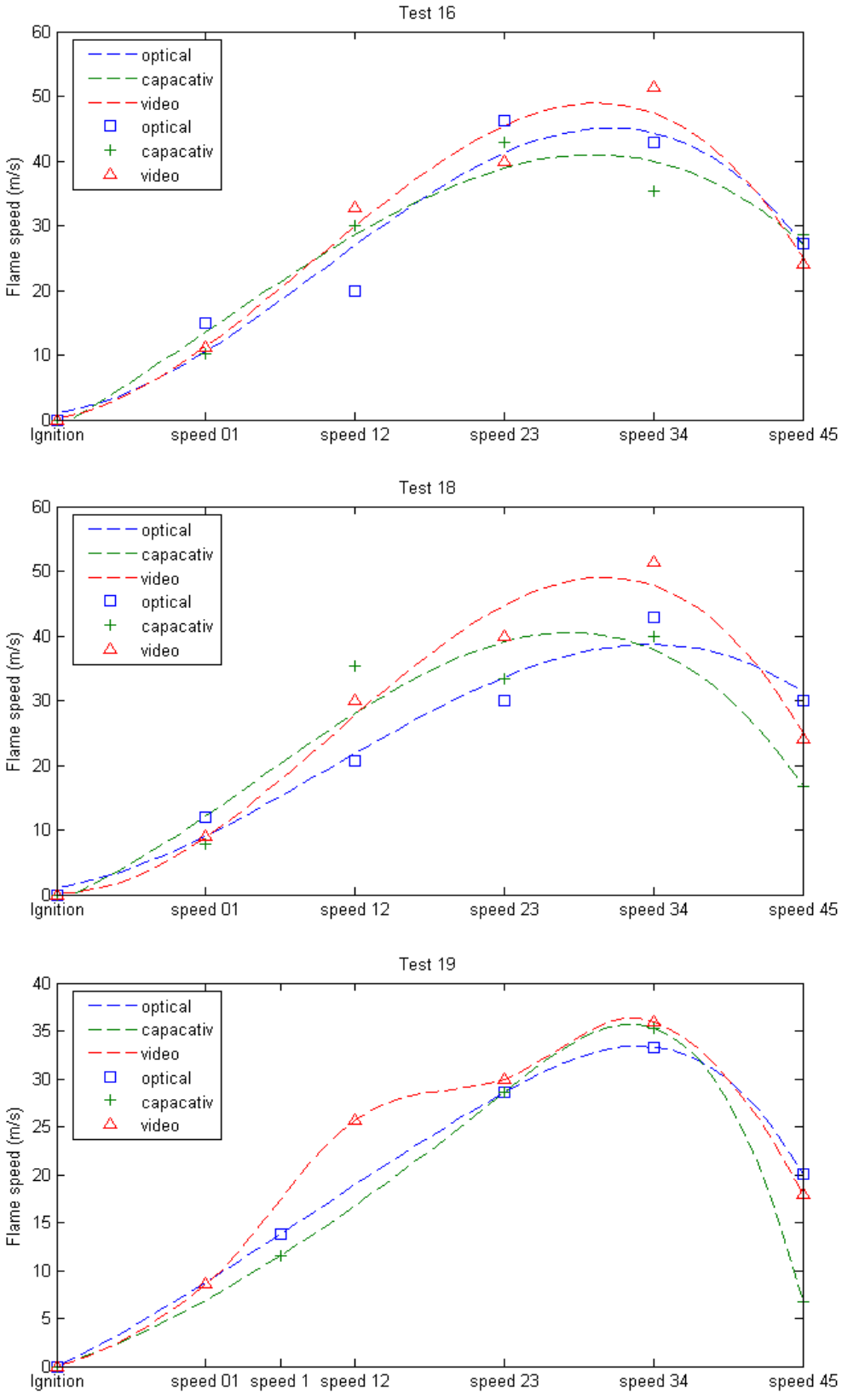

Figure 5-18 *Flame speed measurements for tests with 500 g/m3 of maize starch.*

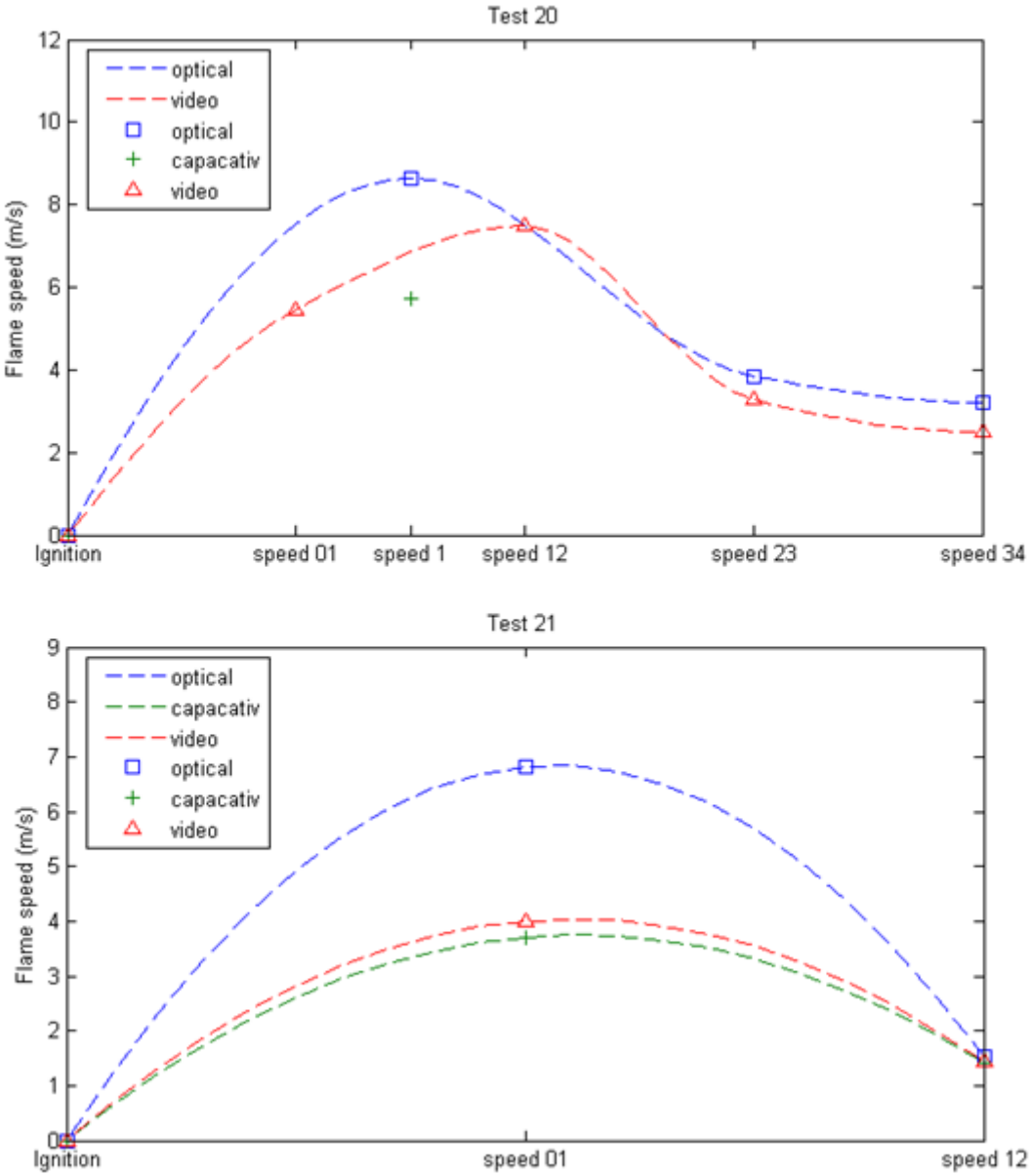

Figure 5-19 *Flame speed measurements for tests with 250 g/m3 of maize starch.*

5.6.1 Discussion of velocity profiles

The results from the flame speed measurements show quite good agreement between the various measurement principles, and the overall trends are consistent. The video and optical methods detect the flame first, and tend yield higher velocities between the point of ignition and the first probe station. The impedance and video analysis show quite good agreement regarding flame acceleration. Some of the results show significant variation, but this is reasonable given the inherent limitations in the various measurement principles when it comes to time resolution. One should keep in mind that the time resolution of the video analysis is 1/600 of a second, the capacitive measurement has a time resolution of 1 ms, and the optical method a estimated resolution of 1 ms. Hence the accuracy of the flame velocity is a function of flame speed:

$$P = \frac{S_f \cdot \Delta t}{L_t} \tag{5.3}$$

Where P is the accuracy, S_f is the measured flame speed, Δt is the time resolution and L_t is the distance between the probe stations.

Much of the deviation between the different measurement techniques is explained by this equation, since the flame speed is so high that the margin of error is larger than the actual deviation. Some of the deviations are related to the nature of the measurement method, as will be discussed in the following.

The experiments with stoichiometric gas mixture gave very high velocities, up to 300 m/s, according to the capacitive measurements for test 6. This high velocity does not agree well with the optical measurement, as it gave a velocity of about 200 m/s. However this is probably a result of poor time resolution compared to the velocity: 1 ms delay in flame arrival at station 4 (which is the time resolution) results in a velocity of 200 m/s. Hence the flame speed is too high for the capacitive method to be applied with a reasonable level of accuracy. If the mean velocity is to be determined within +/- 10%, for a time resolution of 1 ms, the maximum speed should not exceed 60 m/s.

The maximum flame speed in lean gas mixtures (by points, not lines) measured with different methods, gave a large range of results. In the same experiment, the capacitive measurement gave the maximum velocity between stations 1 and 2, the video had a velocity top between station 2 and 3 while the optical measurements showed a top between 3 and 4. The optical analysis gave the peak velocity top between 3 and 4 in all experiments with lean mixture. The capacitive method was the least reliable, as it varied from a top velocity between 1-2 and 3-4. Since the capacitive measurements already suffered from distortion and noise, these measurements are more unreliable. Lean mixtures gave less visible flame detection at probes 3, 4 and 5.

The experiments with rich mixture gave velocities up to 80 m/s, which is also slightly above the mentioned 60 m/s limit. The results of the video analysis and capacitive measurements gave similar velocity curves. The optical measurements suggested higher velocities between probe stations 4 and 5. These results, compared with the above mentioned unreliability of the capacitive method in lean gas mixtures, show that the capacitive probes are not able to measure lean gas flames in a good way, without further perfection of the electronics. The signals are simply too marginal to give good readings.

The dust experiments showed quite similar velocity development measured with the different techniques. This shows that the capacitive probes are able to measure dust flames. Video analysis seems to give a somewhat higher velocity than the two other techniques. Optical probes give less deceleration in the end of the tube, presumably because of the effect of slower flame and early flame arrival detection. The experiments with 250 g/m^3 resulted in flames that extinguished before they reached the end of the tube. The capacitive measurement did not indicate a flame at probe station 3 in test 20 contrary to both video analysis and optical measurements. Without further experiments one can only speculate weather this is due to the illumination of the dust cloud ahead of the flame, or that the probe did not detect the flame even though it actually passed the probe.

5.6.2 Discussion of velocity development, gas versus dust

The maximum flame speed for the dust flames tends to occur further down the tube compared to the experiments with gaseous mixtures. The dust flame may be more dependent upon the turbulence level, which is expected to be higher further down in the tube. The flame in a dust cloud is probably much thicker than the gas flame, something which may affect the location of the maximum speed. The pressure develops more slowly in relation to flame front propagation in a thick flame. This is because the mixture behind the flame front is not fully combusted, thus not fully expanded. If the flame position is plotted along the x-axis, and relative pressure along the y-axis dust explosions would give lower readings at probe station 5. However, this is not the case, as seen in Figure 5-20 where the dust give somewhat the same readings as gas experiments. The development is also similar for gas and dust.

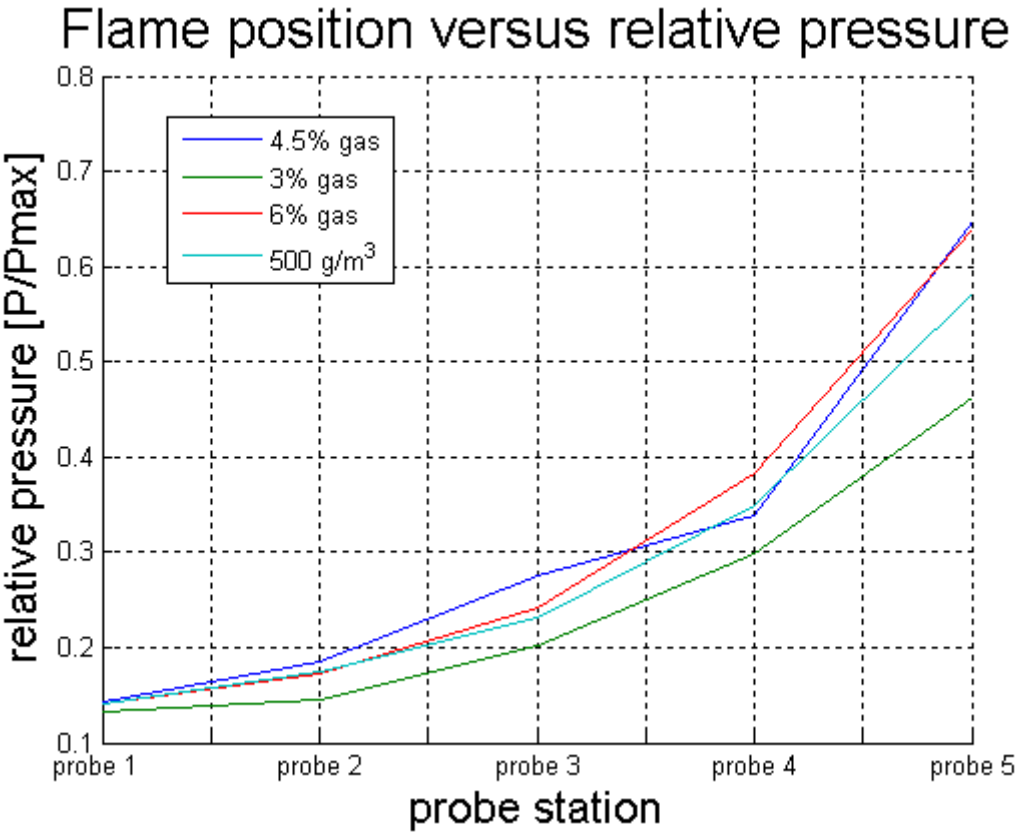

Figure 5-20 *Plotted flame position versus pressure development*

Furthermore some of the dust will drop out of suspension, making the dust concentration lower in the far end of the tube. The maize starch has a maximum KSt value of about 150-160 bar m/s at a concentration of 400 g/m^3. It should be noted that the optical probe measured a

top speed between probe stations 3 and 4 in most of the experiments. It should also be noted that the curve fitting of the velocity profiles is somewhat arbitrary. More experiments are needed to conclude, and hence prove or disprove this trend.

6 Conclusion

The FAT experiment has been instrumented, with a data acquisition and control system built around a NI CAD 6259 card. LabView has been used to program this card, and a computer controls the experiment. The probes containing the different measurement principles were built and tested.

The dispersion system were tested in order to document its effectiveness. Although it worked, the time needed to empty the reservoirs was somewhat long. A shorter dispersion time would give better control of the dispersion process and more flexibility with regard to varying the ignition delay time.

The main effort has been on developing an impedance measurement method for flames. Preliminary tests in a 20 litre explosion vessel proved the functionality of the technology prior to implementation in the FAT. A method for measuring the resonance frequency between a coil and a capacitor (the capacitor is the sensor) were developed, using a sweep generator. However the implementation in the FAT proved only partially successful, as some of the probes gave readings that was difficult to interpret.

6.1 The impedance measurement method

Some impedance measurements gave clear indication of flame arrival and some did not. The reason some of the probes failed to give good measurement is presumably mostly distortion by the diodes due to amplifiers and relatively weak signals. The lean mixtures of gas and dust gave less damping of the resonance and made the interpretation of flame arrival more challenging. Compared to other techniques (optical and video analysis) the capacitive measurements indicated later flame arrival times.

The capacitive probes which gave good readings proved that the measurements principle work. The recordings also gave indications that the method is quite sensitive, and it might be possible to measure dust concentration.

The main drawback of the method developed and tested in this thesis is the time resolution, which is limited to 1 ms. This is particularly important when the flame velocity is high, since a 1 ms difference in the readings may result in completely different flame speeds. The dust flames did not reach velocities where this error is decisive. If the impedance of the flame is needed this problem is not easily solved. However if one is satisfied with only the flame arrival time, the resolution can be dramatically improved.

The preliminary experiments in the 20 litre vessel gave promissing results that were straight forward to analyse and gave a reasonable development of both resonance frequency and damping. This is also possible to achieve in the FAT experiment, and would reveal more valuable information.

6.2 Experiments performed in FAT

Three propane-air mixtures were tested: one lean (3%), one close to stoichiometric mixture, (4.5%) and at last a rich mixture (6%). Dust explosions were also tested, with two different mixtures 500 and 250 g/m^3. The gas experiments proved two things: the time resolution of the impedance measurements and high speed video recordings is to crude, and the leaner mixtures give weaker flame indications. All three measurement techniques gave different flame arrival times. Presumably due to the physical behaviour of the different measured flame properties. For instance, video analysis is a subjective matter, especially when dealing with dust flames.

The experiments also indicate a pariticular differences between gas and dust explosions. The flame thickness might influences the flame acceleration, and whereas gas explosion experiments gave a maximum flame speed near the middle of the tube, dust explosions tended to reach the maximum flame speed closer to the end of the tube. The pressure measurements somewhat contradicts this theory, something which should be further investigated. Unfortunately the limited number of experiments performed this far are not enough to support these findings statistically.

6.3 Future work

The electronics of the probe can be perfected. This would allow further investigation of the measurements. Testing the alternative without the sweep generator would also be interesting. The method has proven its possibilities regarding flame detection. If the information of resistivity and capacitive is not necessary the method should be well suited as a flame arrival detector. The advantage of this method is a well defined area of measurement. It has also a fast response to changes, and should be able to keep up with a very fast flame.

A lot more experiments can be performed in the FAT, with different configurations of obstructions and with venting. One can also vary the type of dust. Also further investigation to find the most dust similar gas mixture should be done. It should also be considered to place a probe at the end of the tube.

References

Bartnecht, W. (1971) "Brenngas-und staubexplosionen." Forschungsbericht F45. Koblenz, Federal republic of Germany: Bundesinstitut für Arbeitsschuttz.

Dobashi, R. (2000). *Welding procedure of fine wire thermocouple.* Personal communication between R. Dobashi and R.K. Eckhoff, November 2000.

Eckhoff, R.K. (2003)*, Dust explosions in the Process industries,* third edition, Gulf Professional Publishing, Amsterdam

Eckhoff, R.K. (2005), *Explosion Hazards in the Process industries*, Gulf Professional Publishing, Houston, TX

Eckhoff, K., Moutrille, M. P. (2003b), *Determination of the laminar burning velocity of biomass dusts,* Confidencial.

Holbrow, P. (2004), DESC: Interconnected vented explosion tests. Report EC/04/30, HSL, Harpur Hill, Buxton, UK

Holbrow, P. (2005a), DESC: Phase 2: Interconnected vented explosion tests. Report EC/04/72, HSL, Harpur Hill, Buxton, UK

Holbrow, P. (2005b), Large scale explosions in vented coupled vessels. In International ESMG symposium, Nürnberg, Germany, 11-13 October 2005 (7pp.).

Huang, S. M., Stott A. L., Green R. G., & Beck M. S. (1988) Electronic transducers for industrial measurement of low value capacitances, J. Phy. E: Instrum. 21, 242-250.

Huang, S. M., Plaskowski A. B., Xie C. G., Beck M. S. (1989) Tomographic imaging of two component flow using capacitance sensors, J. Phy. E: Instrum. 22, 173-177

Kalvatn, I. B. (2009) *Experimental investigation of optical measurement method for detecting dust and gas flames in a flame acceleration,* master thesis.

Klein, A. J. J., van der Voort, M. M., van Zweden, A., & van Ierschot, P. G. A (2005a). Validating CFD-code 'DESC'; Large scale dust explosions in linked enclosed vessels, Report DV2 2005 CO24, TNO, Rijswiik, the Netherlands.

Klein, A. J. J., van der Voort, M. M., & Versloot, N. (2005b) Large scale dust explosions in linked enclosed vessels. In: International ESMG symposium, Nürnberg, Germany, 11-13 October 2005, (9pp.).

Kauffman, C.W., S. R. Srinath, F. I. Tezok, *et al.* (1984) "Turbulent and accelerating dust Flames.", Proceedings of the 20th Symposium (International) on combustion/The Combustion Institute

Pu, K. Y., Mauzurkiewicz J., Jarosinkski J., Kauffman C. W. (1988). *Comparative study of the influence of obstacles on the propagation of dust and gas flames*. Twenty-second symposium (International) on combustion/The Combustion Institute

R. Borghi, In: Bruno C, Casci C (eds) (1984), *Recent Advances in Aerospace Science*, Pergamon, London

Siwek R. (1996). *Determination of technical safety indices and factors influencing hazard evaluation of dusts.* Journal of Loss Prevention in the Process Industries 9, pp.21-31.

Skjold, T. (2003). *Selected aspects of turbulence and combustion in 20-litre explosion vessels*. Cand. Scient. Thesis, University of Bergen

Skjold, T., Eckhoff R. K., Enstad G. A., Kalvatn I. B., van Wingerden M., van Wingerden K. (2008), A modified balloon experiment for dust explosions, *Thirty-second International Symposium on Combustion*, Work-in-Progress Poster Session, Montreal

Tezok, F., Kauffman W. C., Sichel M., Nicholls J. A. (1985). *Turbulent burning velocity Measurments for dust/air mixtures in a constant volume spherical bomb*. Paper presented at 10th International Colloquium on Dynamics of Explosions and reactive systems, Berkley, CA,

"The Temperature Handbook" (2004). Middlesex UK: Labfacility Ltd

U.S. Chemical Safety and Hazard Investigation Board, Investigation Report*, Combustible Dust Hazard Study,* 2006, Report No. 2006-H-1

Waterfall, R. C., R., He, Beck C. M. (1997) Visulizing combustion using electrical impedance tomography, chemical engineering science, vol. 52, no. 13, pp. 2129-2138.

Wikipedia article on resonance, 20.04.2009

William I.G. (1983) The origin of the flame ionization detector Chromatographia Vol. 17 No. 5, May 1983

William I.G., Dewar R.A., (1958) in: Desty D.H. (Ed.), Proc. 2nd Symp. Gas Chromatogr. Discussion Group, Butterworth, London

A - Appendix Experimental Apparatus and Procedures

A-1 Electric Spark Generator

An electric spark generator has been made for preliminary experiments for both this project and others e.g. the modified balloon experiment (shown in appendix C). However, it did not generate enough energy to ignite pure dust clouds and is therefore only used for gas mixtures and hybrid mixtures with gas and dust. The energy generated has been estimated at around 50 mJ. Figure A-2 shows the schematic for the generator. Belonging partlist is shown Table A-1 The electronics of the generator is built into a cabinet with the size of 25 x 20 x 11 cm (L x W x H) and a handle on the top. The electrical circuit board within the spark generator has been made at the UiB.
The basic principle of the generator is to discharge a capacitor that has been loaded by electricity from the regular power net. Either a negative or a positive flank of voltage can manually, or externally trigger the spark generator. The desired setting is chosen on the front panel of the spark generator. The possibility to externally trigger the spark discharge makes it easy to trigger the spark from a computer, thus it is implemented in the Labview program for running the FAT experiment. Figure A-1 below shows the inner parts of the generator.

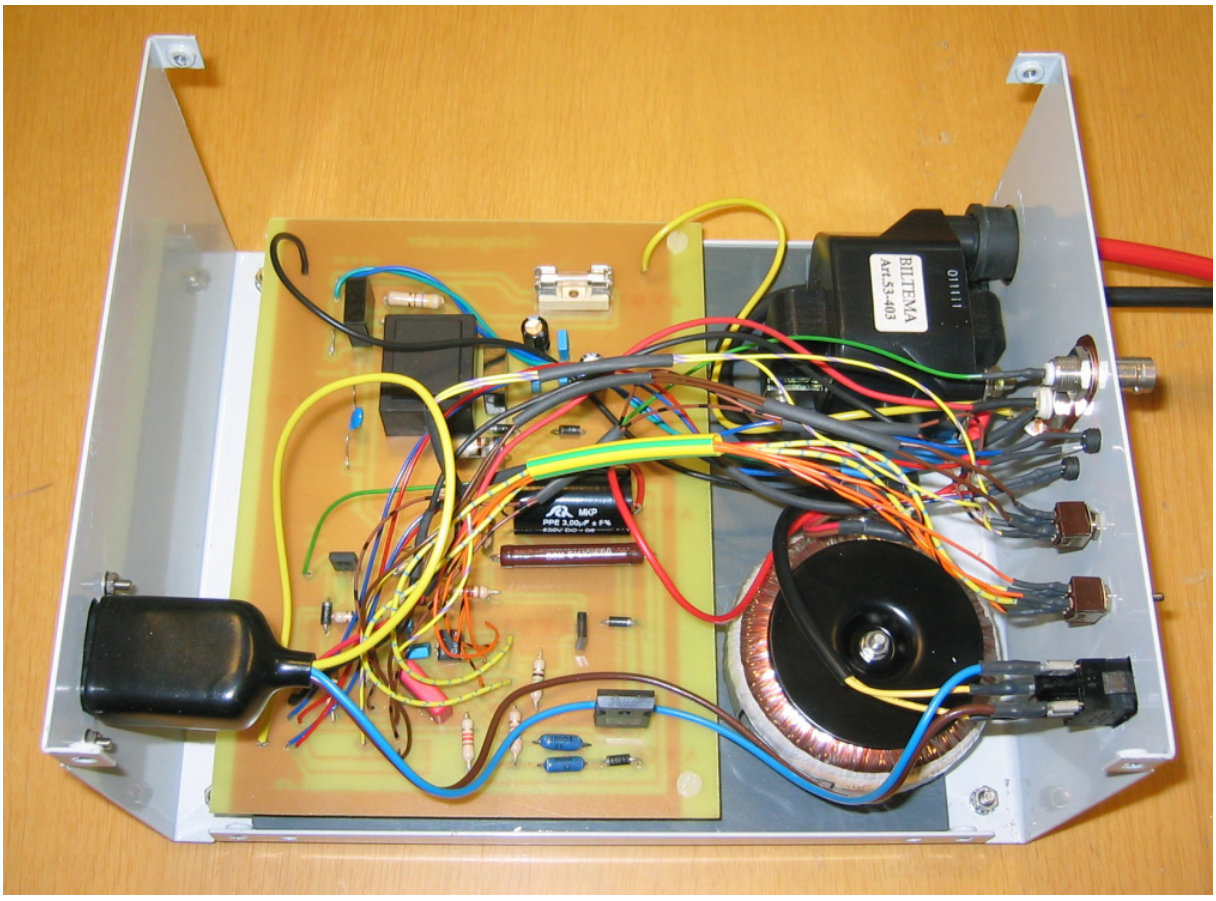

Figure A-1 Inner parts of the electric spark generator

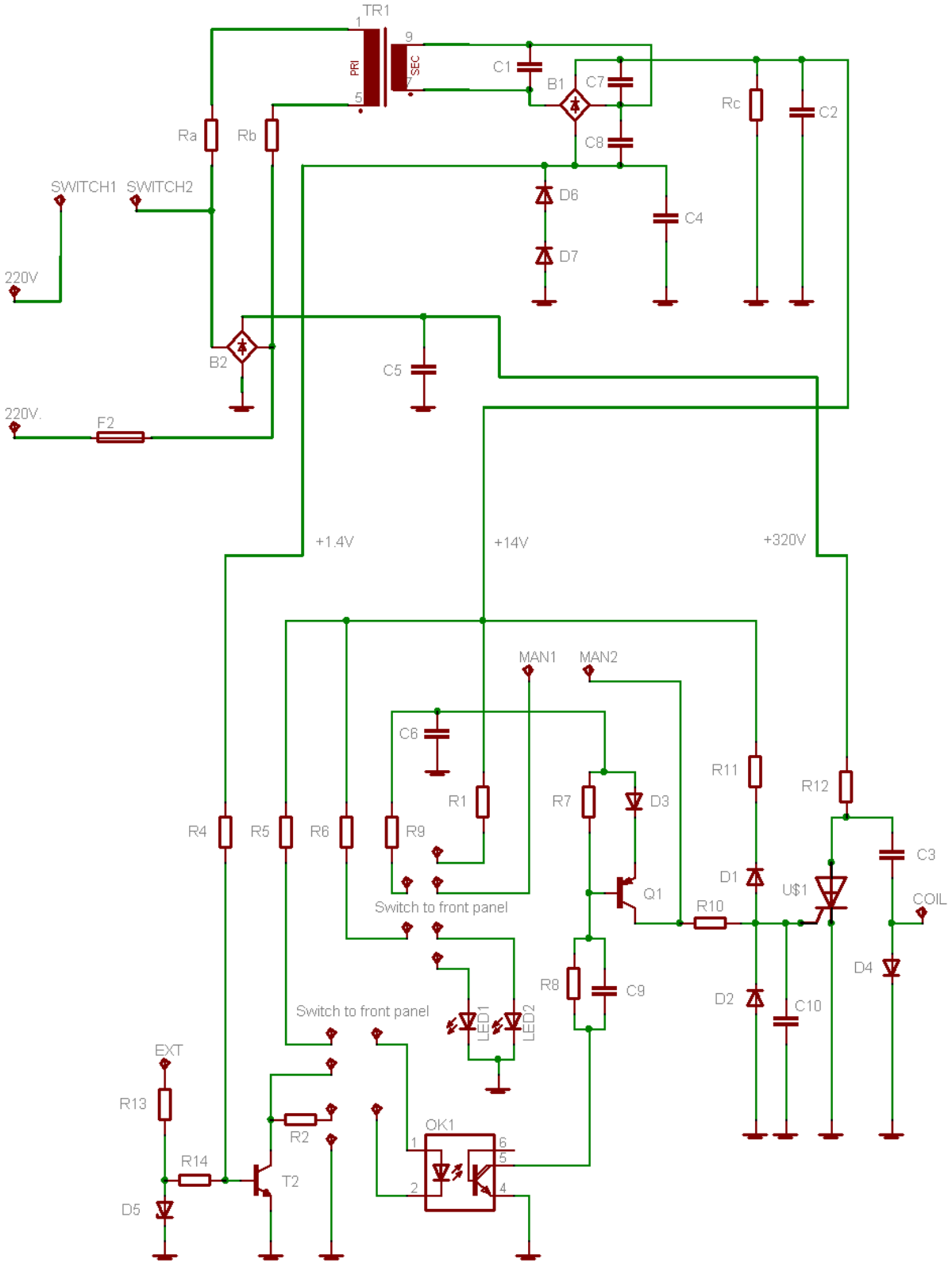

Figure A-2 Electrical circuit for spark generator

Table A-1 Partlist for spark generator

Part	Value	Device	
C3	1u/500V	C-EU275-113X316	capacitor
C6	2.2u	C-EU050-025X075	capacitor
C9	0.1u	C-EU025-024X044	capacitor
C10	0.1u	C-EU050-025X075	capacitor
D1	1N4004	1N4004	diode
D2	1N4004	1N4004	diode
D3	1N4004	1N4004	diode
D4	1N4004	1N4004	diode
D5	1N821	1N821	diode
LED1		LED5MM	led
LED2		LED5MM	led
OK1	4N33	4N33	optocoupler
Q1	BD140	BD140	transistor-pnp
R1	100	R-EU_0207/10	resistor
R2	15	R-EU_0207/10	resistor
R4	10k	R-EU_0207/10	resistor
R5	680	R-EU_0207/15	resistor
R6	1.2k	R-EU_0207/10	resistor
R7	1.2k	R-EU_0207/10	resistor
R8	1.2k	R-EU_0207/10	resistor
R9	220	R-EU_0207/10	resistor
R10	15	R-EU_0207/10	resistor
R11	100	R-EU_0207/10	resistor
R12	58K/2W	R-EU_0617/22	resistor
R13	470	R-EU_0207/10	resistor
R14	120	R-EU_0207/10	resistor
T2	BD139	BD139	transistor
U$1	30TPS08	30TPS08	triac
B1		SKB	rectifier
B2		SKB	rectifier
C1	0.1u	C-EU050-025X075	capacitor
C2	100u	C-EU050-025X075	capacitor
C4	100u	C-EU050-025X075	capacitor
C5	0.01u/400V	C-EU275-093X316	capacitor
C7	0.1u	C-EU050-025X075	capacitor
C8	0.1u	C-EU050-025X075	capacitor
D6	1N4004	1N4004	diode
D7	1N4004	1N4004	diode
F2		SH22,5A	fuse
Ra	470/1W	R-EU_0411/15	resistor
Rb	470/1W	R-EU_0411/15	resistor
Rc	680/1W	R-EU_0411/15	resistor
TR1		EI30-1	trafo
coil		Art.53-403	Biltema

A-2 Thermocouples

A thermocouple basically consists of a junction of two different metals. The junction creates a small voltage which increases with temperature. There is a variety of different thermocouples and they are classified by which materials the junction is made of. The most common type of thermocouples is type k, which is used in this project, where the two materials in use are Nickel-Chromium and Nickel-Aluminium. Its temperature range is from -200°C to 1100°C, its sensitivity is approximately 41µV/°C and they got an accuracy of about ±2.5°C (The temp. handbook). The thermocouples are bought from Elfa and the thickness of the metal wires is 0.3 mm. As shown in Figure A-3 below the use of thermocouples can be very easy using only a voltmeter.

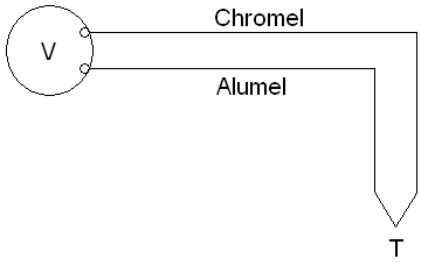

Figure A-3 S*chematic of temperature measurements using a thermocouple and voltmeter*

However, when sampling during continuous measurements, one has to amplify the signal from the thermocouple in order to get a strong signal and clear signal. Figure A-4 shows a thermocouple circuit, including an operational amplifier (AD597). With this circuit an output

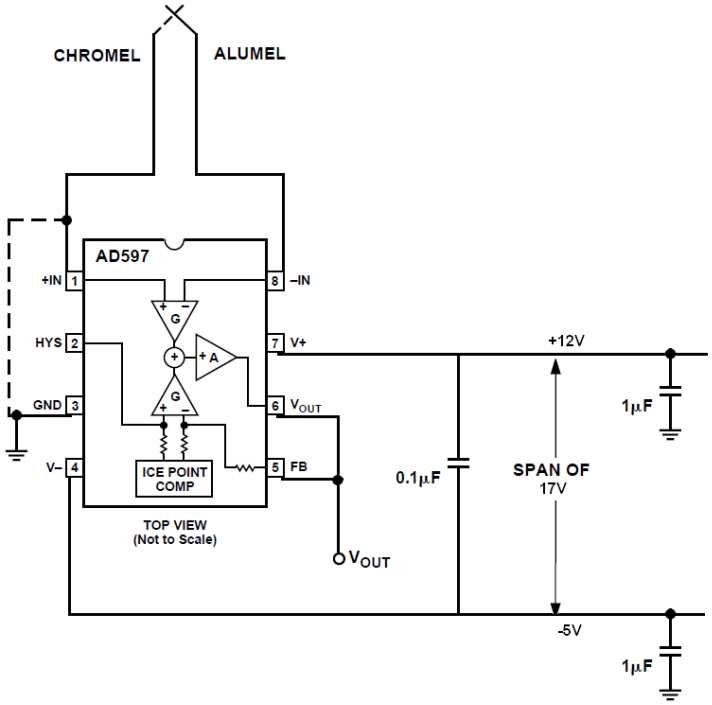

Figure A-4 *A thermocouple circuit including an operational amplifier*

voltage of 0V corresponds to a temperature of 0°C, 0.1V corresponds to 10°C, 1V corresponds to 100°C and so on.

The thermocouple probes are designed to fit both the 20-litre vessel at UiB and the FAT at Gexcon. Figure A-5 shows a picture of one of the thermocouple probes. The probe holders have been made by the mechanics at the Mechanical workshop at UiB, the welding of the thermocouples is done by the use of a self-made welding apparatus.

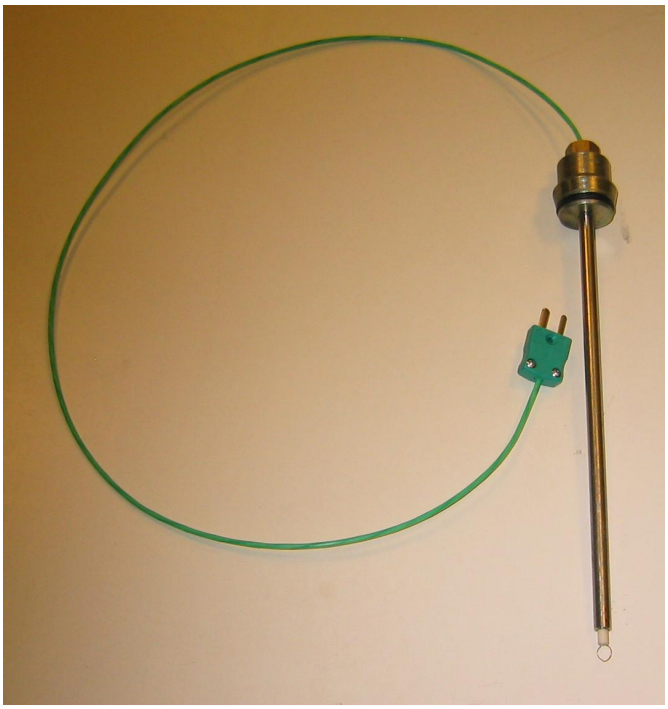

Figure A-5 *Thermocouple probe*

A-3 Welding apparatus for thermocouples

Figure A-6 shows the apparatus that has been made for welding together the two metal wires that the thermoelement consists of. The basic principle behind the apparatus is to first charge a condensator with power from the regular power net via a rectifier, and then to discharge it across the two wires (Figure A-6). This is done by, at one end of the cable, connecting one wire to the positive part of the condensator and the other to the negative part. At the other end of the cable the two wires are gently pushed against eachother until contact is made, and the condensator then discharges through the wires. The wires are then welded together.
To further improve the result, argon is added to the welding point during the process in an attempt to exel oxygen from the welding zone. This will, to some extent, prevent combustion to take place, and the melting/welding of the two materials will be the more dominant process.

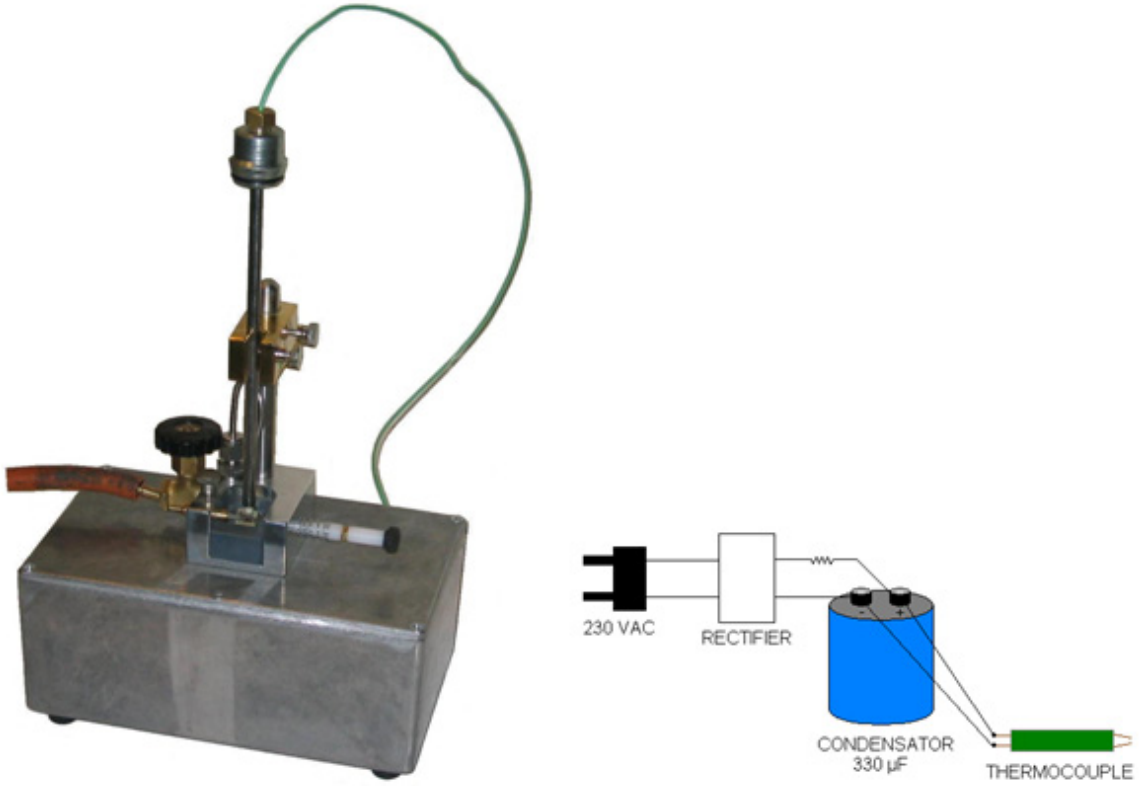

Figure A-6 *Left: welding apparatus for thermocouples. Right: simple schematic for welding apparatus*

A-4 Power supply

A-4.1 5V Power-supply circuit

Within the self-made power-supply, there is a circuit which gives an output voltage of 5V and also consists of a trigger function. The 5 V power supply is mainly used for various measurement instruments. Figure A-7 and Figure A-8 below shows the schematic and print board for this circuit.

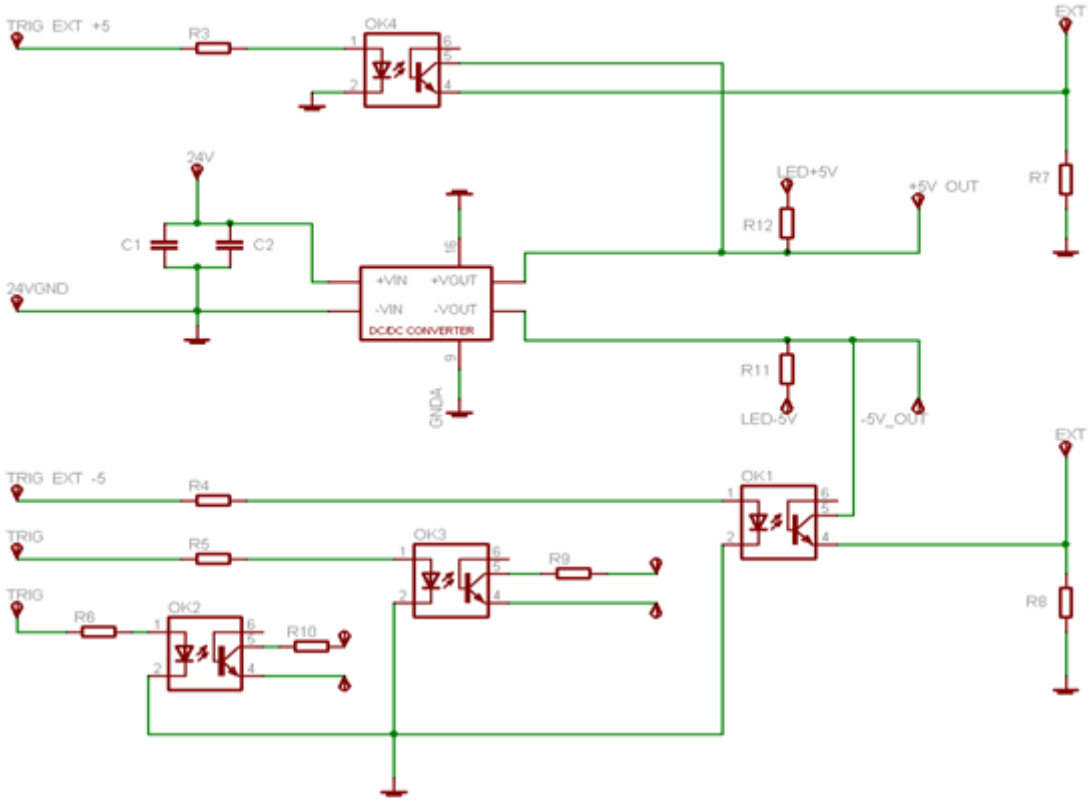

Part	Value	Device	
C1	10u	C2.5/4	capacitor-wima
C2	0.1u	C2.5/4	capacitor-wima
OK1	SFH601G	SFH601G	optocoupler
OK2	SFH601G	SFH601G	optocoupler
OK3	SFH601G	SFH601G	optocoupler
OK4	SFH601G	SFH601G	optocoupler
R3	1k	R-EU_0207/12	resistor
R4	1k	R-EU_0207/12	resistor
R5	1k	R-EU_0207/12	resistor
R6	1k	R-EU_0207/12	resistor
R7	100k	R-EU_0207/12	resistor
R8	100k	R-EU_0207/12	resistor
R9	0	R-EU_0207/12	resistor
R10	0	R-EU_0207/12	resistor
R11	470	R-EU_0207/12	resistor
R12	470	R-EU_0207/12	resistor
U$1	TEN5-2421	TEN5-2421	dc-dc-converter

Figure A-7 *Schematic of 5V circuit with belonging partlist*

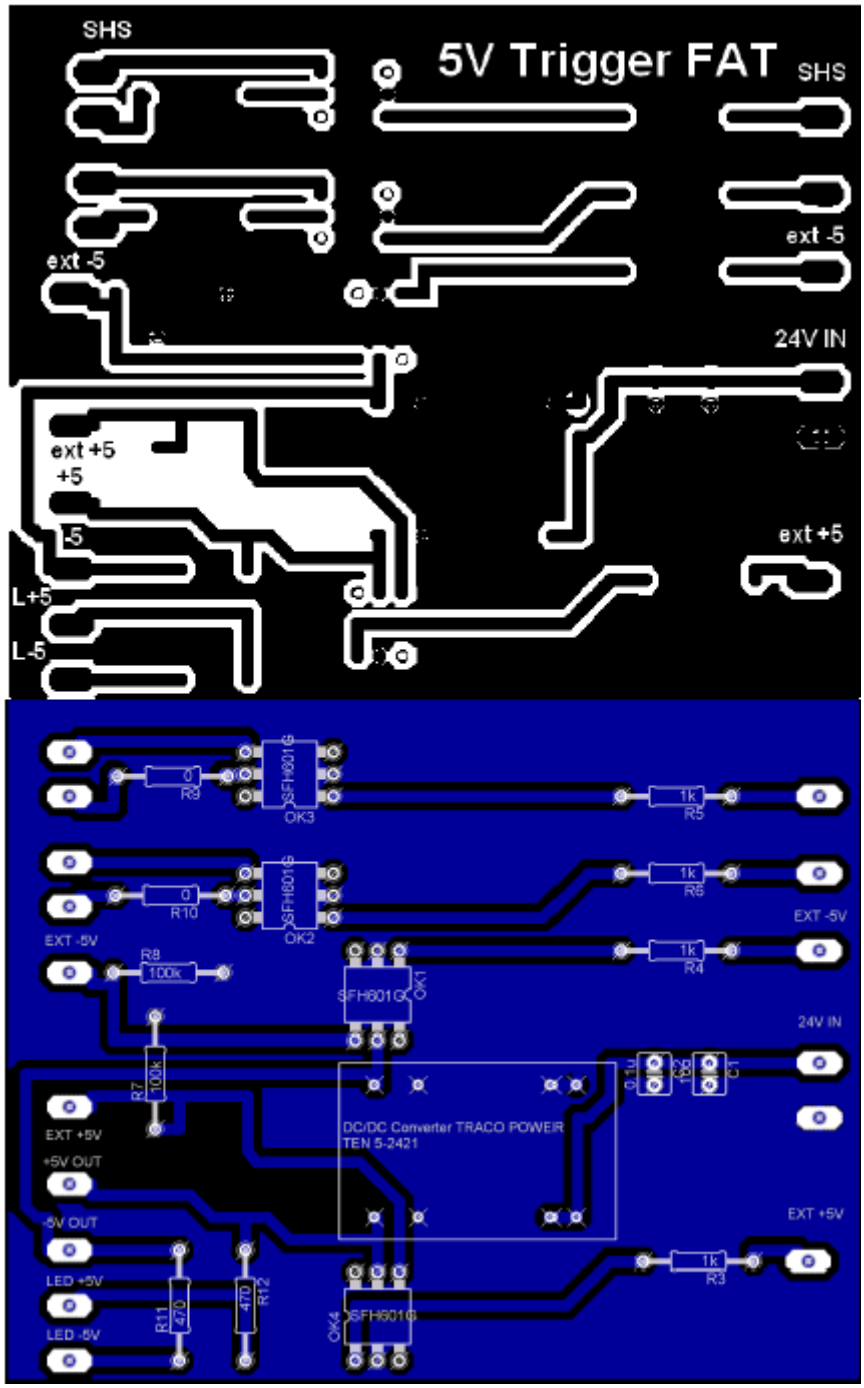

Figure A-8 *Circuit board print of 5 V trigger circuit in scale 1:1, with components added on the bottom picture*

A-4.2 12V Power-supply circuit

Within the self-made power-supply, there is a circuit which gives an output voltage of 12V and also consists of a trigger function. The 12V power supply is used for the thermocouples. In Figure A-9 and Figure A-10 below, the schematic and print board is given for this circuit.

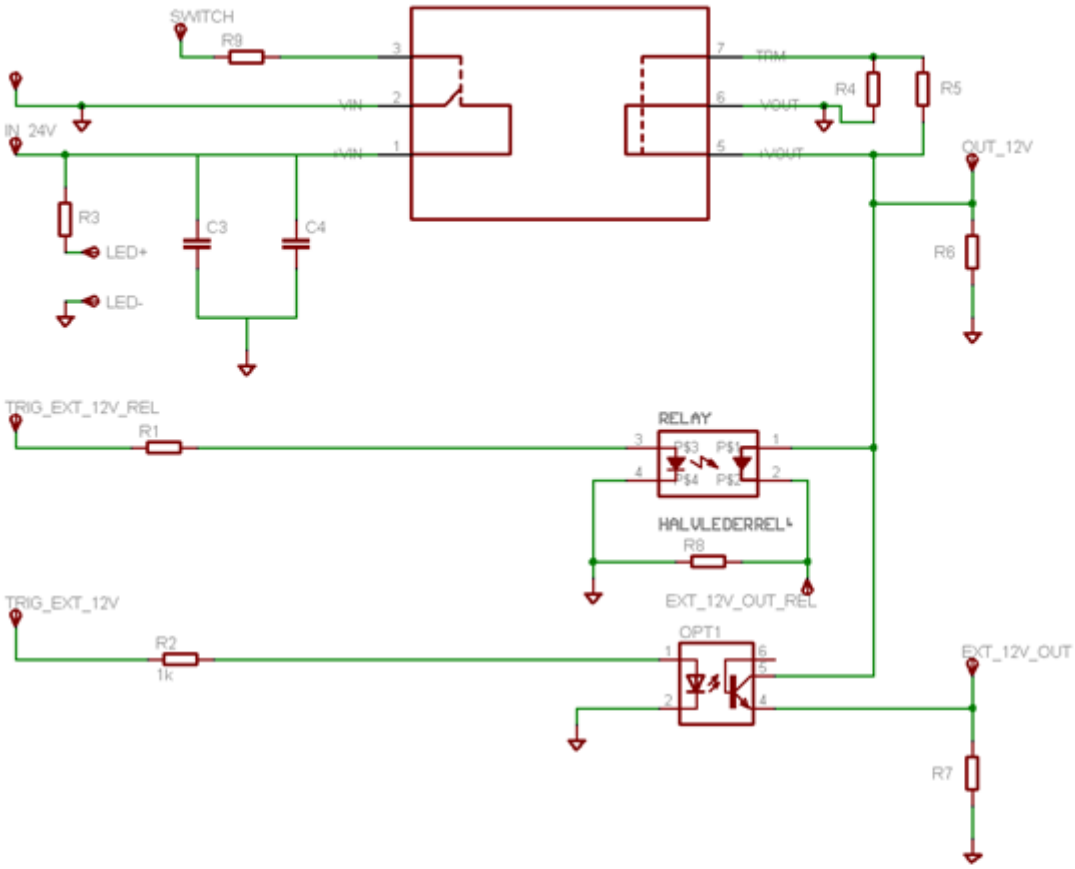

Part	Value	Device	
C3	10u	C2.5/6	capacitor
C4	0.1u	C2.5/6	capacitor
OPT1	SFH601G	SFH601G	optocoupler
R1	0	R-EU_0207/10	resistor
R2	1k	R-EU_0207/12	resistor
R3	1.8k	R-EU_0207/12	resistor
R4	?	R-EU_0309/12	resistor
R5	?	R-EU_0309/12	resistor
R6	100k	R-EU_0309/12	resistor
R7	100k	R-EU_0309/12	resistor
R8	100k	R-EU_0309/12	resistor
R9	0	R-EU_0207/10	resistor
RELAY	HALVLEDERRELÈ	HALVLEDERRELÈ	relay
U$1	TEN25-2412	TEN25-2412	dc-dc-converter

Figure A-9 *Schematic of 12V circuit with belonging partlist*

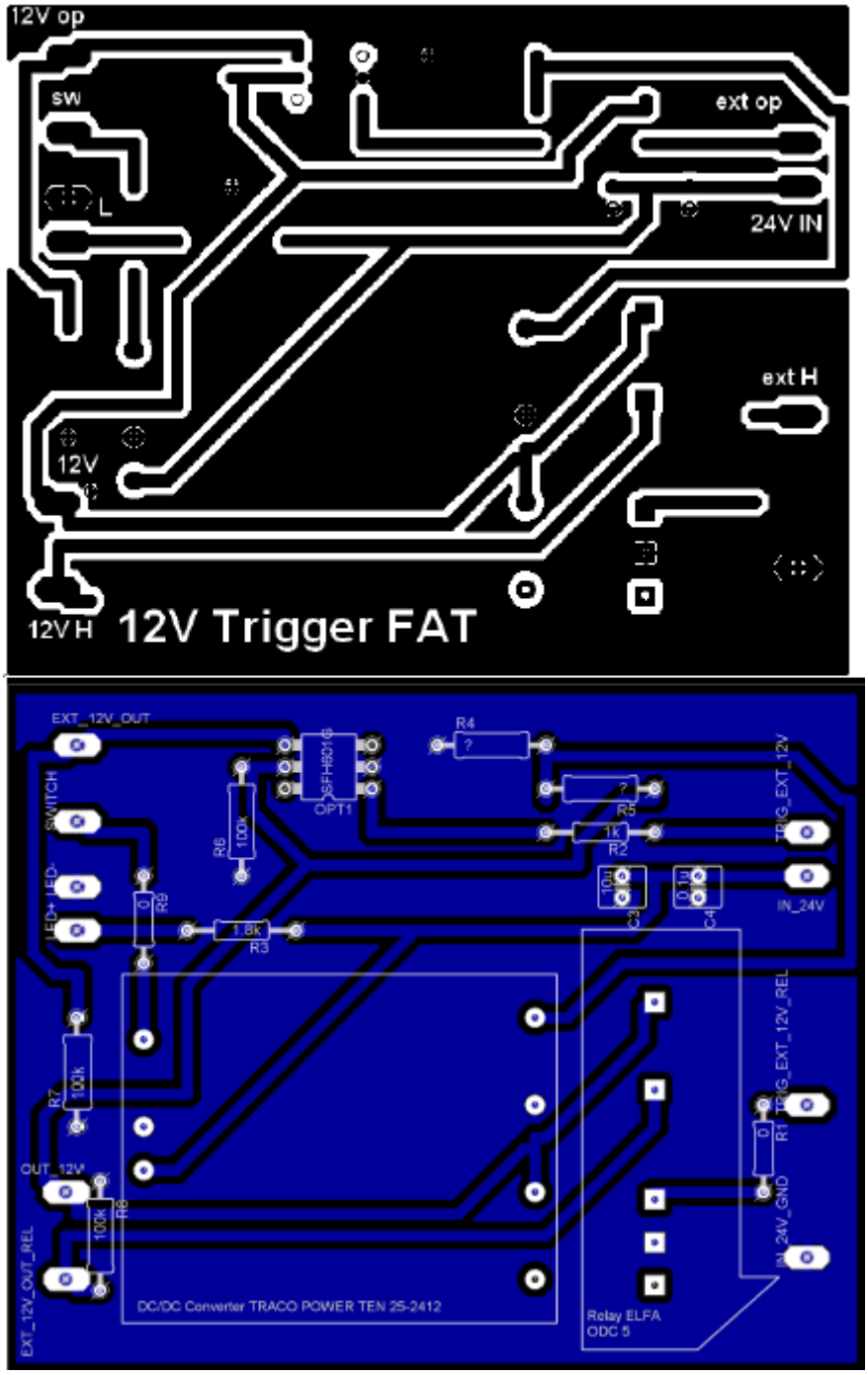

Figure A-10 *Circuit board print for 12 V trigger circuit in scale 1:1, with components added on the bottom picture*

A-4.3 24V Power-supply circuit

Within the self-made power-supply, there is a circuit which gives an output voltage of 24V and consists of a trigger function, which is used for the dispersion valves. In Figure A-11 and Figure A-12below, the schematic and the print board is given for this circuit.

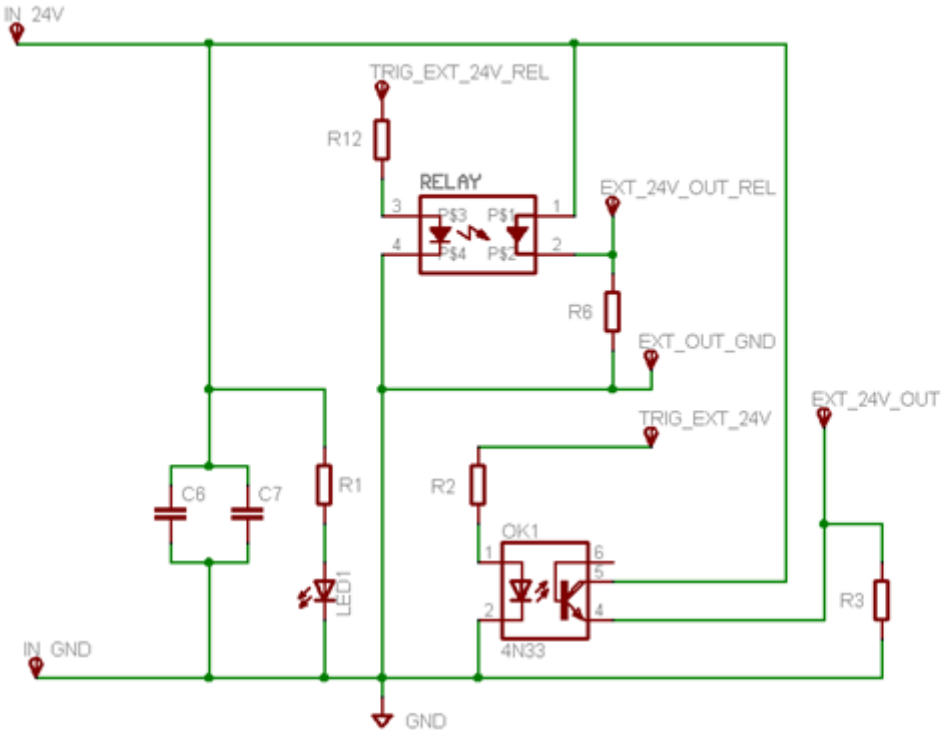

Part	Value	Device	
C6	10u	C-EU050-030X075	capacitor
C7	0.1u	C-EU050-030X075	capacitor
LED1		LED3MM	led
OK1	4N33	4N33	optocoupler
R1	1.8k	R-EU_0411/12	resistor
R2	1.5k	R-EU_0309/12	resistor
R3	100k	R-EU_0204/5	resistor
R6	100k	R-EU_0204/5	resistor
R12	0	R-EU_0411/12	resistor
RELAY	HALVLEDERRELÈ	HALVLEDERRELÈ	relay

Figure A-11 *Schematic of 24V circuit with belonging partlist*

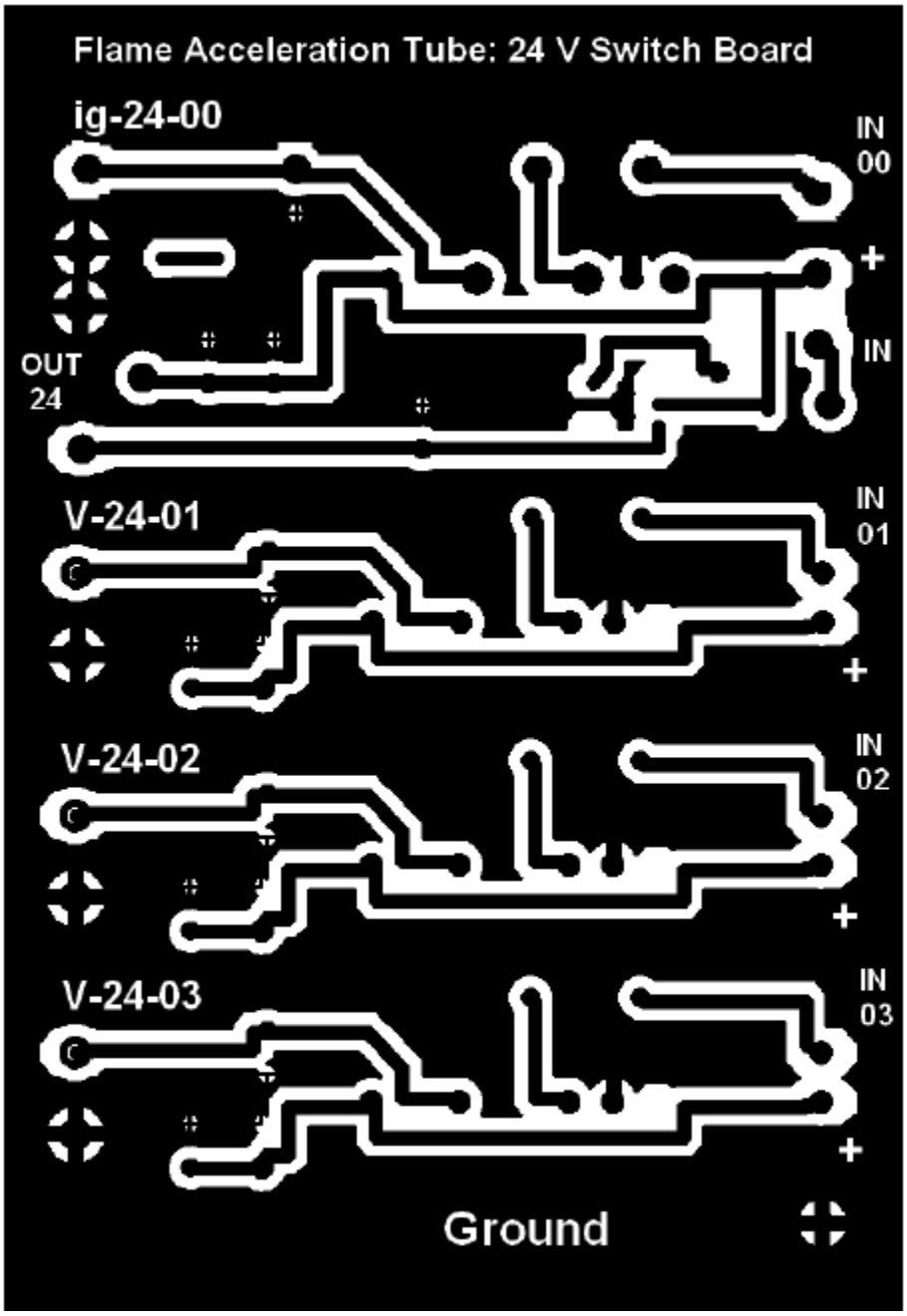

Figure A-12 *Circuit board print of 24 V circuit in scale 1:1*

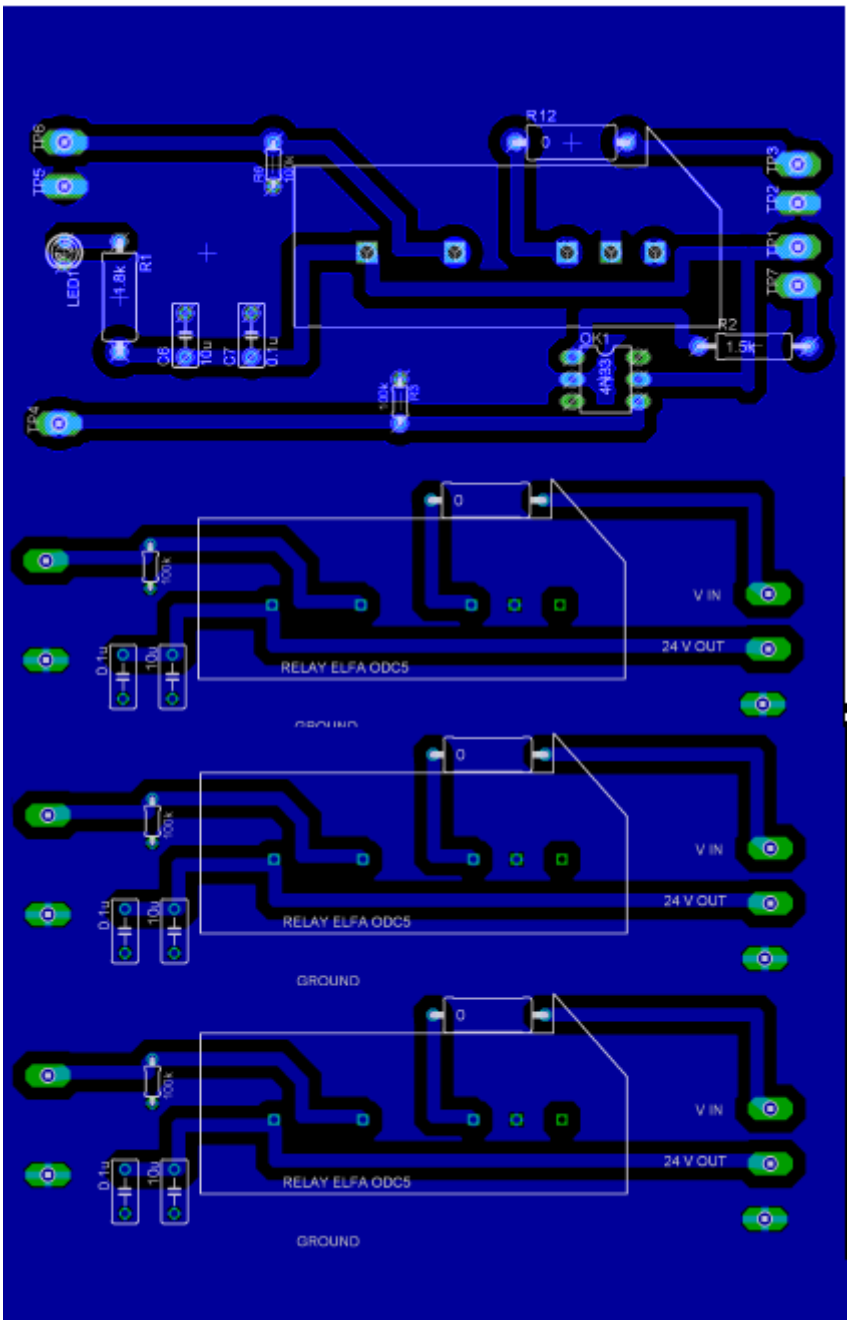

Figure A-13 *Circuit board print with components for 24 V circuit in scale 1:1*

A-5 Mechanical Drawing of the Measurement Probe

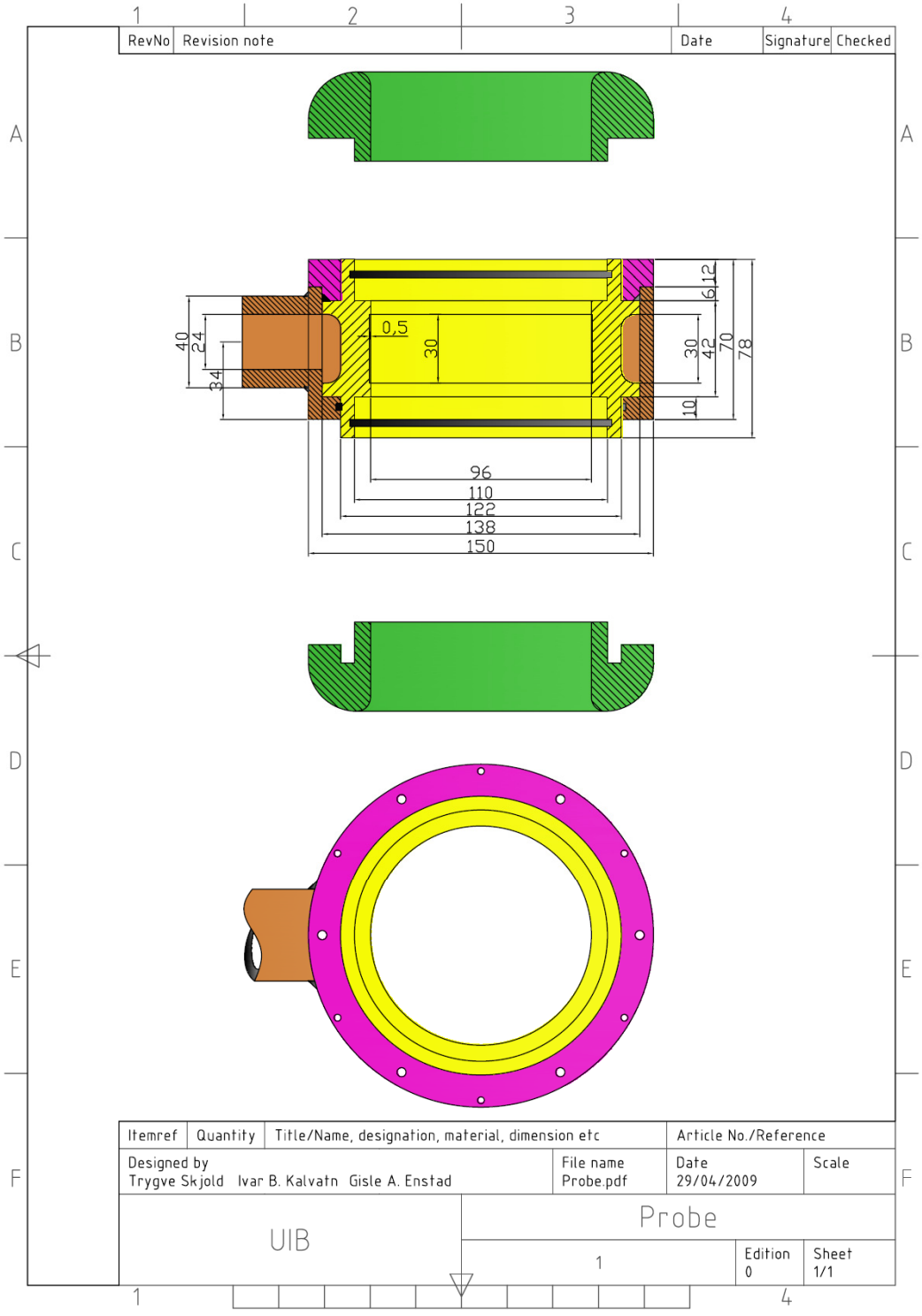

Figure A-14 *Mechanical drawing of the optical/capacative probe*

A-6 User Documents for the FAT

A-6.4 Checklist – FAT

What to check	
Vacuum	_____ barg
Reservoir pressure	_____ barg
Security valve closed	
Specify filename in labview	
Reset signal amplifier for reservoir pressures	
Close reservoir valves	
Check test number	
Secure area	
Spark generator on	

A-6.5 Log

Table A-2 *The log of the experiments performed*

Log						
Propane/air-mixtures						
Test number	consentration	dispersion 1	dispersion 2	dispersion 3	ignition	comment
	vol %					
5	4,5	100	100	100	800	
6	4,5	100	100	100	800	No video
7	4,5	100	100	100	800	
8	2,4	100	100	100	800	No ignition
9	2,8	100	100	100	800	No initial turbulence, 0,4% filled in ignition end
10	3	100	100	100	800	
11	3	100	100	100	800	
12	6	100	100	100	800	
13	6	100	100	100	800	
						chemical igniter
14	3	100	100	100	800	no ignition
15	3	100	100	100	800	no initial turbulence
Maize starch						
Test number	consentration	dispersion 1	dispersion 2	dispersion 3	ignition	comment
	g / m^3					
16	500	100	100	100	800	
17	500	100	100	100	800	no ignition
18	500	100	100	100	800	
19	500	100	100	100	800	
20	250	100	100	100	800	
21	250	100	100	100	800	

A-6.6 User guide for the Labview program for running the experiment

A program was made, based on Labview, in order to run the experiment. In the front panel of the program, shown in Figure A-15, timing of dispersion and ignition can be set. In the block diagram, shown in the same figure, input/output-channel settings can be chosen by the use of the data acquisition (DAQ) assistants. To activate the program, press the arrow button in the upper left corner of the front panel. This button does not start the experiment. To make the program ready to start press the OK button. The experiment can now be activated by the externally trigger switch, which is connected to the NI-logging card. Before every experiment it is important that the file name for the logging file is defined. This can be done via the file path dialog box.

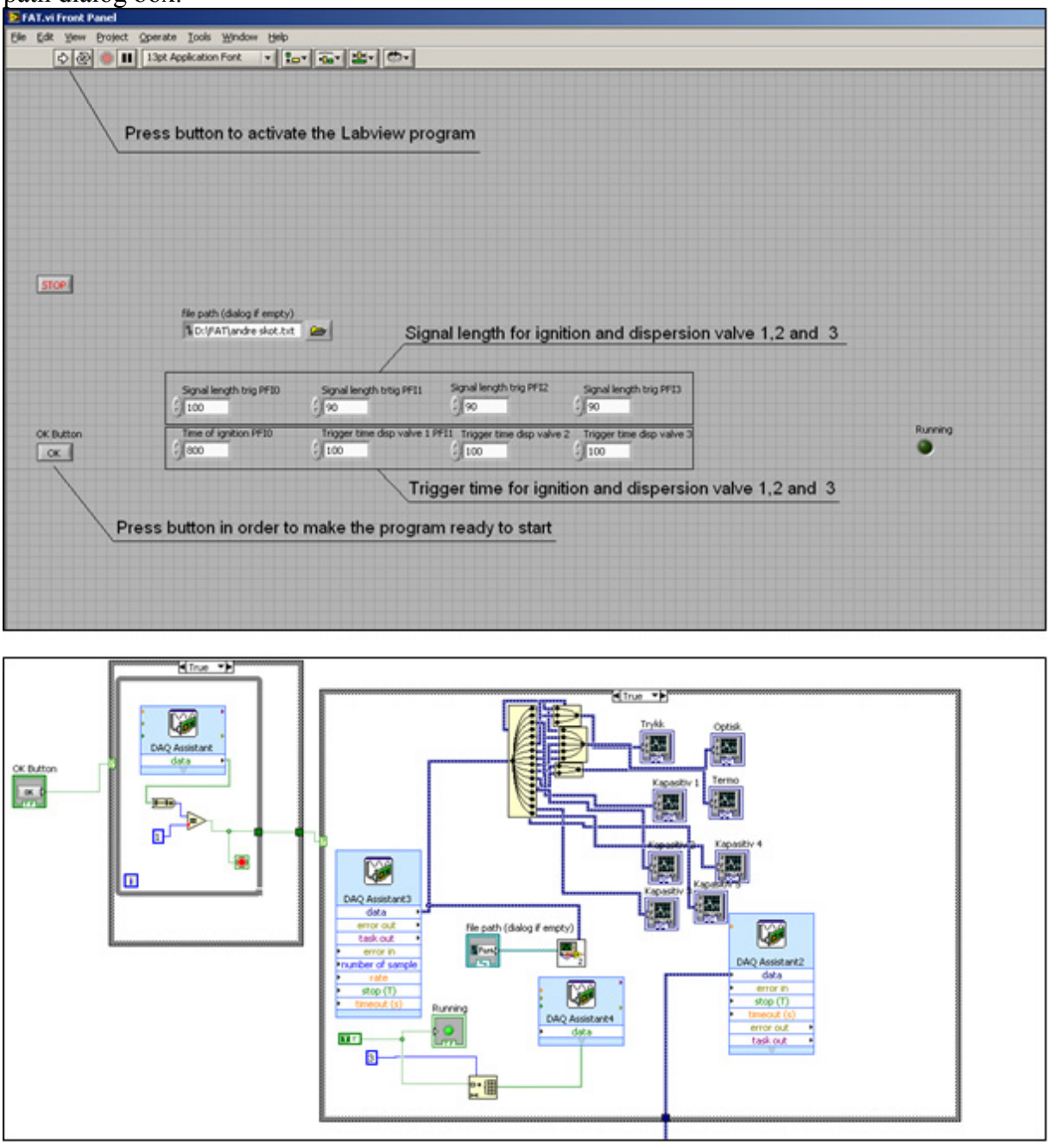

Figure A-15 Upper: front panel for the program. Lower: part of the block diagram with the DAQ assistat

B - Appendix Measurement Data and Analysis

B-1 Flame Arrival/Speed measurements

Pressure measurements are presented in Table B-1, Table B-2 shows data from video observations as well as results from the measurements done with the optical/capacitive probes and the thermoelement in the FAT.

Table B-*1 Results from pressure measurements*

Pressure development for tests in the Flame Acceleration Tube						
Test number	**Probe station**					**Maximum pressure**
	1	2	3	4	5	
	Pressure bar(a)					
6	1,241	1,699	2,715	3,482	5,517	8,58
7	1,168	1,421	1,896	2,208	5,34	8,18
10	1,107	1,2	1,563	2,454	4,198	6,16
11	1,126	1,248	1,835	2,564	3,561	5,78
12	1,189	1,485	2,078	3,261	5,403	7,38
13	1,167	1,4114	1,9861	3,1704	5,316	6,88
16	1,168	1,488	1,983	3,028	4,432	7,28
18	1,166	1,438	1,939	2,9	4,753	7,18
19	1,189	1,461	1,903	2,842	5,181	6,78

Table B-2 Results from measurements after experiments in the FAT

Flame arrival/speed measurements												
		Location										
Test number	Principle	0 (Ignition)	Speed 01	1	Speed 12	2	Speed 23	3	Speed 34	4	Speed 45	5
5	optical probe											
	capacativ probe											
	video	0,000	24	0,025	90	0,032	120	0,037	180	0,040	45	0,053
	thermocouples											
6	optical probe	0,744	20	0,774	75	0,782	150	0,786	200	0,789	100	0,795
	capacativ probe	0,744	17	0,780	120	0,785	120	0,790	300	0,792	75	0,800
	video											
	thermocouples	0,744						0,790				
7	optical probe	0,791	19	0,823	75	0,831	200	0,834	200	0,837	75	0,845
	capacativ probe	0,791	17	0,826	86	0,833	200	0,836	120	0,841	46	0,854
	video	0,000	24	0,025	90	0,032	180	0,035	120	0,040	51	0,052
	thermocouples	0,791						0,842				
8	optical probe											
	capacativ probe											
	video	----------										
	thermocouples											
9	optical probe	0,786	6	0,888	30	0,908	30	0,928	33	0,946	10	1,009
	capacativ probe	0,785	5	0,895	32	0,914	27	0,936	20	0,966	3	1,142
	video	0,000	13	0,047	28	0,068	30	0,088	20	0,118	7	0,203
	thermocouples											
10	optical probe	0,792	4	0,926	26	0,949	32	0,968	33	0,986	8	1,060
	capacativ probe	0,792	4	0,927	22	0,954	38	0,970	12	1,020	16	1,058
	video	0,000	12	0,052	26	0,075	30	0,095	18	0,128	10	0,188
	thermocouples	0,792						0,973				
11	optical probe	0,754	10	0,814	60	0,824	60	0,834	67	0,843	25	0,867
	capacativ probe	0,752	10	0,814	43	0,828	35	0,845	46	0,858		
	video	0,000	21	0,028	51	0,040	51	0,052	36	0,068	17	0,103
	thermocouples	0,754						0,840				
12	optical probe	0,792	18	0,825	50	0,837	100	0,843	100	0,849	50	0,861
	capacativ probe	0,789	15	0,829	75	0,837	75	0,845	60	0,855	30	0,875
	video	0,000	19	0,032	72	0,040	90	0,047	60	0,057	30	0,077
	thermocouples	0,792						0,845				
13	optical probe	0,788	15	0,828	60	0,838	75	0,846	75	0,854	32	0,873
	capacativ probe	0,788	13	0,833	67	0,842	75	0,850	40	0,865	9	0,930
	video	0,000	18	0,033	60	0,043	90	0,050	60	0,060	20	0,090
	thermocouples	0,788						0,849				
14	optical probe											
	capacativ probe											
	video	----------										
	thermocouples											
15	optical probe	0,788	7	0,880	13	0,925	14	0,968	10	1,030	4	1,168
	capacativ probe	0,786	5	0,899	17	0,934				1,100	6	1,200
	video	0,000	6	0,103	13	0,148	16	0,185	7	0,273	3	0,452
	thermocouples											
16	optical probe	0,788	15	0,828	20	0,858	46	0,871	43	0,885	27	0,907
	capacativ probe	0,788	10	0,847	30	0,867	43	0,881	35	0,898	29	0,919
	video	0,000	11	0,053	33	0,072	40	0,087	51	0,098	24	0,123
	thermocouples											
17	optical probe											
	capacativ probe											
	video	----------										
	thermocouples											
18	optical probe	0,788	12	0,838	21	0,867	30	0,887	43	0,901	30	0,921
	capacativ probe	0,788	8	0,865	35	0,882	33	0,900	40	0,915	17	0,951
	video	0,000	9	0,067	30	0,087	40	0,102	51	0,113	24	0,138
	thermocouples											
19	optical probe	0,787		14		0,874	29	0,895	33	0,913	20	0,943
	capacativ probe	0,787		12		0,891	29	0,912	35	0,929	7	1,018
	video	0,000	9	0,070	26	0,093	30	0,113	36	0,130	18	0,163
	thermocouples											
20	optical probe	0,788		9		0,927	4	1,083	3	1,270	----------	
	capacativ probe	0,788		6		0,997						
	video	0,000	5	0,110	8	0,190	3	0,373	2	0,615	----------	
	thermocouples											
21	optical probe	0,787	7	0,875	2	1,269	----------					
	capacativ probe	0,787	4	0,949	1	1,373						
	video	0,000	4	0,150	1	0,570	----------					
	thermocouples											

B-2 Matlab Programs

FileReader
This script reads in a txt file and converts commas to dots. It also organises the data into different files, so that the optical data is put into one, pressure measurement is put into one, and so on.

```
% This program reads measurement data from the logging files and exports
% the measurement data in a file, with a binary format, for each measurement
% channel
clear all
for test = n:m; %n is the staring test number, while m is the ending
fid  = fopen(['test' num2str(test) '.txt'],'r');
A = zeros(200000,16);
for i = 1:200000
Line = fgetl(fid);
Line = strrep(Line,',','.');
line = str2num(Line);
A(i,1:16)=line;
i
end
fclose(fid)
capch = [13,14,15,3,16]
optproch = [1,2,7,8]
thermoch = [10]
prch = [4,5,6]
PrRes = A(:,1:3);
Time = 0:1/50000:4;
PrTub = [Time(1:end-1)', A(:,prch)];
CapPro = [Time(1:end-1)', A(:,capch)];
TempPro = [Time(1:end-1)', A(:,thermoch)];
OptPro = [Time(1:end-1)', A(:,optproch)];
fid = fopen(['cap' num2str(test) '.bin'], 'w+');
count = fwrite(fid, CapPro, 'double');
fclose 'all'
fid = fopen(['opt' num2str(test) '.bin'], 'w+');
count = fwrite(fid, OptPro, 'double');
fclose 'all'
fid = fopen(['Temp' num2str(test) '.bin'], 'w+');
count = fwrite(fid, TempPro, 'double');
fclose 'all'
fid = fopen(['PrTub' num2str(test) '.bin'], 'w+');
count = fwrite(fid, PrTub, 'double');
fclose 'all'
end
```

resan
This is a script used to open, and analyse the data. In this routine the resonance frequency is found.

```
clear
```

```
err = 0;
%Open file
root = 'cap';
fest = 0;
for test = 7:3:13
    test
    fest = fest+1;
    'gf'
    name = ['cap' num2str(test) '.bin'];
    [A] =  FileOpen(name);
    %setting different variables
    %defining which column that holds different information.
    Fk = 0; %frequency
    Rk = 2; %resonant curve
    vFk = 7; %frequency voltage curve
    %If the spark is indicated in a channel, these variables defines the
    %timeinterval which is analysed.
    N = 0.5;    %time before spark
    O = 1;      %time after spark
    %Locating resonant curves if voltage is used as a frequency reference
    [index, jumpovers, Time] = indexer(vFk, A);
    [v2f,k,pf] = voltagefreqency (vFk,vF,A, index);
    %investigating individual probes
    for probe = 1:5
        probe
        Rk = probe + 1;
        [S, Integral(:,probe)] = surfer(A, index,Rk,vF);
        Integral(:,probe) = Integral(:,probe)/mean(Integral(2:20,probe));
        ape(:,fest) = Integral(1:3894,probe);
        VF = sum(vF,2)./numel(vF(1,:));
        SF = sum(S,2)./numel(S(1,:));
        n = 1;
        %identifying and removing noise
        for i = 1:numel(vF(1,:))-1
            VFe = vF(:,i)- VF(:);
            SFe = S(:,i) - SF;
            sumo = find(abs(VFe) > 0.3);
            subo = find(abs(SFe) > 0.7);
            if ~isempty(sumo) || ~isempty(subo)
                jumpy(n) = i;
                n = n + 1;
            end
        end
        clear VF SF VFe SFe sumo subo n
        a = size(A(1,:));
        index(end,2)= a(1,2);
        a = size(index);
        n = 3;  %polynom degree for curve fitting
        ppf = zeros(n+1,a(1,1)-1);
        dppf = zeros(n,a(1,1)-1);
```

```
        ddppf = zeros(n-1,a(1,1)-1);
        eskil = zeros(1,a(1,1)-1);
        %This for loop locates resonance tops. It fitts a polynom to the
        %measured data, derivates this, and locates the top. Also the
        %second derivative in the top is calculated. This can be used to
        %find the capacitance and resistance. Firts loop finds the indicies
        %of top, second does the mentioned calculation.
        for i =  2:a(1,1)-2
                b = max(S(:,i));
                c = find(S(:,i)==b);
                e = c(1); %the indicies of the top
                en = 1;
                if e < 3 %if the top is close to an end special treatment is needed.
                    eng = e;
                    while  (S(e+en,i)  <  S(e+en-1,i)  ||  e  +  en  <  3)  &&  e+en-1  <
numel(S(:,1)) - 3
                        en = en+1;
                    end
                    if e+en-1 < numel(S(:,1)) - 3
                        b = min(gradient(S(:,i)));
                        c = find(gradient(S(:,i))==b);
                        e = c(1)+eng+en-3;
                    else
                        b = max(S(e+en-1:end,i));
                        c = find(S(e+en-1:end,i)==b);
                        e = c(1)+eng+en-3;
                    end
                end
            eskil(i) = e;
        end
        hmm = std(eskil);
        e = floor(mean(eskil));
        resf = zeros(1,a(1,1)-1);
        resa = zeros(1,a(1,1)-1);
        dresaf = zeros(1,a(1,1)-1);
        t = 3;
        for i = 2:a(1,1)-2
            if find(i == jumpovers | i == jumpovers + 1 | i == jumpovers -1) > 0
                'noise removed 1'
                t = t+1;
            elseif find(i == jumpy | i == jumpy + 1 | i == jumpy -1) > 0
                'noise removed 2'
                t = t+1;
            elseif abs(eskil(i)-mean(eskil)) > 10* hmm
                 'noise removed 3'
                 t = t+1;
            else
                e = eskil(i);
                %fitting the polynom to the measured curve
                if e < 5
```

```
                    [pf,s]  =  polyfit(vF(1:e+3,i),S(1:e+3,i),n);  %smoothing  resonant
curve using polynom
                elseif 39-e <  5
                    [pf,s] = polyfit(vF(e-5:end,i),S(e-5:end,i),n); %smoothing resonant
curve using polynom
                else
                    [pf,s] = polyfit(vF(e-4:e+4,i),S(e-4:e+4,i),n); %smoothing resonant
curve using polynom
                end
                dpf(1:n) = 0;
                %finding first and second derivative
                for q = 1:n
                    dpf(q) = pf(q) * (n+1-q);
                end
                ddpf(1:n-1) = 0;
                for q = 1:(n-1)
                    ddpf(q) = dpf(q) * (n-q);
                end
                ppf(:,t-1) = pf;
                dppf(:,t-1) = dpf;
                ddppf(:,t-1) = ddpf;
                %solve the polynom and finds max point
                f = roots(dpf);
                if numel(f) == 0
                    resa(t-1) = 0;
                    resf(t-1) = 0;
                    dresaf(t-1) = 0;
                else
                    for q = 1:(n-1)
                        f(q) = f(q)*isreal(f(q)); %removing imaginary parts
                    end
                    fj = find(abs(vF(e,i)-f) == min(abs(vF(e,i)-f)));
                    %giving the result to different variables
                    resa(t-1) = polyval(pf,f(fj(1)));
                    resf(t-1) = f(fj(1));
                    dresaf(t-1) = polyval(ddpf,f(fj(1)));
                end
                t = t+1;
            end
        end
        %the data can be written to a file, or used directly from the
        %workspace. since Integral is the only used in this thesis, this is
        %the only variable kept. If the others are to be used, the
        %variables must be kept in a matrix, to keep all the probes data.
    end
end
```

indexer

This function finds the indicies of where a resonance curve starts and where it stops.

```
function [index, jumpovers, Time] = indexer(vFk, A)
t = 1;
i = 1;
```

```
%locating resonant curves, which are in the areas where the frequency
%voltage rises
Findus = diff(A(vFk,:));
ind = find(Findus > 0);
ind2 = diff(ind);
ind3 = find(ind2 > 1);
index = zeros(numel(ind3),2);
index(:,2) = ind(ind3);
index(2:end,1) = ind(ind3(1:end-1)+1);
jumpovers = find(index(:,2)-index(:,1) > mean(index(:,2)-index(:,1))+ 2*std(index(:,2)-index(:,1)) | index(:,2)-index(:,1) < mean(index(:,2)-index(:,1))- 2*std(index(:,2)-index(:,1)));
Time = (A(1,index(:,1)+1) + A(1,index(:,2)+1))./2;
```

surfer

This function uses the index variable to organize the data. The area under the resonance curve is also found

```
function [S, Integral] = surfer(A, index,Rk,vF)
a = size(A(1,:));
index(end,2)= a(1,2);
a = size(index);
S = zeros(index(5,2)-index(5,1),a(1,1)-1);
Ssm = zeros(index(5,2)-index(5,1),a(1,1)-1);
%vF = zeros(index(5,2)-index(5,1),a(1,1)-1);
Integral = zeros(a(1,1)-1,1);
%Making matrix for surface plot, and easy acsess to individual
%curves
for i = 2:a(1,1)-1
    vF(:,i) = A(vFk,index(i,1):index(i,1)+38))
    S(:,i) = (A(Rk,index(i,1):index(i,1)+38))+0.8;
    Integral(i) = sum(S(2:end,i).*diff(vF(:,i))); %this is the key parameter to find flame arrival
end
%end
```

Voltagefrequency

This function was intended to convert the voltage frequency into a frequency. The linear correlation approach was however not accurate enough.

```
function [v2f,k,pf] = voltagefrequency (vFk,vF,A, index)
%this function converts the voltage into a frequency, based on mesured
%resonant frequencies. The output is to be used in this formula:
%F(vF) = vF * v2f + k where F is the frequncy, vF is the voltage frequncy
%v2f and k is calculated here.
'voltagefrequency'
Freq = [40.5E6 41E6 41.25E6 41.5E6 41.75E6 42E6 42.25E6 42.5E6];
Probe(:,1) = [-0.11 -0.361 0.01 0.701 1.558 2.038 1.958 1.323];
Probe(:,2) = [-0.340 0.718 1.442 1.755 1.612 1.367 1.182 0.832];
Probe(:,3) = [-.731 -0.705 -0.644 -0.555 -0.503 -0.503 -0.514 -0.520];
Probe(:,4) = [-0.207 0.741 1.166 1.179 0.910 0.650 0.460 0.255];
Probe(:,5) = [-0.752 -0.544 -0.450 -0.270 -0.060 0.06 0.03 -0.060];
Probe = Probe + 0.8;
A(2:6,:) = A(2:6,:)+0.8;
```

```
%In order to find maximum point a polynom is fitted to measured curve, and
%the resulting resonant frequncy is found. Probe 1 and 4 is used, since
%these have the most different resonance frequncy
for i = 1:3:4
    b = max(Probe(:,i));        %finding max point of measured frequency response curve
    c = find(Probe(:,i)==b);
    e = c(1);
    [pf,s] = polyfit(Freq(e-2:e+2),Probe(e-2:e+2,i)',3);
    dpf(1:3) = 0;
    %finding first derivative
    for q = 1:3
        dpf(q) = pf(q) * (3+1-q);
    end
    f = roots(dpf);
    fj = find(abs(Freq(e)-f) == min(abs(Freq(e)-f)));
    Fres(i) = f(fj);
    %this resonant frequncy, Fres,corresponds to a voltage, which is found in
    %experimental data.
    Rk = i+1;
    [S, Integral] = surfer(A, index, Rk,vF);
    Eser = (sum(S(:,2:200),2))./199; %averaging 200 first resonant curves
    Vese = (sum(vF(:,2:200),2))./199;
    b = max(Eser(12:end));
    c = find(Eser(12:end)==b);
    e = c(1);
    [pf,s] = polyfit(Vese(e-2+12:e+2+12),Eser(e-2+12:e+2+12),3);
    dpf(1:3) = 0;
    %finding first derivative
    for q = 1:3
        dpf(q) = pf(q) * (3+1-q);
    end
    f = roots(dpf);
    fj = find(abs(A(vFk,index(3,1)+e)-f) == min(abs(A(vFk,index(3,1)+e)-f)));
    Volt(i) = f(fj);
end
%assuming that the frequncy is a linear function of the voltage
v2f = (Fres(4)-Fres(1))/(Volt(4)-Volt(1));
k = Fres(4) - v2f*Volt(4);
A(2:6,:) = A(2:6,:)-0.8;
```

titled

This function calculates a response curve for a given probe
function [fcurve, curve] = titled(probe)

```
Vinn = 1;
%Settings for probe
switch probe
    case 1
        L = 4.9285E-7;
        Cc = 0E-12;
        Cs = 25.9E-12;
        Cx = 3E-12;
```

```
    Rx = 1000000;
    Rc = 10;
    Rs = 0.06;
    k = 0;
    Probe = [-0.11 -0.361 0.01 0.701 1.558 2.038 1.958 1.323]+0.8;
    res = 42E6*2*pi * sqrt(-1);
case 2
    L = 5.19E-7;
    Cc = 0E-12;
    Cs = 25.9E-12;
    Cx = 3E-12;
    Rx = 1000000;
    Rc = 9;
    Rs = 0.06;
    k = 0;
    Probe = [-0.340 0.718 1.442 1.755 1.612 1.367 1.182 0.832]+0.8;
    res = 41.5E6*2*pi * sqrt(-1);
case 3
    L = 4.98E-7;
    Cc = 0E-12;
    Cs = 25.9E-12;
    Cx = 3E-12;
    Rx = 1000000;
    Rc = 10;
    Rs = 0.06;
    k = 0;
    Probe = [-.731 -0.705 -0.644 -0.555 -0.503 -0.503 -0.514 -0.520]+0.8;
    res = 41.750E6*2*pi * sqrt(-1);
case 4
    L = 5.1145E-7;
    Cc = 0E-12;
    Cs = 25.9E-12;
    Cx = 3E-12;
    Rx = 1000000;
    Rc = 10;
    Rs = 0.06;
    k = 0;
    Probe = [-0.207 0.741 1.166 1.179 0.910 0.650 0.460 0.255]+0.8;
    res = 41.5E6*2*pi * sqrt(-1);
case 5
    L = 4.935E-7;
    Cc = 0E-12;
    Cs = 25.9E-12;
    Cx = 3E-12;
    Rx = 1000000;
    Rc = 10;
    Rs = 0.06;
    k = 0;
    Probe = [-0.752 -0.544 -0.450 -0.270 -0.060 0.06 0.03 -0.060]+0.8;
    res = 42E6*2*pi * sqrt(-1);
```

```
end

%Making curve


for E = 37E6 * 2*pi:2*pi*1e4:44E6 * 2*pi;
    k = k + 1;
    S = E * sqrt(-1);
    curve(k)                                                                                =
abs(Vinn*(2*Rs*Rx*Cx*S+2*Rs+Rx)/(L*S+Rc+Rc*Cc*S^2*L+2*Rs*Rx*Cx*S+2*Rs+Rx+2*Rs*Rx*Cx*S^4
*Cs*Rc*Cc*L+2*Rs*Rx*Cx*S^2*Cs*Rc+2*Rs*Rx*Cx*S^3*Cs*L+2*Rs*Rx*Cx*S^3*Cc*L+2*Rs*S^3*Cs*Rc
*Cc*L+2*Rs*S*Cs*Rc+2*Rs*S^2*Cs*L+2*Rs*Cc*S^2*L+Rx*S^3*Cs*Rc*Cc*L+Rx*S*Cs*Rc+Rx*S^2*Cs*L
+Rx*Cc*S^2*L+Rx*Cx*S*Rc+Rx*Cx*S^2*L+Rx*Cx*S^3*Rc*Cc*L));
    fcurve(k)  = E/(pi*2);
end


S = res;
p1                                                                                      =
Vinn*(2*Rs*Rx*Cx*S+2*Rs+Rx)/(L*S+Rc+Rc*Cc*S^2*L+2*Rs*Rx*Cx*S+2*Rs+Rx+2*Rs*Rx*Cx*S^4*Cs*
Rc*Cc*L+2*Rs*Rx*Cx*S^2*Cs*Rc+2*Rs*Rx*Cx*S^3*Cs*L+2*Rs*Rx*Cx*S^3*Cc*L+2*Rs*S^3*Cs*Rc*Cc*
L+2*Rs*S*Cs*Rc+2*Rs*S^2*Cs*L+2*Rs*Cc*S^2*L+Rx*S^3*Cs*Rc*Cc*L+Rx*S*Cs*Rc+Rx*S^2*Cs*L+Rx*
Cc*S^2*L+Rx*Cx*S*Rc+Rx*Cx*S^2*L+Rx*Cx*S^3*Rc*Cc*L);


Freq = [40.5E6 41E6 41.25E6 41.5E6 41.75E6 42E6 42.25E6 42.5E6];
Probe = (abs(p1)/max(abs(Probe)))*Probe;
```

C - Appendix Abstracts for Work in Progress Poster

Abstract for work in progress posters are presented in the following pages. The first is a poster that is to be presented at the 22nd International Colloquium on the Dynamics of Explosions and Reactive Systems (ICDERS) in Minsk, Belarus. This poster describes the ongoing work with the FAT. The second poster was presented last year in Montreal, Canada at the 32nd International Symposium on Combustion, and it is about the modified balloon experiment for dust explosions. This experiment were performed at the workshop at the UiB, and also worked as a preliminary experiment to the FAT-project.

Experimental investigation of the influence of obstacles on flame propagation in propane-air mixtures and dust-air suspensions in a 3.6 m flame acceleration tube

Trygve Skjold [1,2], Ivar B. Kalvatn [1], Gisle A. Enstad [1] & Rolf K. Eckhoff [1]

[1] University of Bergen, Dept. Physics & Technology, Allégaten 55, Bergen, Norway
[2] GexCon AS, Fantoftvegen 38, Bergen, Norway

1 Introduction

Dust explosions pose a hazard whenever a sufficient amount of combustible material is present as fine powder, there is a possibility of dispersing the material forming an explosive dust cloud within a relatively confined volume of air, and there is an ignition source present. Detailed modelling of industrial dust explosions from first principles is a formidable task, and current methods for mitigating the effects of industrial dust explosions therefore rely on empirical correlations obtained from a limited number of experiments. Recent efforts at simulating the course of dust explosions by combining computational fluid dynamics (CFD) and correlations for turbulent flame propagation with combustion parameters derived from standardized experimental tests have produced promising results [1]. However, the results indicate that the correlations for turbulent burning velocity used in various CFD codes for gaseous fuel-air mixtures are less successful in reproducing the experimental trends observed for dust explosions [1, 2]. The aim of the present work is to investigate these discrepancies further, and to develop improved models that can benefit future use of CFD-codes in consequence assessments for industrial plants. This paper describes an experimental study performed in a 3.6 metres flame acceleration tube on the influence of obstacles on flame propagation in two types of combustible mixtures: propane-air mixtures, and mechanical suspensions of maize starch in air.

2 Experiments

The experimental approach is similar to that of Pu *et al.* [3], but with a somewhat larger apparatus, and with an up-to-date data acquisition system. The flame acceleration tube consists of three equal sections of length 1.2 metres, and internal cross-section 0.27 m × 0.27 m (Figure1). The tests described here are limited to constant volume explosions, but the tube also allows for vented explosions. For gaseous fuels, the explosive mixture is prepared by evacuating the tube and controlling the addition of gas by monitoring the pressure. Tests are typically performed with initial turbulence generated by injecting air from a high pressure reservoir, and this secures thorough mixing prior to ignition. For solid fuels, air from the high pressure reservoir disperses the dust in a pre-dispersion chamber, before the dust is injected into the vessel through nozzles (Figure 2). An ignition source, either a spark or a chemical igniter, initiates the combustion process in one end of the tube. Different types of sensors (thermocouples, capacitive sensors, optical sensors, and high-speed video) measure flame arrival along the length of the tube, and piezoelectric pressure transducers measure pressure development inside the tube.

Correspondence to: trygve@gexcon.com

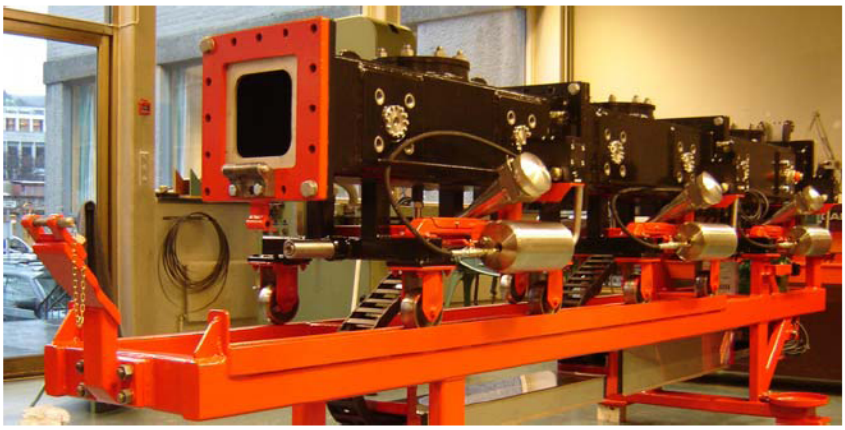

Figure 1 The 3.6 meter flame acceleration tube.

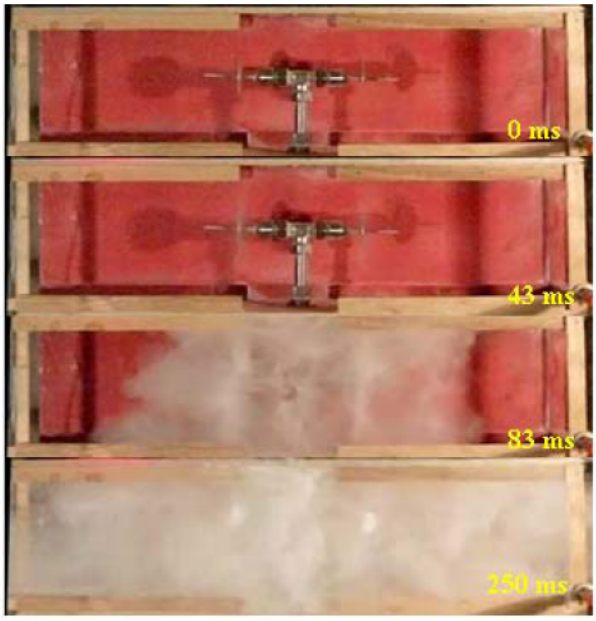

Figure 1 Sequence of pictures from initial testing of the dispersion system in a replica of a 1 metre section with the same cross section area as the flame acceleration tube.

References

[1] Skjold, T., Pu, Y.K., Arntzen, B.J., Hansen, O.J., Storvik, I.E., Taraldset, O.J. & Eckhoff, R.K. (2005). Simulating the influence of obstacles on accelerating dust and gas flames. Poster, *Twentieth International Colloquium on Dynamics of Explosive and Reactive Systems* (ICDERS), July 31 - August 5, Montreal, Canada.

[2] Skjold, T. (2007). Review of the DESC project. *Journal of Loss Prevention in the Process Industries*, **20**: 291-302.

[3] Pu, Y.K., Mazurkiewicz, J., Jarosinski, J. & Kauffman, C.W. (1988). Comparative study of the influence of obstacles on the propagation of dust and gas flames. Twenty-second *Symposium (Int.) on Combustion*: 1789-1797.

A MODIFIED BALLOON EXPERIMENT FOR DUST EXPLOSIONS

T. Skjold [1, 2 *], R.K. Eckhoff [1], G.A. Enstad [1], I.B. Kalvatn [1], M. van Wingerden [2], K. van Wingerden [2]

[1] *Department of Physics and Technology, University of Bergen, Norway;* [2] *GexCon AS, Norway*

trygve.skjold@ift.uib.no

Dust explosions continue to cause serious accidents in the powder handling industries, and the available methods for predicting the course of dust explosions in complex geometries are still of limited use in many practical situations [1]. Dust explosions are inherently complex phenomena, involving transient turbulent particle-laden flow with chemical reactions, often in complex geometries. Nevertheless, recent modelling efforts involving computational fluid dynamics (CFD) have produced promising results [2]. A conventional way of characterizing the reactivity of combustible powders is the maximum rate of pressure rise in constant volume explosion vessels. Although such parameters are convenient to measure, and often provide a useful way of classifying dust samples, they reveal limited information on the actual burning velocity and the structure of the flame. Moreover, the effect of pressure on the rate of combustion complicates the interpretation of the experimental results.

The purpose of the present study is to investigate dust explosions by an alternative experimental method, namely the traditional balloon experiment. A previous study resulted in an experimental apparatus that produced promising results [3]. Rotational flow from a high-pressure reservoir fluidizes the dust in a pre-dispersion chamber, before the suspension flows into the balloon through a pipe and a specially designed nozzle. In the first version, a small blasting cap ignited the dust cloud inside the balloon after a preset ignition delay time. A high-speed video camera captures the dispersion process and the subsequent explosion. The figure below shows some selected frames from one of these experiments. However, the blasting cap produced sparks that could ignite the flammable mixture some distance away from the original point of ignition, and even punctuate the balloon on some occasions. Furthermore, it was not always straightforward to support the balloon in an upright position. Hence, in the present contribution, the flow from the pre-dispersion chamber will enter the balloon from above (hanging balloon), and an electric discharge will ignite the flammable mixture at a specified ignition delay time. The experimental program includes tests with both maize starch and flammable gas (propane).

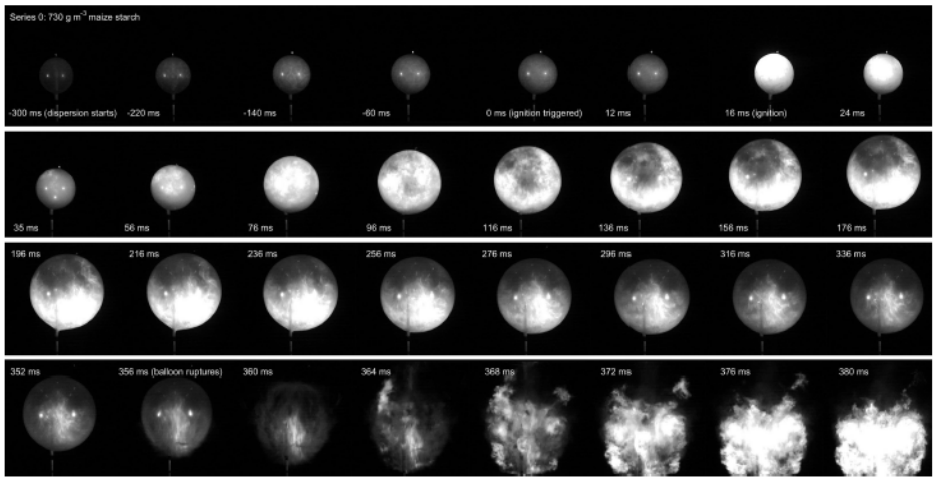

Although the experimental setup is relatively simple, the results may reveal fundamental differences in the structure of turbulent flames involving combustible dusts and flammable gases. The results are also valuable for validating sub-grid models describing the initial phase of flame propagation in CFD codes.

[1] Eckhoff, R.K. (2003). *Dust explosions in the process industries.* Third edition, Gulf Professional Publishing, Amsterdam.

[2] Skjold, T. (2007). Review of the DESC project. *Journal of Loss Prevention in the Process Industries*, 20, 291-302.

[3] Skjold, T. & Eckhoff, R.K. (2006). A balloon experiment for dust explosions. *Thirty-first Symposium (Int.) on Combustion*, Work-in-Progress Poster Session, August 6-11 2006, Heidelberg, 606.